Journal of Immunology Research

Cell Death Signaling and Mechanisms of Systemic Inflammation 2022

Lead Guest Editor: Yi-Song Qian
Guest Editors: Menghao Huang, Teng Guan, Quanwen Liu, and Xiaojiaoyang Li

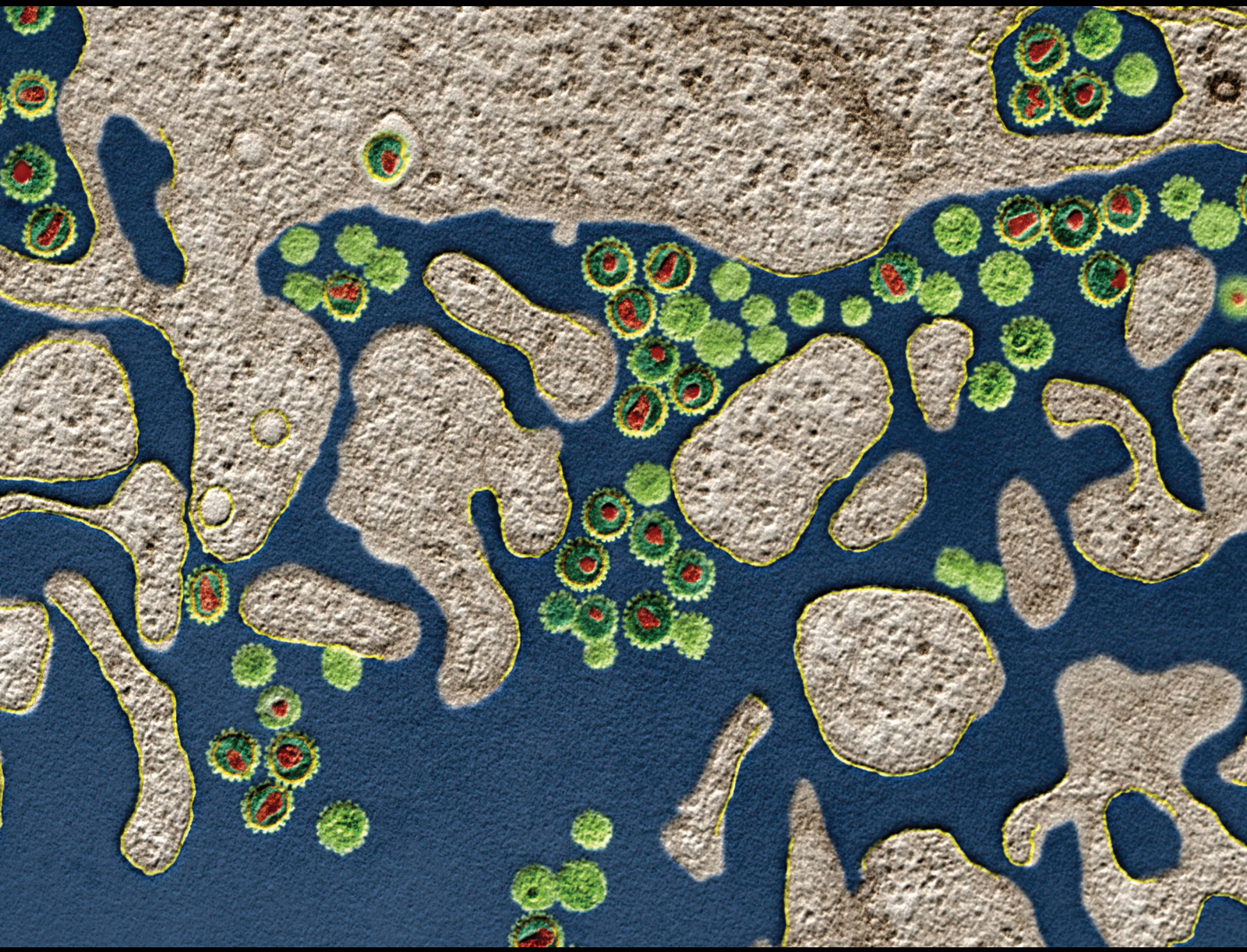

Cell Death Signaling and Mechanisms of Systemic Inflammation 2022

Journal of Immunology Research

Cell Death Signaling and Mechanisms of Systemic Inflammation 2022

Lead Guest Editor: Yi-Song Qian
Guest Editors: Menghao Huang, Teng Guan, Quanwen Liu, and Xiaojiaoyang Li

Contents

Hindawi
Journal of Immunology Research
Volume 2023, Article ID 5509652, 8 pages
https://doi.org/10.1155/2023/5509652

Review Article

Role of Extracellular microRNAs in Sepsis-Induced Acute Lung Injury

Chenlu Xiong,[1] Xuan Huang,[2] Shibiao Chen,[1] and Yong Li[1]

[1]*Department of Anesthesiology, Medical Center of Anesthesiology and Pain, The First Affiliated Hospital of Nanchang University, Nanchang, China*
[2]*The National Engineering Research Center for Bioengineering Drugs and the Technologies, Institute of Translational Medicine, Nanchang University, Nanchang, China*

Correspondence should be addressed to Shibiao Chen; chenlaoshi1111@163.com and Yong Li; liyong@ncu.edu.cn

Received 11 October 2022; Revised 13 May 2023; Accepted 5 June 2023; Published 19 June 2023

Academic Editor: Arif Siddiqui

Acute lung injury (ALI) is a life-threatening pathological disease characterized by the damage of pulmonary endothelial cells and epithelial cell barriers by uncontrolled inflammation. During sepsis-induced ALI, multiple cells cooperate and communicate with each other to respond to the stimulation of inflammatory factors. However, the underlying mechanisms of action have not been fully identified, and the modes of communication therein are also being investigated. Extracellular vesicles (EVs) are a heterogeneous population of spherical membrane structures released by almost all types of cells, containing various cellular components. EVs are primary transport vehicles for microRNAs (miRNAs), which play essential roles in physiological and pathological processes in ALI. EV miRNAs from different sources participated in regulating the biological function of pulmonary epithelial cells, endothelial cells, and phagocytes by transferring miRNA through EVs during ALI induced by sepsis, which has great potential diagnostic and therapeutic values. This study aims to summarize the role and mechanism of extracellular vesicle miRNAs from different cells in the regulation of sepsis-induced ALI. It provides ideas for further exploring the role of extracellular miRNA secreted by different cells in the ALI induced by sepsis, to make up for the deficiency of current understanding, and to explore the more optimal scheme for diagnosis and treatment of ALI.

1. Introduction

Acute lung injury (ALI) is a life-threatening pathological disease, which remains major cause of morbidity, mortality, and healthcare burden of critically ill patients [1]. ALI is characterized by pulmonary inflammation, damage to the alveolar–capillary barrier and hypoxemia [2]. The pathophysiology of sepsis-induced ALI has not been fully elucidated. There are many risk factors for ALI, such as severe shock, infection, mechanical injury, and so on, among which the most common risk factor is severe sepsis [3]. The lung is the initial and most vulnerable target organ during sepsis, and about 25%–50% of septic patients may develop ALI or even acute respiratory distress syndrome (ARDS) [4]. It is noteworthy that the mortality rate of sepsis-induced ALI is higher than that caused by other risk factors [5]. Despite major advances in supportive care recently, the mortality rate for patients with ALI has decreased over time but is still as high as 40% [6]. Undoubtedly, the identification of new therapeutic targets and preventive approaches that are innovative, safe, and effective is crucial for the successful treatment of sepsis-induced ALI.

Extracellular vesicles (EVs) have recently emerged as key mediators in the pathogenesis of sepsis and ALI [7, 8]. The potential of harnessing EVs in the diagnosis and treatment of diseases is now being actively explored [9]. EV is a heterogeneous group of endogenous nanosized spherical membrane structures released by almost all types of cells, which is initially considered as a process of discarding membrane proteins in cells [10]. With the progress of research, it has been found that EVs are closely related to intercellular material transmission and signal communication, which can be released into a variety of bodily fluids including blood, urine, saliva, and bronchoalveolar lavage fluid (BALF) [11]. After ALI, there are abundant

Table 1: Exo-miRNA involved in sepsis-induced ALI.

Derived from cell types	Exo-miRNA	Target cell types	Mechanisms	Reference no.
Mesenchymal stem cells	Exo-mir-30b-3p	Epithelial cells	Cell membrane repair	[18]
	Exo-mir-377-3p	Epithelial cells	RPTOR/autophagy	[19]
	Exo-miR-126	Endothelial cells	PI3K/Akt signaling/apoptosis	[20]
	Exo-miR-27a-3p	Macrophage	Macrophage polarization/NF-*k*B signalling	[21]
	Exo-miR-145	Macrophage	Macrophage phagocytosis	[22]
Macrophage	Exo-miR-223/142	Macrophage	NLRP3 inflammasome activity	[23]
	Exo-miR-155		SOCS-1 signaling	[24]
Neutrophils	Exo-miR-223	Epithelial cell	PARP-1 inhibition	[25]
Endothelial progenitor cells	Exo-miR-126	Endothelial cells	Raf/ERK signaling	[26]
	Exo-miR-10a/b-5p	Endothelial cells	miR-10a/b-5p/adam15 axis	[27]
	Exo-miR-126-3p/5p	Endothelial cells	Restore lung permeability	[28]
Endothelial cells	Exo-miR-125b-5p		miR-125b-5p/TOP2A/VEGF axis	[29]
Epithelial cells	Exo-miR-92a-3p	Alveolar macrophages	NF-*k*B signalling	[30]
	Exo-miR-17/221	Macrophage	Integrin β1 recycling	[31]

EVs detected in BALF, which originated from different cells. Furthermore, BALF EVs differ significantly in lung injury caused by sterile or infectious stimuli [12]. In the lipopolysaccharide (LPS)-induced ALI model, EVs were packaged with microRNA (miRNA) and cytokines, and then secreted to BALF [13].

EVs are composed of small lipid bilayers surrounding vesicles, which contain cellular components such as cytosolic proteins, DNA, and RNA [14]. Among them, there is a large amount of RNA in EVs, which can exchange genetic information between cells via carrying out intercellular communication by transferring messenger RNA and miRNA [15]. Extracellular miRNA plays a crucial role in the occurrence, maintenance, and resolution of a variety of diseases including ALI, which can be used as a new diagnostic and therapeutic target for various noncancer diseases (such as metabolic abnormalities) [16, 17]. Consequently, a growing number of studies have focused on the roles of extracellular miRNAs in lung injury and inflammation.

Here, we intend to update the latest knowledge about the roles of extracellular miRNAs in sepsis-induced ALI (Table 1), and discuss their diagnostic and therapeutic potential as facilitators of cell communication via miRNA as well as the relevance of microorganism-derived EVs.

2. Extracellular Vesicles (EVs)

EVs are composed of small lipid bilayers around vesicles with diameters ranging from 40 to 1,000 nm [32]. Three main subtypes of EVs have been classified based on the mechanisms of formation, the membrane compositions, and the size of EVs, including exosomes (50–150 nm), macrovesicles (100–1,000 nm), and apoptotic bodies (500–5,000 nm) [33]. Most notably, migrasomes are a recently discovered type of EVs with diameters of about 50–100 nm, which are characteristically generated along retraction fibers in migrating cells [34] (Figure 1). Although several comparative proteomics studies have provided a list of proteins that may be specific for the identified EV subtypes, EV isolation methods to date only enable enrichment but not distinct separation of these EV subpopulations [35], thus the current article collectively refers to all vesicles released by cells as EVs. These EVs transfer cytosolic proteins, nucleic acids, or lipids to target cells [14], inducing transferring cellular components and changes in target-cell phenotypes and functions [36, p. 96]. According to the type of secretory cells, a group of cell type-specific proteins will be displayed in the EVs, which explain their specific fate and function.

The content of EVs is influenced by the environmental conditions and cell type, and other factors (e.g., infection or artificial expression of molecules), and hence it will directly affect the fate and function of EVs [37]. EV is involved in inflammation inhibition, immune regulation, transportation, and transmission of genetic information [38–40]. For instance, after ALI, there are abundant EVs detected in BALF, which originated from different cells, when subjected to the addition of plasma obtained from septic patients, or, the addition of pure LPS. In the LPS-induced ALI model, EVs were secreted in BALF, packaged with miRNA and cytokines, suggesting a complicated relationship between several cellular pathways occurring in sepsis [13].

Although, the components of EVs during the development of lung injury and inflammation are highly regulated, such as proteins, lipids, DNA, and RNA molecules, only RNA compositions are robustly increased in each EVs after normalization with the number of EVs. It seems that different miRNAs containing EVs play specific functional roles after specific stimuli [41]. The function and mechanism of these EVs-containing miRNAs in sepsis remain unclear, which may have the great potential to be diagnostic biomarkers and therapeutic targets [42].

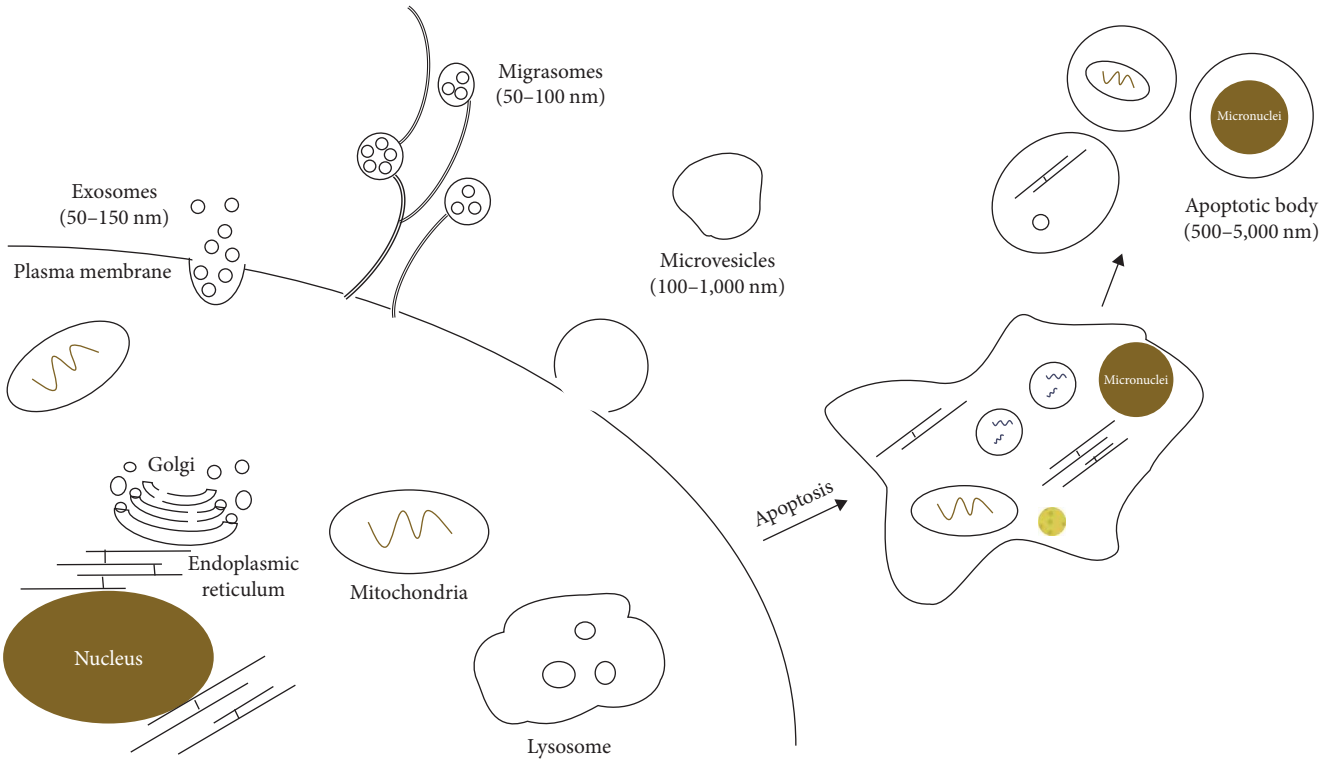

Figure 1: Subtypes of extracellular vesicles (EVs).

3. Extracellular miRNAs

In 2007, Valadi et al. [43] found that both mRNA and miRNA existed in exosomes of mast cells, which can be delivered into another cell through a specific and regulated process and be functional in this new location. This genetic communication between cells may occur in the extracellular microenvironment but could also occur at a distance by traffic of exosomes through the systemic circulation in a similar way to hormones [44]. More importantly, if exosomes deliver a specific mRNA or miRNA, it may be more effective in affecting the recipient cell by modifying the protein production and gene expression of the recipient cell. Furthermore, those extracellular miRNAs bypass the transcriptional control of receptor cells through the intercellular transfer of foreign bodies and regulate the expression of target genes in receptor cells of different tissues [45]. As noncoding RNAs (ncRNAs), miRNAs are enriched in exosomes while others are barely present, which may share the same specific sequence (such as the EXO motif), suggesting a potential regulatory mechanism for the sorting of specific sets of miRNAs into exosomes [45].

miRNA is highly stable due to its small size compared with long mRNAs, which are identified to be differentially expressed in different stages of the disease and contribute to the diagnosis, treatment determination, and prognosis [46]. EVs containing miRNAs may be the emerging targets for developing novel therapeutic and diagnostic agents. As novel endocrine factors, extracellular miRNA can be used as a new diagnostic and therapeutic target for various noncancer diseases (such as metabolic disease), which plays a crucial role in the occurrence, maintenance, and resolution of a variety of diseases, including ALI [47, 48].

4. Extracellular miRNAs in Sepsis-Induced ALI

4.1. Extracellular miRNAs Derived from Mesenchymal Stem Cells. In severe bacterial pneumonia, microbubbles derived from human mesenchymal stem cells (MSCs) are as effective as parental stem cells [49]. EVs of human bone marrow-derived mesenchymal stem cells (hBMSCs) have been studied as therapeutic methods in various ALI models because they can reduce inflammation, lung permeability, and bacterial pneumonia [49–51]. MSC-EVs contain a large amount of RNA, including miRNAs [52, 53], which can not only regulate gene expression and transcription but also transfer into target cells and mediate gene expression and regulate cell function [43].

Accumulated evidence has revealed that MSC can play a role in sepsis-induced ALI [54, 55] because they can secrete paracrine factors such as growth factors, anti-inflammatory cytokines, and antimicrobial peptides [56–58]. Keratinocyte growth factor (KGF) is a paracrine factor secreted by hBMSCs. It has been proved that KGF can repair ALI induced by *Escherichia coli* endotoxin and bacteria perfused into the human lung in vitro, partially restore lung protein permeability, and reduce alveolar inflammation [55, 59]. MSC can transfer miR-30b-3p into mouse alveolar epithelial cells (AECs) through exosomes to inhibit the expression of SAA3 and increase the expression of

KGF, thereby promoting the proliferation of LPS-treated AECs and inhibiting their apoptosis, which plays a role in reducing the inflammatory response and repairing endothelial cells against ALI [18]. Hao et al. [22] reported that bone marrow MSCs secreted EVs carrying miR-145 and transferred them to macrophages, which inhibited the activity of MRP1, thus enhancing the production and antibacterial activity of LTB4 through LTB4/BLT1 signal transduction, and increased the phagocytosis of macrophage cells to *E. coli*.

Autophagy is a powerful degradation pathway that plays a crucial role in various diseases [60]. Exosomes released by human umbilical cord mesenchymal stem cells (HucMSCs) induce autophagy in LPS-induced ALI, protecting against ALI [19]. The overexpression of miR-377-3p in HucMSCs exosomes can reduce LPS-induced ALI by targeting the inhibition of mTOR regulatory-related protein which stimulated the autophagy of LPS-treated human alveolar epithelial cells [19].

MSCs from various tissues and adipose-derived mesenchymal stem cells (ADSCs) are a group of attractive pluripotent MSCs due to their abundance and easy accessibility [61]. Compared with bone marrow-derived MSCs and ADSCs are more easily obtained by minimally invasive methods. In sepsis, dead cells release extracellular histones, which can induce endothelial injury and lead to ALI and multiple organ failure (MOF) [62–64]. MiR-126 was significantly increased in histone-treated ADSCs and exosomes derived from histone-treated ADSCs, which can activate PI3K/Akt signal and inhibit endothelial cell apoptosis [20]. Therefore, ADSCs can indirectly protect endothelial cells through the paracrine effect of exosomes.

4.2. Extracellular miRNAs Derived from Macrophage. Macrophages, the first responders of all immunoregulatory cells, are involved in the initiation and progression of lung inflammation and play a central role in the pathogenesis of ALI, which could be a new biomarker and treatment of ALI [65, 66]. Macrophage extracellular vesicle-mediated miRNA may provide a new therapeutic strategy in a cell-specific manner [67]. Compared with other delivery methods, microvesicles have some potential advantages as a carrier for delivering exogenous nucleotides [68]. Macrophages can be obtained from the blood of the host. Thus Zhang et al. [23] thought that the microbubbles secreted by macrophages to deliver miRNA molecules as therapeutic agents may trigger a less immune response, increase efficacy, and have fewer nontarget effects.

Infectious stimuli can increase miR-223/142 levels in microvesicles secreted by macrophages, and thus miR-223/142 in the circulation may serve as a potential marker to indicate lung macrophage activation or inflammation, and predict lung inflammation and its changes after bacterial infection [23]. Intracellular miR-223/142 was delivered via microvesicle-mediated delivery, and miR-223 and miR-142 synergistically inhibited activation of the NLRP3 inflammasome in macrophages by inhibiting NLRP3 and ASC, respectively, leading to suppression of lung inflammation [23]. MiR-155 belongs to a multifunctional miRNA family and has been reported to be associated with multifactorial-induced lung inflammation [69]. Macrophage-derived miR-155 mediates the expression of inflammatory factors in LPS-induced ALI through SOCS-1 and promotes inflammation [24].

Macrophage polarization occurs when macrophages phenotypically mount a specific phenotype and functional response to different pathophysiological conditions and surrounding microenvironments [70]. In the rehabilitation phase of ALI/ARDS, recruited macrophages then shift from the M1 to the M2 phenotype [71]. Wang et al. [21] found miR-27a-3p carried in EVs transferred from bone marrow MSCs to macrophages, which induced M2 macrophage polarization, inhibited the expression of NFKB1, and alleviated LPS-induced lung injury. Phagocytosis of dying cells and pathogens from a host by macrophages is also an efficient process for the resolution of inflammation [72, 73].

4.3. Extracellular miRNAs Derived from Polymorphonuclear Neutrophils. During ALI, inflammatory cells, mainly polymorphonuclear neutrophils, are in close contact with AECs. Many researchers have studied the intercellular communication of neutrophils in ALI, including paracrine cross talk between neutrophils and lung parenchymal cells [74]. Neutrophils secrete EVs carrying bioactive substances, including miRNA, which mediate intercellular communication and horizontal transfer of genetic material [75]. Neudecker et al. [25] found that miR-223 can transfer from neutrophils to lung epithelial cells through EVs, mediate PARP-1 inhibition, and has anti-inflammatory and protective effects on ALI. PARP-1, a miR-223 target gene in lung epithelial cells, is related to inflammation and ischemia-reperfusion tissue injury. miR-223 limits excessive lung inflammation during ALI by inhibiting PARP-1.

4.4. Extracellular miRNAs Derived from Endothelial Progenitor Cells and Endothelial Cells. Endothelial dysfunction is the pathophysiologic basis of ALI syndromes with dysfunction in several aspects, including coagulation, fibrinolysis, permeability, leukocyte recruitment, and vascular tone [76]. The mechanisms supporting these functions are highly complex, but some independent regulatory factors can be regulated explicitly for some independent factors without damaging other protective innate immune responses [77].

Endothelial progenitor cells (EPCs) can promote the proliferation, migration, and tube formation of endothelial cells, thereby reducing vascular leakage and inflammation, and improving bacterial clearance in sepsis-induced lung injury, pneumonia, and ALI [78, 79]. EPCs can migrate from bone marrow and then locate at the site of tissue injury, which has been studied as a possible therapeutic approach [80]. Moreover, it can secrete exosomes for intercellular communication to attenuate LPS-induced lung injury [28].

Wu et al. [26] suggested that EPCs secrete exosomes to transfer miR-126 to endothelial cells, and miR-126 regulates endothelial cell proliferation, migration, and tube formation by targeting spred-1 to activate Raf/ERK signaling. Jin et al. [27] believed that EPCs increase the expression of miR-10a/b-5p in lung tissue and pulmonary microvascular endothelial cells of ALI induced by LPS. MiR-10a/b-5p reduces the protein level of adam15 and promotes the proliferation of

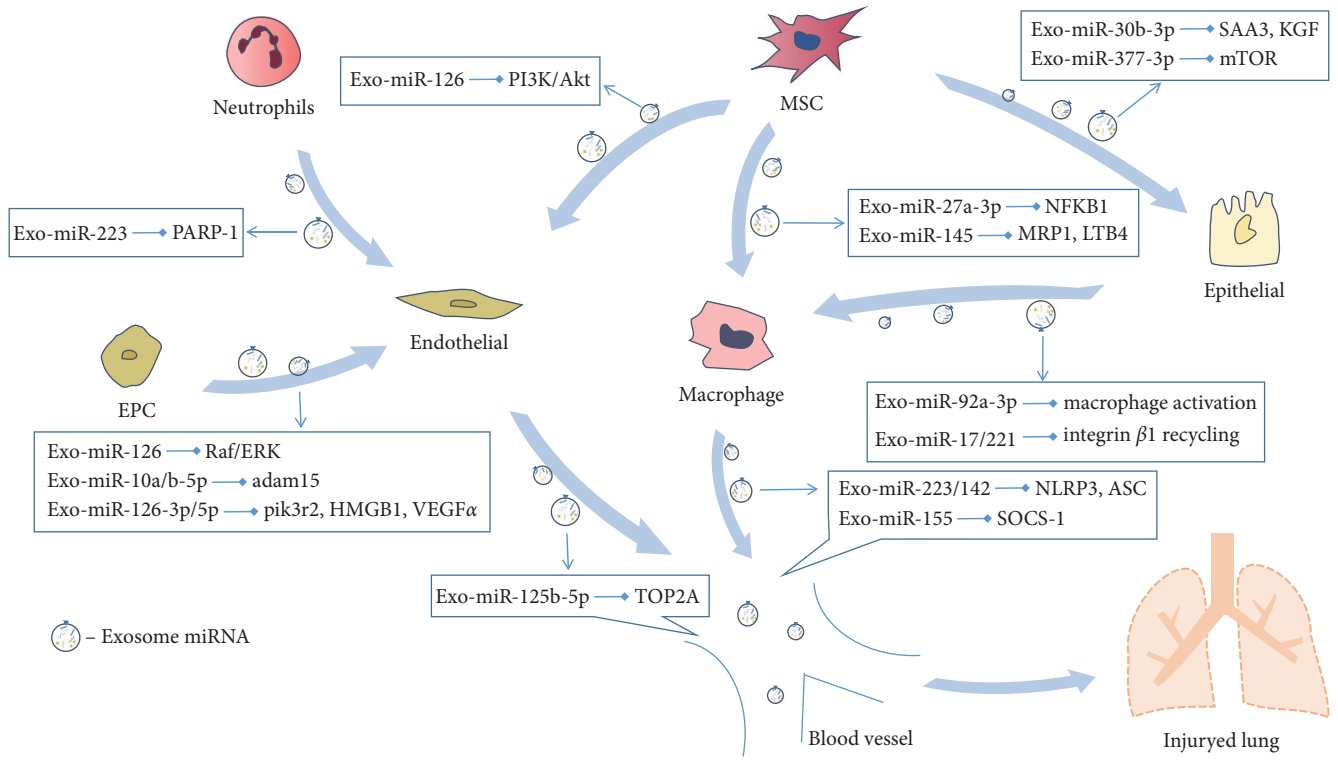

FIGURE 2: Extracellular microRNAs in sepsis-induced ALI. During sepsis-induced ALI, Exo-miRs released from different cells (such as neutrophils, MSCs, and EPCs) were transported by extracellular vesicles (EVs) and transferred to recipient cells (such as macrophage, endothelial cells, and epithelial cells), where they regulate posttranscriptional gene expression.

multisegmented microvascular endothelial cells induced by LPS. In addition, EPCs play a therapeutic role in ALI by promoting LPS-induced MPMVEC proliferation by regulating the miR-10a/b-5p/adam15 axis. Zhou et al. [28] suggested that both miR-126-3p and 5p in endothelial progenitor cell exosomes could increase the expression of tight junction proteins, including claudin1, claudin4, and occludin, by inhibiting phosphoinositide-3-kinase regulatory subunit 2 (pik3r2) and HMGB1 to restore alveolar barrier integrity and attenuate alveolar edema and lung injury. The overexpression of miR-126-3p could target pik3r2, whereas the overexpression of miR-126-5p inhibited inflammatory factor HMGB1 and permeability factor VEGFα. In addition, miR-126-5p delivered by exosomes inhibits VEGFα expression, further reducing ALI-induced lung permeability decline.

Endothelial cells can also secrete exosomes to attenuate sepsis-induced ALI. Jiang et al. [29] demonstrated that miR-125b-5p was upregulated in endothelial cell-derived exosomes to protect sepsis-induced ALI by inhibiting TOP2A and inflammatory responses in lung tissues of ALI mice. Amplified miR-125b-5p promoted the expression of vascular endothelial growth factor in lung tissue while decreasing vascular endothelial growth factor levels in ALI mice serum. Exosomes and exosomal miR-125b-5p (Exo-miR-125b-5p) also inhibited apoptosis in mice with ALI lung tissue.

4.5. Extracellular miRNAs Derived from Lung Epithelial Cell. Common features of ALI/ARDS include a solid inflammatory response in the lung parenchyma, severe damage of epithelial and endothelial cell barriers leading to alveolar edema, decreased lung compliance, impaired gas exchange, and hypoxemia [81]. As the first line of defense against injury, the alveolar epithelium plays an essential role in maintaining lung integrity and function during the development of ALI [82]. Liu et al. [30] showed that AECs exposed to LPS or sepsis released more exosomes than normal AECs, and there was a significant difference in the expression profile of miRNA in exosomes compared with the control group, in which miR-92a-3p was significantly increased in the exosomes of AECs after LPS treatment. The exosomes produced by LPS-treated AECs can promote the activation of alveolar macrophages and enhance the inflammatory response of alveolar macrophages. Macrophages activated by miR-92a-3p in the exosomes released by AECs have specific effects on lung injury, but the exact mechanism of miR-92a-3p-induced macrophage activation is unclear. Pulmonary epithelial-derived vesicles regulate macrophage migration and microvascular function by delivering miRNA-17/221-induced integrin β1 recycling. The transmission of miRNA in EVs from lung epithelial cells may provide a new way for the treatment of ALI [31].

5. Conclusion

This review aimed to summarize the mechanisms by which different cells regulate the repair of ALI through extracellular vesicle transfer of miRNAs and to provide ideas for further exploring the role of extracellular miRNAs secreted by different cells in sepsis-induced ALI (Figure 2). This review also aimed to make up for the lack of existing knowledge and

explore a better scheme for the diagnosis and treatment of ALI.

Data Availability

Data sharing is not applicable to this article as no new data were created or analyzed in this study.

Conflicts of Interest

The authors declare that they have no conflicts of interest.

Acknowledgments

This work was supported by grants from the National Natural Science Foundation of China (82060023, 31960147, and 82160133), Jiangxi Provincial Natural Science Foundation (20202ACBL206015, 20224BAB206007, 20212ACB216005, and 20212BAB206086).

References

[1] M. A. Matthay, R. L. Zemans, G. A. Zimmerman et al., "Acute respiratory distress syndrome," *Nature Reviews Disease Primers*, vol. 5, Article ID 18, 2019.

[2] L. B. Ware, "Pathophysiology of acute lung injury and the acute respiratory distress syndrome," *Seminars in Respiratory and Critical Care Medicine*, vol. 27, no. 4, pp. 337–349, 2006.

[3] G. Bellani, J. G. Laffey, T. Pham et al., "Epidemiology, patterns of care, and mortality for patients with acute respiratory distress syndrome in intensive care units in 50 countries," *JAMA*, vol. 315, no. 8, pp. 788–800, 2016.

[4] J. Cohen, "The immunopathogenesis of sepsis," *Nature*, vol. 420, pp. 885–891, 2002.

[5] J. E. Sevransky, G. S. Martin, C. Shanholtz et al., "Mortality in sepsis versus non-sepsis induced acute lung injury," *Critical Care*, vol. 13, Article ID R150, 2009.

[6] R. D. Stapleton, B. M. Wang, L. D. Hudson, G. D. Rubenfeld, E. S. Caldwell, and K. P. Steinberg, "Causes and timing of death in patients with ARDS," *Chest*, vol. 128, no. 2, pp. 525–532, 2005.

[7] C. Quan, M. Wang, H. Chen, and H. Zhang, "Extracellular vesicles in acute respiratory distress syndrome: recent developments from bench to bedside," *International Immunopharmacology*, vol. 100, Article ID 108118, 2021.

[8] S. M. Kronstadt, A. E. Pottash, D. Levy, S. Wang, W. Chao, and S. M. Jay, "Therapeutic potential of extracellular vesicles for sepsis treatment," *Advanced Therapeutics*, vol. 4, no. 7, Article ID 2000259, 2021.

[9] L. Cheng and A. F. Hill, "Therapeutically harnessing extracellular vesicles," *Nature Reviews Drug Discovery*, vol. 21, pp. 379–399, 2022.

[10] B.-T. Pan and R. M. Johnstone, "Fate of the transferrin receptor during maturation of sheep reticulocytes in vitro: selective externalization of the receptor," *Cell*, vol. 33, no. 3, pp. 967–978, 1983.

[11] G. van Niel, D. R. F. Carter, A. Clayton, D. W. Lambert, G. Raposo, and P. Vader, "Challenges and directions in studying cell–cell communication by extracellular vesicles," *Nature Reviews Molecular Cell Biology*, vol. 23, pp. 369–382, 2022.

[12] H. Lee, D. Zhang, D. L. Laskin, and Y. Jin, "Functional evidence of pulmonary extracellular vesicles in infectious and noninfectious lung inflammation," *The Journal of Immunology*, vol. 201, no. 5, pp. 1500–1509, 2018.

[13] Z. Yuan, B. Bedi, and R. T. Sadikot, "Bronchoalveolar lavage exosomes in lipopolysaccharide-induced septic lung injury," *Journal of Visualized Experiments*, vol. 135, Article ID e57737, 2018.

[14] M. P. Zaborowski, L. Balaj, X. O. Breakefield, and C. P. Lai, "Extracellular vesicles: composition, biological relevance, and methods of study," *BioScience*, vol. 65, no. 8, pp. 783–797, 2015.

[15] K. M. Kim, K. Abdelmohsen, M. Mustapic, D. Kapogiannis, and M. Gorospe, "RNA in extracellular vesicles," *WIREs RNA*, vol. 8, no. 4, Article ID e1413, 2017.

[16] A. Etheridge, I. Lee, L. Hood, D. Galas, and K. Wang, "Extracellular microRNA: a new source of biomarkers," *Mutation Research/Fundamental and Molecular Mechanisms of Mutagenesis*, vol. 717, no. 1-2, pp. 85–90, 2011.

[17] Y. Gon, T. Shimizu, K. Mizumura, S. Maruoka, and M. Hikichi, "Molecular techniques for respiratory diseases: microRNA and extracellular vesicles," *Respirology*, vol. 25, no. 2, pp. 149–160, 2020.

[18] X. Yi, X. Wei, H. Lv et al., "Exosomes derived from microRNA-30b-3p-overexpressing mesenchymal stem cells protect against lipopolysaccharide-induced acute lung injury by inhibiting SAA3," *Experimental Cell Research*, vol. 383, no. 2, Article ID 111454, 2019.

[19] X. Wei, X. Yi, H. Lv et al., "MicroRNA-377-3p released by mesenchymal stem cell exosomes ameliorates lipopolysaccharide-induced acute lung injury by targeting RPTOR to induce autophagy," *Cell Death & Disease*, vol. 11, Article ID 657, 2020.

[20] Y. Mizuta, T. Akahoshi, J. Guo et al., "Exosomes from adipose tissue-derived mesenchymal stem cells ameliorate histone-induced acute lung injury by activating the PI3K/Akt pathway in endothelial cells," *Stem Cell Research & Therapy*, vol. 11, Article ID 508, 2020.

[21] J. Wang, R. Huang, Q. Xu et al., "Mesenchymal stem cell-derived extracellular vesicles alleviate acute lung injury via transfer of miR-27a-3p," *Critical Care Medicine*, vol. 48, no. 7, pp. e599–e610, 2020.

[22] Q. Hao, V. Gudapati, A. Monsel et al., "Mesenchymal stem cell-derived extracellular vesicles decrease lung injury in mice," *The Journal of Immunology*, vol. 203, no. 7, pp. 1961–1972, 2019.

[23] D. Zhang, H. Lee, X. Wang et al., "A potential role of microvesicle-containing miR-223/142 in lung inflammation," *Thorax*, vol. 74, no. 9, pp. 865–874, 2019.

[24] W. Wang, Z. Liu, J. Su et al., "Macrophage micro-RNA-155 promotes lipopolysaccharide-induced acute lung injury in mice and rats," *American Journal of Physiology Lung Cellular and Molecular Physiology*, vol. 311, no. 2, pp. L494–L506, 2016.

[25] V. Neudecker, K. S. Brodsky, E. T. Clambey et al., "Neutrophil transfer of *miR-223* to lung epithelial cells dampens acute lung injury in mice," *Science Translational Medicine*, vol. 9, no. 408, Article ID eaah5360, 2017.

[26] X. Wu, Z. Liu, L. Hu, W. Gu, and L. Zhu, "Exosomes derived from endothelial progenitor cells ameliorate acute lung injury by transferring miR-126," *Experimental Cell Research*, vol. 370, no. 1, pp. 13–23, 2018.

[27] Y. Jin, C. Yang, X. Sui, Q. Cai, L. Guo, and Z. Liu, "Endothelial progenitor cell transplantation attenuates lipopolysaccharide-induced acute lung injury via regulating miR-10a/b-5p," *Lipids in Health and Disease*, vol. 18, Article ID 136, 2019.

[28] Y. Zhou, P. Li, A. J. Goodwin et al., "Exosomes from endothelial progenitor cells improve outcomes of the lipopolysaccharide-

induced acute lung injury," *Critical Care*, vol. 23, Article ID 44, 2019.

[29] L. Jiang, J. Ni, G. Shen et al., "Upregulation of endothelial cell-derived exosomal microRNA-125b-5p protects from sepsis-induced acute lung injury by inhibiting topoisomerase II alpha," *Inflammation Research*, vol. 70, pp. 205–216, 2021.

[30] F. Liu, W. Peng, J. Chen et al., "Exosomes derived from alveolar epithelial cells promote alveolar macrophage activation mediated by miR-92a-3p in sepsis-induced acute lung injury," *Frontiers in Cellular and Infection Microbiology*, vol. 11, Article ID 646546, 2021.

[31] H. Lee, D. Zhang, J. Wu, L. E. Otterbein, and Y. Jin, "Lung epithelial cell-derived microvesicles regulate macrophage migration via microRNA-17/221-induced integrinβ_1 recycling," *The Journal of Immunology*, vol. 199, no. 4, pp. 1453–1464, 2017.

[32] J. A. Welsh, J. A. Holloway, J. S. Wilkinson, and N. A. Englyst, "Extracellular vesicle flow cytometry analysis and standardization," *Frontiers in Cell and Developmental Biology*, vol. 5, Article ID 78, 2017.

[33] C. Théry, K. W. Witwer, E. Aikawa et al., "Minimal information for studies of extracellular vesicles 2018 (MISEV2018): a position statement of the international society for extracellular vesicles and update of the MISEV2014 guidelines," *Journal of Extracellular Vesicles*, vol. 7, no. 1, Article ID 1535750, 2018.

[34] L. Ma, Y. Li, J. Peng et al., "Discovery of the migrasome, an organelle mediating release of cytoplasmic contents during cell migration," *Cell Research*, vol. 25, pp. 24–38, 2015.

[35] F. Cocozza, E. Grisard, L. Martin-Jaular, M. Mathieu, and C. Théry, "SnapShot: extracellular vesicles," *Cell*, vol. 182, no. 1, Article ID 262.e1, 2020.

[36] N. Iraci, T. Leonardi, F. Gessler, B. Vega, and S. Pluchino, "Focus on extracellular vesicles: physiological role and signalling properties of extracellular membrane vesicles," *International Journal of Molecular Sciences*, vol. 17, no. 2, Article ID 171, 2016.

[37] G. van Niel, G. D'Angelo, and G. Raposo, "Shedding light on the cell biology of extracellular vesicles," *Nature Reviews Molecular Cell Biology*, vol. 19, pp. 213–228, 2018.

[38] R. Jean-Toussaint, Z. Lin, Y. Tian et al., "Therapeutic and prophylactic effects of macrophage-derived small extracellular vesicles in the attenuation of inflammatory pain," *Brain, Behavior, and Immunity*, vol. 94, pp. 210–224, 2021.

[39] S. Martire, F. Montarolo, M. Spadaro et al., "A first phenotypic and functional characterization of placental extracellular vesicles from women with multiple sclerosis," *International Journal of Molecular Sciences*, vol. 22, no. 6, Article ID 2875, 2021.

[40] S. Gurung, D. Perocheau, L. Touramanidou, and J. Baruteau, "The exosome journey: from biogenesis to uptake and intracellular signalling," *Cell Communication and Signaling*, vol. 19, Article ID 47, 2021.

[41] H. Lee, E. Abston, D. Zhang, A. Rai, and Y. Jin, "Extracellular vesicle: an emerging mediator of intercellular crosstalk in lung inflammation and injury," *Frontiers in Immunology*, vol. 9, Article ID 924, 2018.

[42] M. Helena Vasconcelos, H. R. Caires, A. Ābols, C. P. R. Xavier, and A. Linē, "Extracellular vesicles as a novel source of biomarkers in liquid biopsies for monitoring cancer progression and drug resistance," *Drug Resistance Updates*, vol. 47, Article ID 100647, 2019.

[43] H. Valadi, K. Ekström, A. Bossios, M. Sjöstrand, J. J. Lee, and J. O. Lötvall, "Exosome-mediated transfer of mRNAs and microRNAs is a novel mechanism of genetic exchange between cells," *Nature Cell Biology*, vol. 9, pp. 654–659, 2007.

[44] R. Bayraktar, K. Van Roosbroeck, and G. A. Calin, "Cell-to-cell communication: microRNAs as hormones," *Molecular Oncology*, vol. 11, no. 12, pp. 1673–1686, 2017.

[45] Q. Fan, L. Yang, X. Zhang et al., "The emerging role of exosome-derived non-coding RNAs in cancer biology," *Cancer Letters*, vol. 414, pp. 107–115, 2018.

[46] M. V. Iorio and C. M. Croce, "MicroRNA dysregulation in cancer: diagnostics, monitoring and therapeutics. A comprehensive review," *EMBO Molecular Medicine*, vol. 4, no. 3, pp. 143–159, 2012.

[47] J. Li, Y. Zhang, Y. Ye et al., "Pancreatic β cells control glucose homeostasis via the secretion of exosomal miR-29 family," *Journal of Extracellular Vesicles*, vol. 10, no. 3, Article ID e12055, 2021.

[48] S. Rajasekaran, D. Pattarayan, P. Rajaguru, P. S. Sudhakar Gandhi, and R. K. Thimmulappa, "MicroRNA regulation of acute lung injury and acute respiratory distress syndrome," *Journal of Cellular Physiology*, vol. 231, no. 10, pp. 2097–2106, 2016.

[49] A. Monsel, Y.-G. Zhu, S. Gennai et al., "Therapeutic effects of human mesenchymal stem cell-derived microvesicles in severe pneumonia in mice," *American Journal of Respiratory and Critical Care Medicine*, vol. 192, no. 3, pp. 324–336, 2015.

[50] J. Park, S. Kim, H. Lim et al., "Therapeutic effects of human mesenchymal stem cell microvesicles in an ex vivo perfused human lung injured with severe *E. coli* pneumonia," *Thorax*, vol. 74, no. 1, pp. 43–50, 2019.

[51] Q. Hao, Y.-G. Zhu, A. Monsel et al., "Study of bone marrow and embryonic stem cell-derived human mesenchymal stem cells for treatment of *Escherichia coli* endotoxin-induced acute lung injury in mice," *Stem Cells Translational Medicine*, vol. 4, no. 7, pp. 832–840, 2015.

[52] T. S. Chen, R. C. Lai, M. M. Lee, A. B. H. Choo, C. N. Lee, and S. K. Lim, "Mesenchymal stem cell secretes microparticles enriched in pre-microRNAs," *Nucleic Acids Research*, vol. 38, no. 1, pp. 215–224, 2010.

[53] L. Cheng, R. A. Sharples, B. J. Scicluna, and A. F. Hill, "Exosomes provide a protective and enriched source of miRNA for biomarker profiling compared to intracellular and cell-free blood," *Journal of Extracellular Vesicles*, vol. 3, no. 1, Article ID 23743, 2014.

[54] Y.-G. Zhu, Q. Hao, A. Monsel, X.-M. Feng, and J.-W. Lee, "Adult stem cells for acute lung injury: remaining questions and concerns," *Respirology*, vol. 18, no. 5, pp. 744–756, 2013.

[55] Y.-G. Zhu, X.-M. Feng, J. Abbott et al., "Human mesenchymal stem cell microvesicles for treatment of *Escherichia coli* endotoxin-induced acute lung injury in mice," *Stem Cells*, vol. 32, no. 1, pp. 116–125, 2014.

[56] N. Gupta, A. Krasnodembskaya, M. Kapetanaki et al., "Mesenchymal stem cells enhance survival and bacterial clearance in murine *Escherichia coli* pneumonia," *Thorax*, vol. 67, no. 6, pp. 533–539, 2012.

[57] A. Krasnodembskaya, Y. Song, X. Fang et al., "Antibacterial effect of human mesenchymal stem cells is mediated in part from secretion of the antimicrobial peptide LL-37," *Stem Cells*, vol. 28, no. 12, pp. 2229–2238, 2010.

[58] A. Krasnodembskaya, G. Samarani, Y. Song et al., "Human mesenchymal stem cells reduce mortality and bacteremia in gram-negative sepsis in mice in part by enhancing the phagocytic activity of blood monocytes," *American Journal of Physiology Lung Cellular and Molecular Physiology*, vol. 302, no. 10, pp. L1003–L1013, 2012.

[59] J. W. Lee, X. Fang, N. Gupta, V. Serikov, and M. A. Matthay, "Allogeneic human mesenchymal stem cells for treatment of

E. coli endotoxin-induced acute lung injury in the ex vivo perfused human lung," *Proceedings of the National Academy of Sciences*, vol. 106, no. 38, pp. 16357–16362, 2009.

[60] S. Saha, D. P. Panigrahi, S. Patil, and S. K. Bhutia, "Autophagy in health and disease: a comprehensive review," *Biomedicine & Pharmacotherapy*, vol. 104, pp. 485–495, 2018.

[61] C. G. da Silva, L. S. de Sá Barretto, E. G. Lo Turco et al., "Lipidomics of mesenchymal stem cell differentiation," *Chemistry and Physics of Lipids*, vol. 232, Article ID 104964, 2020.

[62] J. S. Ibañez-Cabellos, C. Aguado, D. Pérez-Cremades et al., "Extracellular histones activate autophagy and apoptosis via mTOR signaling in human endothelial cells," *Biochimica et Biophysica Acta (BBA) - Molecular Basis of Disease*, vol. 1864, no. 10, pp. 3234–3246, 2018.

[63] Z. Xu, Y. Huang, P. Mao, J. Zhang, and Y. Li, "Sepsis and ARDS: the dark side of histones," *Mediators of Inflammation*, vol. 2015, Article ID 205054, 9 pages, 2015.

[64] E. Silk, H. Zhao, H. Weng, and D. Ma, "The role of extracellular histone in organ injury," *Cell Death & Disease*, vol. 8, Article ID e2812, 2017.

[65] M. Divangahi, I. L. King, and E. Pernet, "Alveolar macrophages and type I IFN in airway homeostasis and immunity," *Trends in Immunology*, vol. 36, no. 5, pp. 307–314, 2015.

[66] M. Kopf, C. Schneider, and S. P. Nobs, "The development and function of lung-resident macrophages and dendritic cells," *Nature Immunology*, vol. 16, pp. 36–44, 2015.

[67] J. Lan, L. Sun, F. Xu et al., "M2 macrophage-derived exosomes promote cell migration and invasion in colon cancer," *Cancer Research*, vol. 79, no. 1, pp. 146–158, 2019.

[68] K. Khalaj, R. L. Figueira, L. Antounians, G. Lauriti, and A. Zani, "Systematic review of extracellular vesicle-based treatments for lung injury: are EVs a potential therapy for COVID-19?" *Journal of Extracellular Vesicles*, vol. 9, no. 1, Article ID 1795365, 2020.

[69] A. Rodriguez, E. Vigorito, S. Clare et al., "Requirement of *bic/microRNA-155* for normal immune function," *Science*, vol. 316, no. 5824, pp. 608–611, 2007.

[70] N. Wang, H. Liang, and K. Zen, "Molecular mechanisms that influence the macrophage M1–M2 polarization balance," *Frontiers in Immunology*, vol. 5, Article ID 614, 2014.

[71] L. K. Johnston, C. R. Rims, S. E. Gill, J. K. McGuire, and A. M. Manicone, "Pulmonary macrophage subpopulations in the induction and resolution of acute lung injury," *American Journal of Respiratory Cell and Molecular Biology*, vol. 47, no. 4, pp. 417–426, 2012.

[72] A. M. Joffe, M. H. Bakalar, and D. A. Fletcher, "Macrophage phagocytosis assay with reconstituted target particles," *Nature Protocols*, vol. 15, pp. 2230–2246, 2020.

[73] I. Kourtzelis, G. Hajishengallis, and T. Chavakis, "Phagocytosis of apoptotic cells in resolution of inflammation," *Frontiers in Immunology*, vol. 11, Article ID 553, 2020.

[74] V. Dengler, G. P. Downey, R. M. Tuder, H. K. Eltzschig, and E. P. Schmidt, "Neutrophil intercellular communication in acute lung injury. Emerging roles of microparticles and gap junctions," *American Journal of Respiratory Cell and Molecular Biology*, vol. 49, no. 1, pp. 1–5, 2013.

[75] Y.-J. Youn, S. Shrestha, Y.-B. Lee et al., "Neutrophil-derived trail is a proinflammatory subtype of neutrophil-derived extracellular vesicles," *Theranostics*, vol. 11, no. 6, pp. 2770–2787, 2021.

[76] Y. Hao, Z. Wang, F. Frimpong, and X. Chen, "Calcium-permeable channels and endothelial dysfunction in acute lung injury," *Current Issues in Molecular Biology*, vol. 44, no. 5, pp. 2217–2229, 2022.

[77] J. Joffre, J. Hellman, C. Ince, and H. Ait-Oufella, "Endothelial responses in sepsis," *American Journal of Respiratory and Critical Care Medicine*, vol. 202, no. 3, pp. 361–370, 2020.

[78] J.-P. Cao, X.-Y. He, H.-T. Xu, Z. Zou, and X.-Y. Shi, "Autologous transplantation of peripheral blood-derived circulating endothelial progenitor cells attenuates endotoxin-induced acute lung injury in rabbits by direct endothelial repair and indirect immunomodulation," *Anesthesiology*, vol. 116, no. 6, pp. 1278–1287, 2012.

[79] H. Fan, A. J. Goodwin, E. Chang et al., "Endothelial progenitor cells and a stromal cell-derived factor-1alpha analogue synergistically improve survival in sepsis," *American Journal of Respiratory and Critical Care Medicine*, vol. 189, no. 12, pp. 1509–1519, 2014.

[80] R. Sun, J. Huang, and B. Sun, "Mobilization of endothelial progenitor cells in sepsis," *Inflammation Research*, vol. 69, pp. 1–9, 2020.

[81] A. P. Wheeler and G. R. Bernard, "Acute lung injury and the acute respiratory distress syndrome: a clinical review," *The Lancet*, vol. 369, no. 9572, pp. 1553–1564, 2007.

[82] J. A. Whitsett and T. Alenghat, "Respiratory epithelial cells orchestrate pulmonary innate immunity," *Nature Immunology*, vol. 16, pp. 27–35, 2015.

Hindawi
Journal of Immunology Research
Volume 2023, Article ID 1774260, 15 pages
https://doi.org/10.1155/2023/1774260

Research Article

Identification of Hub Biomarkers and Immune and Inflammation Pathways Contributing to Kawasaki Disease Progression with RT-qPCR Verification

Hongjun Ba,[1,2] **Lili Zhang**,[1] **Huimin Peng**,[1] **Xiufang He**,[1] **Yuese Lin**,[1] **Xuandi Li**,[1] **Shujuan Li**,[1] **Ling Zhu**,[1] **Youzhen Qin**,[1] **Xing Zhang**,[3] **and Yao Wang**[4]

[1]*Department of Pediatric Cardiology, Heart Center, First Affiliated Hospital of Sun Yat-sen University, 58# Zhongshan Road 2, Guangzhou 510080, China*
[2]*Key Laboratory on Assisted Circulation, Ministry of Health, 58# Zhongshan Road 2, Guangzhou 510080, China*
[3]*Department of Cardiology, Kunming Children's Hospital, 288 Qianxing Road, Xishan District, Kunming 650034, Yunnan, China*
[4]*Cancer Hospital, Guangzhou Medical University, Guangzhou 510095, China*

Correspondence should be addressed to Xing Zhang; zhichi828@126.com and Yao Wang; wangyao@gzhmu.edu.cn

Received 28 September 2022; Revised 21 November 2022; Accepted 18 March 2023; Published 6 April 2023

Academic Editor: Yisong Qian

Background. Kawasaki disease (KD) is characterized by a disordered inflammation response of unknown etiology. Immune cells are closely associated with its onset, although the immune-related genes' expression and possibly involved immune regulatory mechanisms are little known. This study aims to identify KD-implicated significant immune- and inflammation-related biomarkers and pathways and their association with immune cell infiltration. *Patients and Methods*. Gene microarray data were collected from the Gene Expression Omnibus database. Differential expression analysis, weighted gene coexpression network analysis (WGCNA), least absolute shrinkage and selection operator (LASSO) regression, Gene Ontology (GO), Kyoto Encyclopedia of Genes and Genomes (KEGG), and gene set enrichment analysis (GSEA) were used to find KD hub markers. GSEA was used to assess the infiltration by 28 immune cell types and their connections to essential gene markers. Receiver operating characteristic (ROC) curves were used to examine hub markers' diagnostic effectiveness. Finally, hub genes' expressions were validated in Chinese KD patients by reverse transcription-quantitative polymerase chain reaction (RT-qPCR). *Results*. One hundred and fifty-one unique genes were found. Among 10 coexpression modules at WGCNA, one hub module exhibited the strongest association with KD. Thirty-six overlapping genes were identified. Six hub genes were potential biomarkers according to LASSO analysis. Immune infiltration revealed connections among activated and effector memory $CD4^+$ T cells, neutrophils, activated dendritic cells, and macrophages. The six hub genes' diagnostic value was shown by ROC curve analysis. Hub genes were enriched in immunological and inflammatory pathways. RT-qPCR verification results of *FCGR1B* ($P<0.001$), *GPR84* ($P<0.001$), *KREMEN1* ($P<0.001$), *LRG1* ($P<0.001$), and *TDRD9* ($P<0.001$) upregulated expression in Chinese KD patients are consistent with our database analysis. *Conclusion*. Neutrophils, macrophages, and activated dendritic cells are strongly linked to KD pathophysiology. Through immune-related signaling pathways, hub genes such as *FCGR1B*, *GPR84*, *KREMEN1*, *LRG1*, and *TDRD9* may be implicated in KD advancement.

1. Introduction

Kawasaki disease (KD), often called cutaneous lymph node syndrome, was initially described by Tomisaku Kawasaki in 1967 [1]. Children under 5 years of age are primarily affected by KD. KD is an acute systemic immune vasculitis caused by infectious factors that can be complicated by coronary artery lesions (CAL). CAL caused by KD are a common heart disease in some countries and regions. On the other hand, the steps leading to the development of KD are not fully understood. The diagnosis of KD depends on typical clinical manifestations. However, some children with KD have atypical manifestations and are easily misdiagnosed with other diseases, leading to an increased risk of coronary artery damage

due to delayed diagnosis and treatment [2, 3]. Therefore, identifying a biomarker to diagnose KD helps with early diagnosis and treatment, reducing the risk of damage to the coronary arteries.

Although much research has been conducted, the pathogenesis of KD is not completely known. Recent research has suggested that immune cells may play a role in KD development and its associated symptoms. Alterations in the monocyte development locus can be observed during the acute phase of KD infection [4]. When KD is in its acute phase, $CD8^+$ T cell expression decreases significantly [5]. Immunohistochemical analysis of coronary arteries of deceased patients with KD showed the presence of monocytes, macrophages, neutrophils, monocytes, macrophages, and activated $CD8^+$ T cells [6] and IgA^+ plasma cells [7, 8] in the arterial wall. Furthermore, immune regulatory genes such as *CXCL8* and *CCL5*, among others, have the potential to play a crucial role in the progression of KD [9]. These findings imply that genes related to the immune system may be involved in the pathogenesis of KD.

Bioinformatic analysis approaches include least absolute shrinkage and selection operator (LASSO) and weighted gene coexpression network analysis (WGCNA). WGCNA aggregates similar-expressed genes into a single module using clustering. This approach has substantial biological consequences and can effectively screen for target-related genes [10, 11]. Unlike traditional Cox and logistic regression methods, the LASSO regression method aims to gain insight into the exact degree of connection between two inextricably connected variables. The accuracy of character-related gene screening may be improved by LASSO analysis of WGCNA genes [12]. The WGCNA and LASSO technologies were used to identify important KD biomarkers. Using DEGs, or differentially expressed genes, these biomarkers were identified. The immune-related signaling pathways linked with DEGs were then identified using Gene Ontology (GO), the Kyoto Encyclopedia of Genes and Genomes (KEGG), and gene set enrichment analysis (GSEA). This study is the first to evaluate 28 immune cell infiltrates using a single GSEA sample (ssGSEA) to better understand the pathogenesis of KD and treatment goals. Finally, we validated the screening of hub genes in Chinese KD patients.

2. Materials and Methods

2.1. Data Extraction. The Gene Expression Omnibus database (https://www.ncbi.nlm.nih.gov/geo/) was used to get microarray expression data and clinical information relevant to KD (GSE18606 [13], GSE73461 [14], and GSE68004 [15]). In the GSE18606 dataset, 47 samples were taken from 38 patients diagnosed with KD, and nine healthy individuals served as controls. Within the GSE73461 dataset, there were 78 KD and 55 control samples. The GSE68004 collection included 113 samples: 76 patients with KD and 37 healthy controls. GSE18606 and GSE73461 were added to the metadata queues (training groups) in preparation for future integration investigations. The training group was validated using the GSE68004 dataset as the test group.

2.2. Identification of DEGs. For data normalization and probe annotation, the "limma" and "GEOquery" packages included in R software (version 4.0.1) were applied. The screening criterion for DEGs consisted of an adjusted *P*-value of <0.05 and a log fold change (FC) of more than 1 [16, 17].

2.3. Construction of Gene Coexpression Network. The WGCNA package of the R program was used to build a weighted coexpression network from the expression profile data of the training group (in addition to GSE18606 and GSE73461), and 25% of the genes that were the most distinct from the median were selected for the investigation [10]. The "goodSampleGenes" function was used to validate the accuracy of the data. The "pickSoftThreshold" function was used to calculate and confirm that the optimal soft threshold (β) had been attained. Clustering was performed to identify the modules most similar in terms of their topological overlap after the matrix data were converted into an adjacency matrix. After the module characteristic genes of the modules had been calculated, a hierarchical clustering tree diagram was built according to the comparable modules that were present in the cluster tree of the feature genes. This investigation integrated phenotypic and modular data to determine gene significance (GS) and modular importance. Furthermore, a determination was made about the value of genetic and clinical information, and research was carried out on the correlation between modules and models. The method was determined to compute the degree of each gene's module membership (MM), and the GS values of each module were analyzed. The adjacency matrix was constructed by a weighted correlation coefficient. Subsequently, the adjacency matrix was transformed into a topological overlap matrix (TOM). Then, hierarchical clustering was performed to identify modules, and the eigengene was calculated. Finally, we assessed the correlation between phenotype (KD or control samples) and each module by Pearson's correlation analysis and identified KD-related modules. The genes in these modules were considered KD-related module genes.

2.4. Screening and Validation of Hub Genes. To use them as possible hub genes, priority was given to genes exhibiting the highest level of intermodular connection. Generally, genes that are more important biologically have more significant absolute amount of GS. The default was used as the basis for the candidate gene screening criteria of GS absolute value >0.50 and MM absolute value >0.80. It was determined that the genes with the highest intermodular connection levels should be prioritized for use as potential hub genes. In general, genes with greater biological relevance have higher levels of absolute GS.

2.5. Immune Cell Infiltration and Its Association with Hub Genes. In the training group, the relative amounts of infiltration of each of the 28 different types of immune cells were measured using the ssGSEA technique [18]. The varying degrees of expression of each of the 28 different types of immune cells are shown as a violin diagram. The "ggplot2" software application was used to display the results of a calculation that determined the Spearman correlation between the hub gene and the 28 immune cells.

2.6. Functional Enrichment Analysis. The R packages "clusterProfiler" and "enrichment plot" were utilized to study DEGs according to GO, KEGG, and GSEA. GSEA analysis was performed based on all genes. The level of statistical significance was obtained when P was <0.05 [19]. The ssGSEA method was used to determine the relative amounts of infiltration of 28 different types of immune cells in the training group [18]. It was shown using a violin diagram how the different types of immune cells each had a distinct amount of differential expression. The "cor.test" function was utilized to calculate the Spearman correlation between the hub gene and the 28 immune cells. ggplot2 software application was used for visualization.

2.7. Validation of Hub Genes. Reverse transcription-quantitative polymerase chain reaction (RT-qPCR) assays were performed to verify the reliability of bioinformatics-based results. A total of 20 study participants were recruited from the First Affiliated Hospital of Sun Yat-sen University, including 10 KD patients and 10 healthy controls. All subjects gave written informed consent in accordance with the Declaration of Helsinki. The protocol was approved by the Ethics Committee of the First Affiliated Hospital of Sun Yat-sen University ([2022]514). Peripheral venous blood was collected from each participant; then, total RNA was extracted from each sample using TRIzol Reagent (Invitrogen, United States) according to the manufacturer's instructions. The cDNA was synthesized using the SuperScript III Reverse Transcriptase Kit (Invitrogen, United States). RT-qPCR was performed with Power SYBR Green PCR Master Mix (TransGen Biotech, China) on an ABI 7,500 fast real-time PCR system. The amplification reaction procedure was as follows: 95°C for 10 min, followed by 95°C for 15 s and 60°C for 1 min for 40 cycles [20]. GAPDH was selected as the internal control for mRNA, and the relative expression level of mRNA was calculated by the relative quantification ($2^{-\Delta\Delta Ct}$) method. Primer sequences are listed in *Supplementary 1*.

3. Results

The study's flowchart is shown in Figure 1.

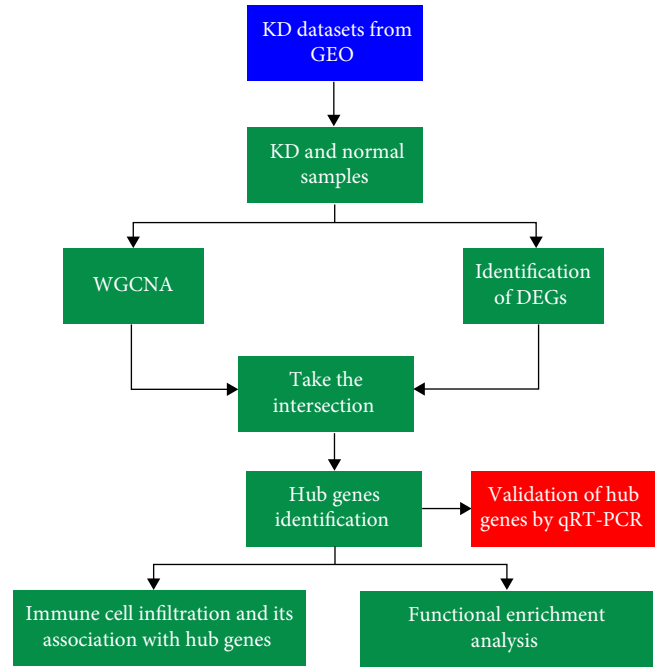

Figure 1: Flowchart of the research process.

3.1. Coexpression Network Construction and Identification of Hub Modules. The data from 10,869 genes in the top 25% of absolute departure from the median were pooled to produce the WGCNA. An identification procedure for missing values was carried out, and outliers were removed. The value of $\beta = 3$ was determined to be the soft threshold (scale-free $R^2 = 0.85$, slope $= -1.21$), which agreed with the scale-free network (*Supplementary 2 and 3*). A coexpression matrix was constructed using a one-step method, and 10 gene modules were obtained using the dynamic mixed shear method (Figure 2(a)). The correlation between the above modules and KD and healthy controls was displayed using heat maps. A hub module (blue module, comprising 315 genes) had the strongest connection with KD (cor = 0.69; P = 6e-24) (Figures 2(b) and 2(c)). In addition, there was a strong correlation between GS and MM inside the blue module (cor = 0.78; P = 1e-200), suggesting that the two may be connected (Figure 2(d)). In addition, the blue module served as the primary focus for the subsequent analyses.

3.2. Identification of DEGs and Screening of Hub Genes. After correcting the P-values to <0.05 and |logFC| to >1, a total of 151 DEGs were identified, 132 and 19 of which had an increase and a decrease in expression, respectively. These DEGs were discovered using a volcano plot (Figure 3(a)). The applicant completed the screening process since their absolute GS score was >0.50 and their absolute MM score was >0.80. Based on these overlaps, 36 DEGs were identified as intersecting (Figure 3(b)). Six hub genes, namely, Fc gamma RI (*FCGR1*), G protein-coupled medium-chain fatty acid receptor (*GPR84*), haptoglobin (*HP*), kringle-containing transmembrane protein 1 (*KREMEN1*), leucine-rich α-2-glycoprotein 1 (*LRG1*), and tudor domain-containing protein 9 (*TDRD9*), were identified by LASSO analysis (Figures 3(c) and 3(d)).

3.3. Functional Enrichment Analysis of DEGs. We found the biological activities and signaling pathways linked with KD-related DEGs by researching the GO and KEGG pathways. According to the findings of the GO enrichment study, DEGs were much more prevalent in immunological and inflammatory processes (such as activation of cells, including white blood cells, involved in immune responses, positive regulation of cytokine production, and acute inflammatory reactions) (Figure 4). Based on an analysis of the KEGG signaling network, DEGs enriched immune and inflammatory disorders (e.g., inflammatory bowel disease and asthma), immune-related pathways (e.g., cytokine–cytokine receptor interaction), and infectious diseases (e.g., inflammatory bowel disease and asthma) (Figure 5). These results showed that

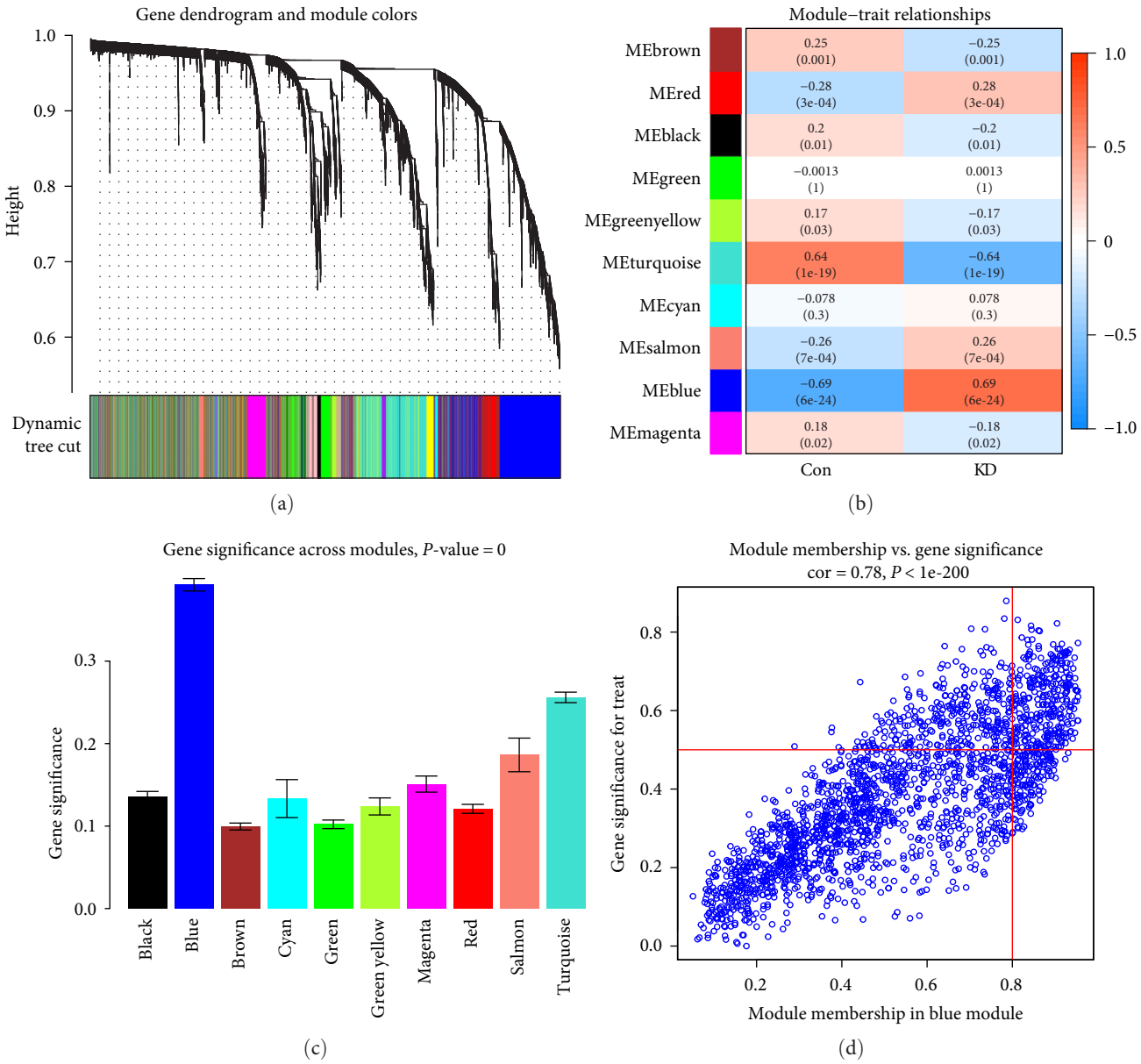

Figure 2: Development of the creation of WGCNA modules: (a) cluster dendrogram of genes whose median absolute deviation is among the top 25% of the range. The lines in the diagram represent a gene, and the colors denote the coexpression modules associated with those genes; (b) a heatmap illustrates the relationships between the modules and the traits. A powerful connection was found between the blue module and KD; (c) a representation of the distribution of the mean gene significance between KD-related modules; (d) a scatter plot shows the connection between membership in the blue module of the gene module and the level of relevance of the gene. Abbreviations: KD, Kawasaki disease; WGCNA, weighted gene coexpression network analysis.

abnormal signaling pathways and cellular processes cause the progression of KD.

3.4. Identification of Hub Gene Expression Levels and Diagnostic Value. As part of the verification process, box plots were utilized to examine the expression levels produced by six different hub genes. *FCGR1B* ($P < 0.001$), *GPR84* ($P < 0.001$), *HP* ($P < 0.001$), *KREMEN1* ($P < 0.001$), and *LRG1* ($P < 0.001$) all had significantly higher expression levels in KD tissues than in healthy control tissues (Figure 6(a)). Subsequently, the levels of expression of these six hub genes were examined using a second external dataset known as GSE68004, and it was demonstrated that they were accurate (Figure 6(b)).

An investigation of the receiver operating characteristic (ROC) curve was conducted to evaluate how sensitive or specific a diagnosis of KD is. As a result, the values of the area under the curve (AUC) for the six key genes could be compared. Because the AUC values for the six hub genes were higher than 0.94, it was clear that these genes have a solid diagnostic value for KD (Figure 7(a)). We conducted further

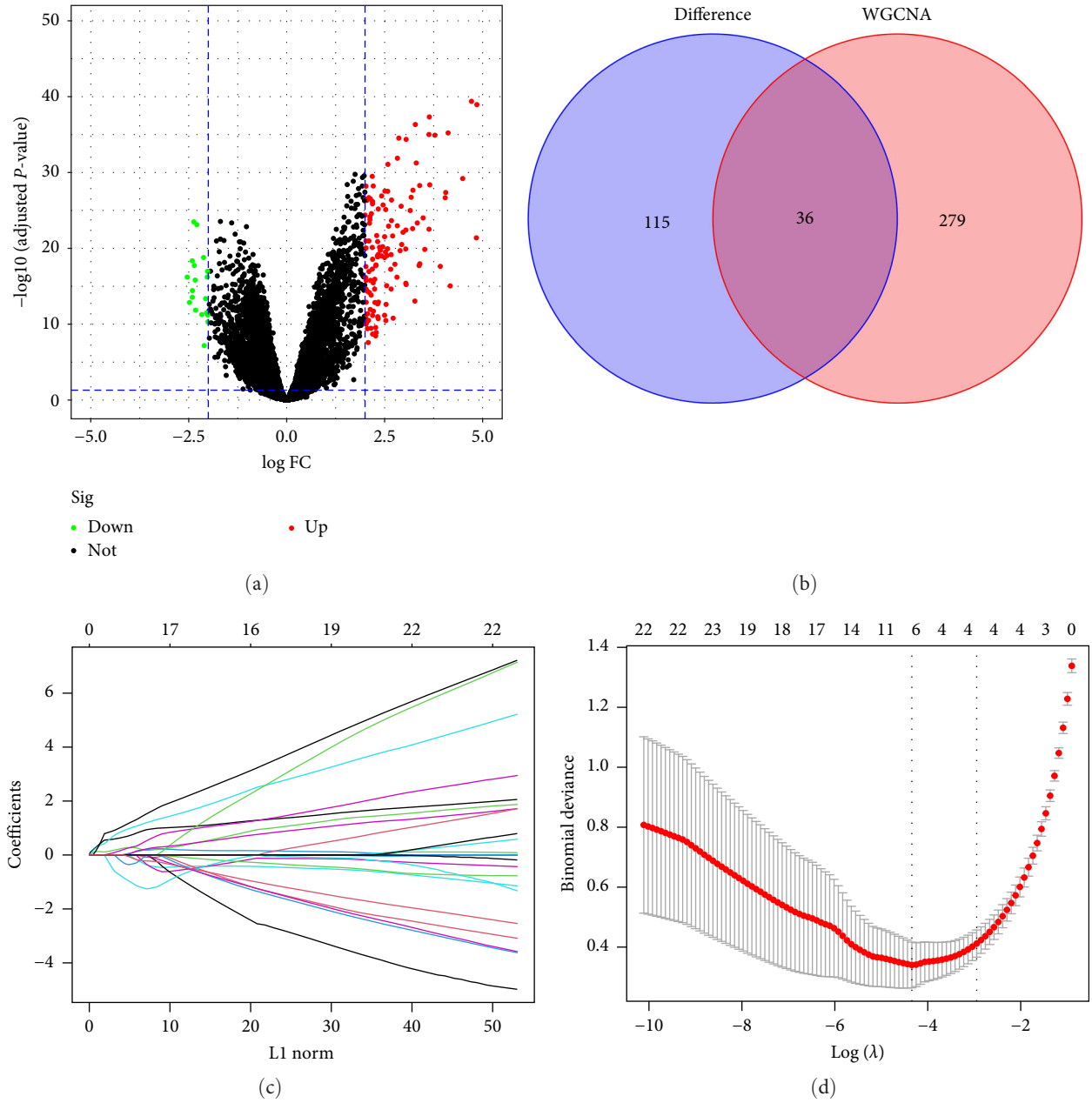

Figure 3: Detection of differentially expressed genes and selection of hub genes: (a) a volcano plot shows DEGs that compare healthy control tissues with those affected by KD; (b) a Venn diagram depicting the intersection of DEGs and the blue module. Thirty-six DEGs were identified as intersecting; (c) comparing LASSO regression with partial likelihood deviance while altering log (l) in 10-fold cross-validations. Vertical dashed lines mark the ideal (lambda.min) values defined by the minimal criterion (1-SE criterion); (d) LASSO coefficient profiles were produced from 10-fold cross-validation for the six hub genes. Abbreviations: DEGs, differentially expressed genes; KD, Kawasaki disease; LASSO, least absolute shrinkage and selection operator.

tests to establish the diagnostic importance of the six hub genes in the GSE68004 dataset. AUC values >0.90 were observed for each of the six hub genes (Figure 7(b)).

3.5. Correlation between Immune Cell Infiltration and Hub Genes. The ssGSEA approach was applied to evaluate the differences in immune cell infiltration between patients with KD and healthy controls. This was done to determine a relationship between KD and healthy controls. Figure 8(a) shows the distribution of the 28 immune cells in the training group. It was discovered that tissues of KD patients have a significantly higher level of infiltration of activated and effector memory $CD4^+$ T cells, monocytes, neutrophils, and macrophages than healthy tissues. This study was conducted on the topic of immune cell infiltration. This study supports the hypothesis that these cells are necessary to develop KD (Figure 8(b)).

According to the findings of an investigation into the connections between 28 distinct types of immune cells and

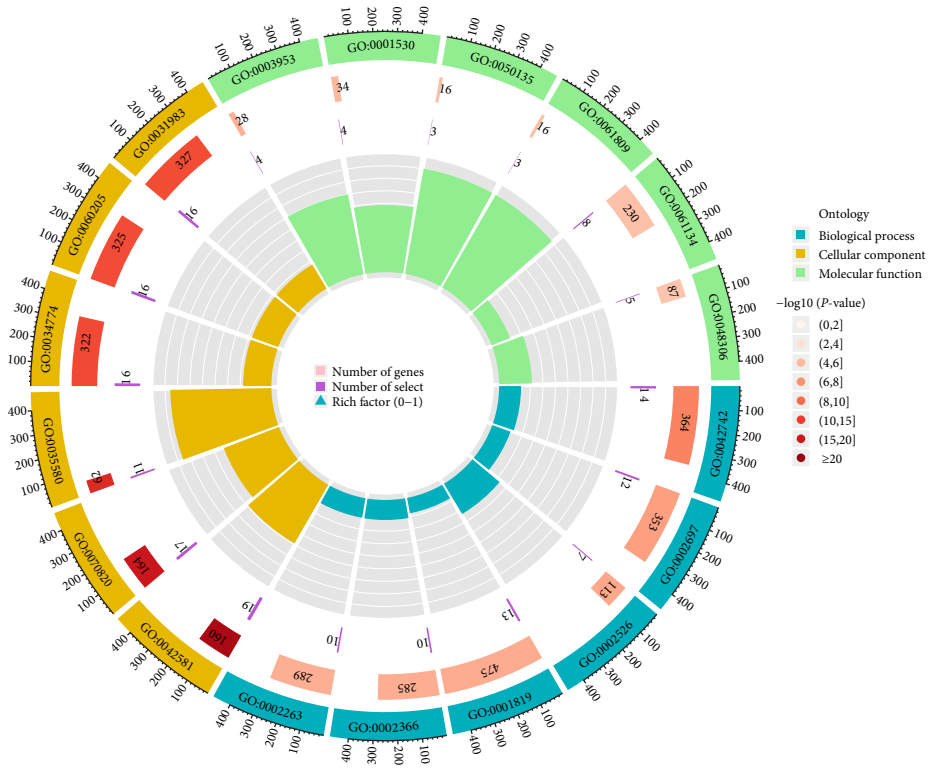

ID	Description
GO:0031983	Vesicle lumen
GO:0060205	Cytoplasmic vesicle lumen
GO:0034774	Secretory granule lumen
GO:0035580	Specific granule lumen
GO:0070820	Tertiary granule
GO:0042581	Specific granule
GO:0002263	Cell activation involved in immune response
GO:0002366	Leukocyte activation involved in immune response
GO:0001819	Positive regulation of cytokine production
GO:0002526	Acute inflammatory response
GO:0002697	Regulation of immune effector process
GO:00042742	Defense response to bacterium
GO:0048306	Calcium-dependent protein binding
GO:0061134	Peptidase regulator activity
GO:0061809	NAD+ nucleotidase, cyclic ADP-ribose generating
GO:0050135	NAD (P)+ nucleosidase activity
GO:0001530	Lipopolysaccharide binding
GO:0003953	NAD+ nucleosidase, activity

FIGURE 4: Using GO keywords in the study of differentially expressed genes in biological processes, the first lap represents the top 18 GO keywords, while the outer lap indicates the total number of genes. During the second pass, the number of genes already present in the genomic background and the *P*-values linked with the enrichment of DEGs for biological processes were retrieved. In the third lap, we compare the number of genes that were elevated (dark purple) with the number of genes that were downregulated (light purple). The fourth circuit represents the enrichment factor of each GO word in the diagram in the figure. Abbreviations: DEG, differentially expressed genes; GO, Gene Ontology.

hub genes, there are positive associations between neutrophils and *FCGR1B* (cor = 5.655; $P < 0.001$), *GPR84* (cor = 4.281; $P < 0.001$), *HP* (cor = 3.918; $P < 0.001$), *KREMEN1* (cor = 7.367; $P < 0.001$), *LRG1* (cor = 7.552; $P < 0.001$), and *TDRD9* (cor = 5.321; $P < 0.001$) (Figure 8(c)).

Positive correlations were found between activated dendritic cells (DCs) and the following genes: *FCGR1B* (cor = 5.807; $P < 0.001$), *GPR84* (cor = 5.861; $P < 0.001$), *HP* (cor = 5.995; $P < 0.001$), *KREMEN1* (cor = 5.169; $P < 0.001$), *LRG1* (cor = 7.448; $P < 0.001$), and *TDRD9* (cor = 5.503; $P < 0.001$). Positive correlations were found between macrophages and the following genes: *FCGR1B* (cor = 4.609; $P < 0.001$), *GPR84* (cor = 4.979; $P < 0.001$), *HP* (cor = 3.890; $P < 0.001$), *KREMEN1* (cor = 6.242; $P < 0.001$), *LRG1* (cor = 6.348; $P < 0.001$), and *TDRD9* (cor = 4.983; $P < 0.001$).

Negative correlations were found between effector memory $CD4^+$ T cells and *FCGR1B* (cor = −4.995; $P < 0.001$), *GPR84* (cor = −5.485; $P < 0.001$), *HP* (cor = −4.987; $P < 0.001$), *KREMEN1* (cor = −4.732; $P < 0.001$), *LRG1* (cor = −7.058; $P < 0.001$), and *TDRD9* (cor = −5.765; $P < 0.001$).

Negative correlations were found between central memory $CD4^+$ T cells and *FCGR1B* (cor = −4.399; $P < 0.001$), GPR84 (cor = −4.897; $P < 0.001$), *HP* (cor = −4.977; $P < 0.001$), *KREMEN1* (cor = −3.654; $P < 0.001$), *LRG1* (cor = −6.304; $P < 0.001$), and *TDRD9* (cor = −5.739; $P < 0.001$).

In addition, a negative connection was seen between the six hub genes and effector memory $CD8^+$ T cells and central memory $CD8^+$ T cells (Figure 8(c)). These findings support the hypothesis that specific immune cells play an essential role in the development of KD.

3.6. Enrichment Analysis of GSEA Immune Signature Gene Sets. To investigate the most likely mechanism that keeps immune function intact throughout the course of KD, we used the Molecular Signatures Database (MsigDB) of immunological signature genes as a reference for GSEA of DEGs. This analysis focused on genes that were expressed at different levels. Eight hundred and thirty-three gene sets showed substantially higher enrichment, as shown by a normalized enriched score (NES) >1 and a false discovery rate (FDR) q-value <0.05. It was shown that neutrophils and peripheral blood mononuclear cells (PBMCs) have much more significant enrichment in these genes. The 15 gene sets that are the most enriched are given in Table 1. The findings of this investigation support the hypothesis that immune-related genes play a significant role in the onset of KD and its progression (Figure 9).

3.7. RT-qPCR Validation of Hub Genes in Chinese KD Patients. To further verify the expression of the 10 hub genes in KD patients, we detected their expression in 20 peripheral

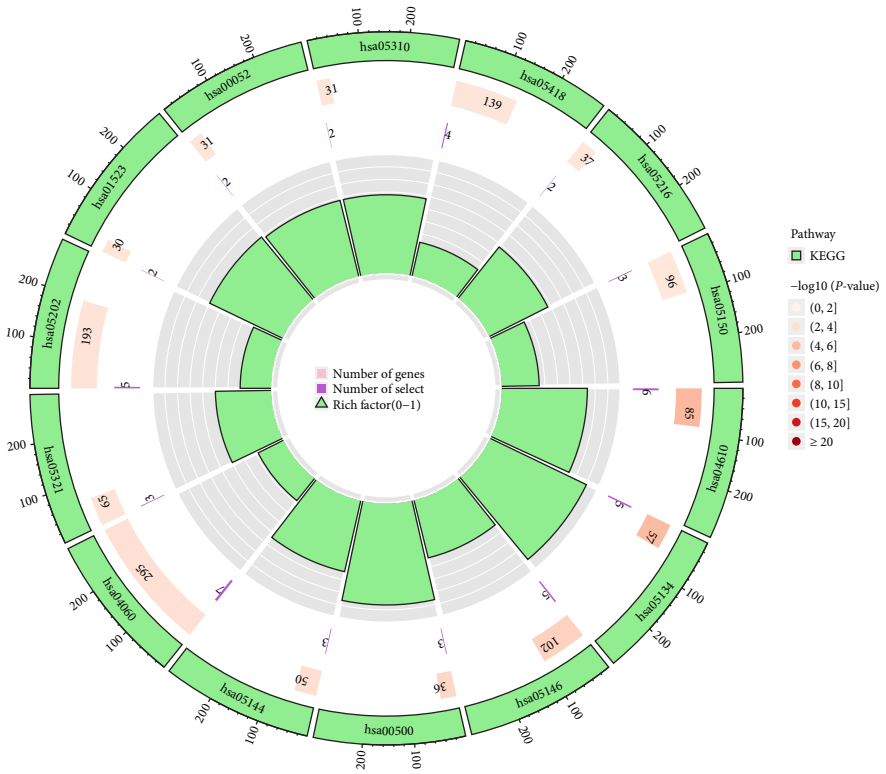

ID	Description
hsa04610	Complement and coagulation cascades
hsa05134	Legionellosis
hsa05146	Amoebiasis
hsa00500	Starch and sucrose metabolism
hsa05144	Malaria
hsa04060	Cytokine–cytokine receptor interaction
hsa05321	Inflammatory bowel disease
hsa05202	Transcriptional misregulation in cancer
hsa01523	Antifolate resistance
hsa00052	Galactose metabolism
hsa05310	Asthma
hsa05418	Fluid shear stress and atherosclerosis
hsa05216	Thyroid cancer
hsa05150	*Staphylococcus aureus* infection

FIGURE 5: Utilizing terminology from the KEGG database to research DEGs in metabolic processes, organismal systems, and human diseases. The first lap depicts the top 14 KEGG keywords, while the outer lap represents the total number of genes in the human genome. In the second lap, the *P*-values for DEG enrichment are displayed along with the total number of genes present in the genetic background. In the third lap, we compare the number of genes that were elevated (dark purple) with the number of genes that were downregulated (light purple). The enrichment factor for each KEGG term is presented in the fourth circuit of the scheme. Abbreviations: DEGs, differentially expressed genes; KEGG, Kyoto Encyclopedia of Genes and Genomes.

venous blood samples from 10 KD patients and 10 samples from healthy individuals. The results showed that the expression of *FCGR1B* ($P<0.001$), *GPR84* ($P<0.001$), *KREMEN1* ($P<0.001$), *LRG1* ($P<0.001$), and *TDRD9* ($P<0.001$) was significantly upregulated in KD patients compared with the control group, while *HP* ($P>0.05$) was not significantly upregulated in KD patients compared to the normal group (Figure 10 and *Supplementary 4*).

4. Discussion

In recent years, the widespread application of high-throughput microarray technology has resulted in developing more rapid and effective bioinformatics methods to screen critical genes associated with disease mechanisms, occurrence, and progression. These methods have been made possible because of the widespread application of high-throughput microarray technology. Because of this, effective ways of diagnosing diseases, designing new drugs, and treating existing patients have been developed. Our research revealed that immunological responses, positive regulation of cytokine production, and acute inflammatory responses were more prevalent in DEGs in patients with KD compared to healthy controls. Based on these findings, specific pathways were implicated in the development of KD [21, 22].

Previous research found that neutrophils, monocytes, and macrophages increased considerably in peripheral blood samples from individuals with acute KD [23]. Interleukin (IL)-6, a soluble receptor for tumor necrosis factor, rises considerably during the acute phase of KD [24, 25]. When KEGG signaling pathways were examined, DEGs were shown to be more abundant in immunological and inflammatory diseases (such as inflammatory bowel disease and asthma), immune-related pathways (such as cytokine–cytokine receptor interaction), and viral diseases (e.g., inflammatory bowel disease and asthma). These results provide additional credence to the hypothesis that the development of KD is closely related to infection-induced immunological abnormalities.

WGCNA differs from traditional DEG-based screening methods. It overcomes the disadvantages of traditional methods that only allow the partial analysis of datasets, thus possibly missing key regulatory molecules and making it challenging to explore and study the entire biological system. The network of individual biological interactions has been systematically mapped, and core prognosis-associated molecules have been identified [26, 27]. In this study, genes strongly linked to KD were found using WGCNA. The results of this study were then compared with those of another study that examined DEG to determine whether there were significant differences or correlations between the two sets of genes. Subsequently, six hub

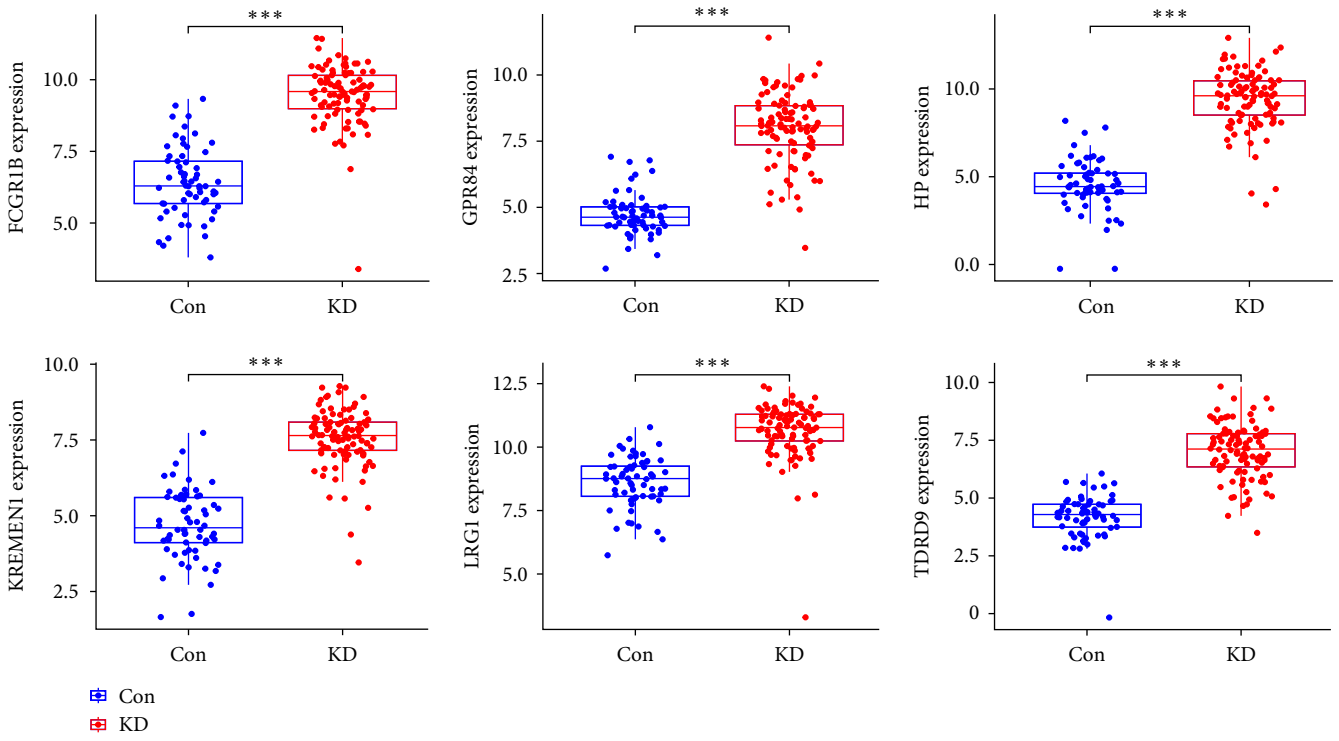

(a)

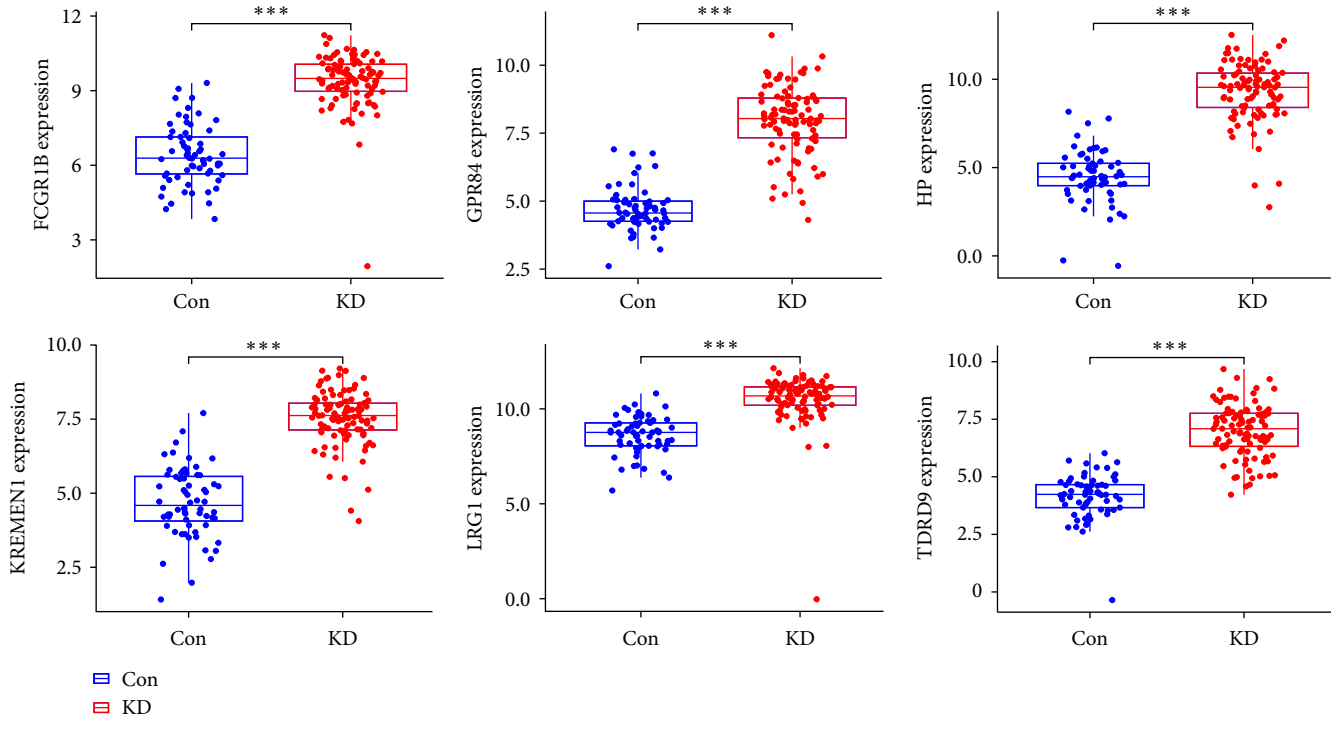

(b)

Figure 6: Hub genes' validation performed at the level of gene expression: (a) verification of the expression of hub genes in the training population (merging GSE18606 and GSE73461 datasets). KD patients had higher levels of *FCGR1B*, *GPR84*, *HP*, *KREMEN1*, *LRG1*, and *TDRD9* than healthy controls; (b) the validation of the hub genes in the test group (GSE68004) yielded results that overlapped with the results of the training group. Abbreviation: KD, Kawasaki disease. $^{***}P<0.001$.

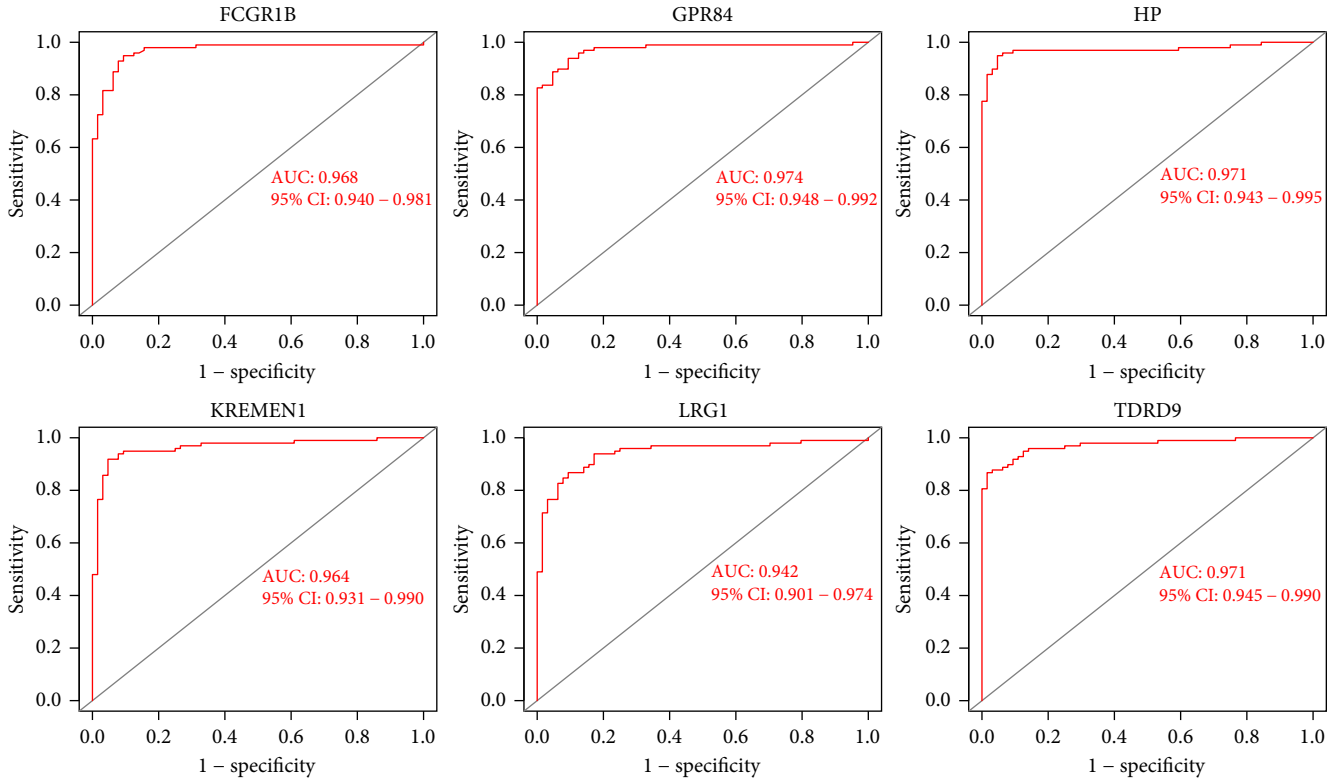

(a)

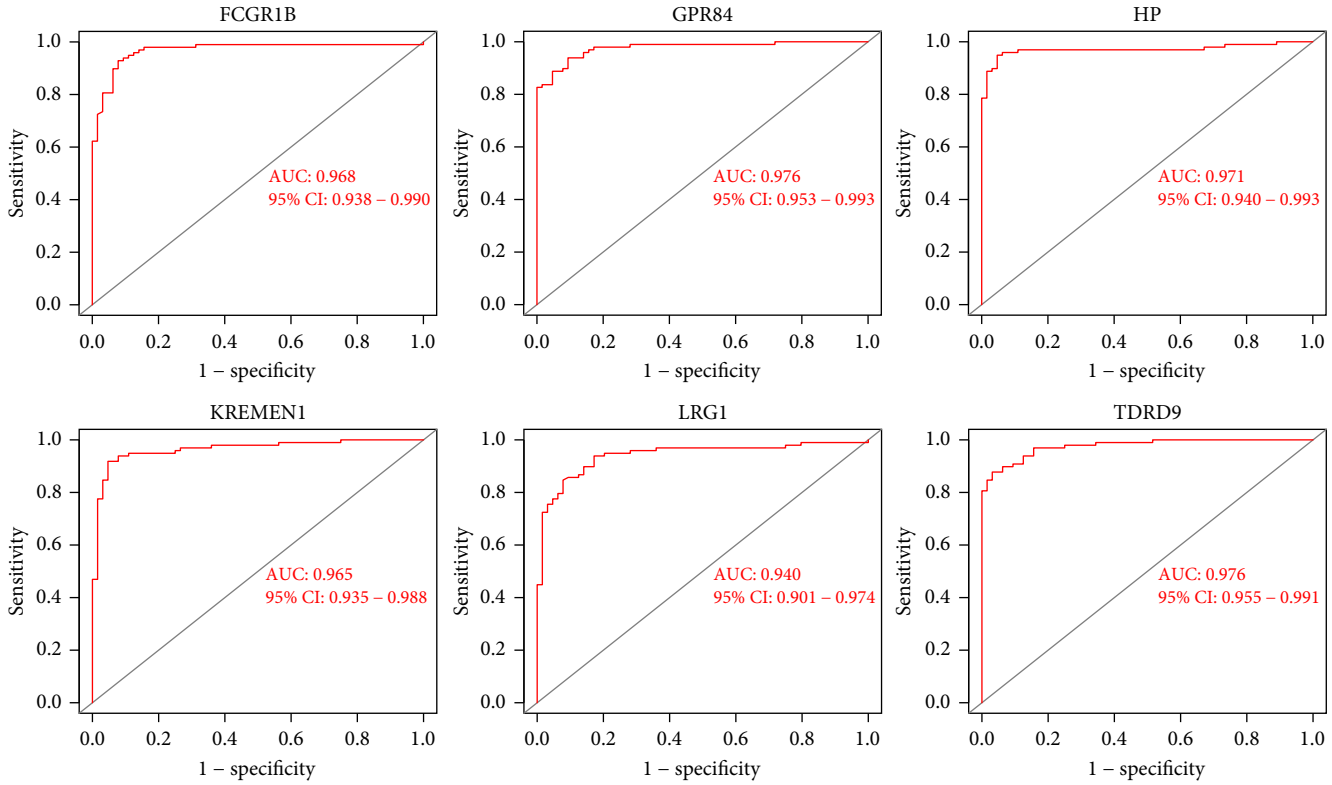

(b)

Figure 7: Validation of hub genes in the diagnostic value: (a) validation of diagnostically relevant hub genes (fusion of GSE18606 and GSE73461). ROC curves and area under the curve (AUC) data were utilized to examine the capability to distinguish KD from healthy controls with high sensitivity and specificity; (b) results from the validation of the hub genes in the test group (GSE68004) were comparable to those obtained in the training group. According to these data, the diagnostic sensitivity of these six hub genes for KD is at the higher end of the spectrum. Abbreviations: AUC, area under the curve; KD, Kawasaki disease; ROC, receiver operating characteristic.

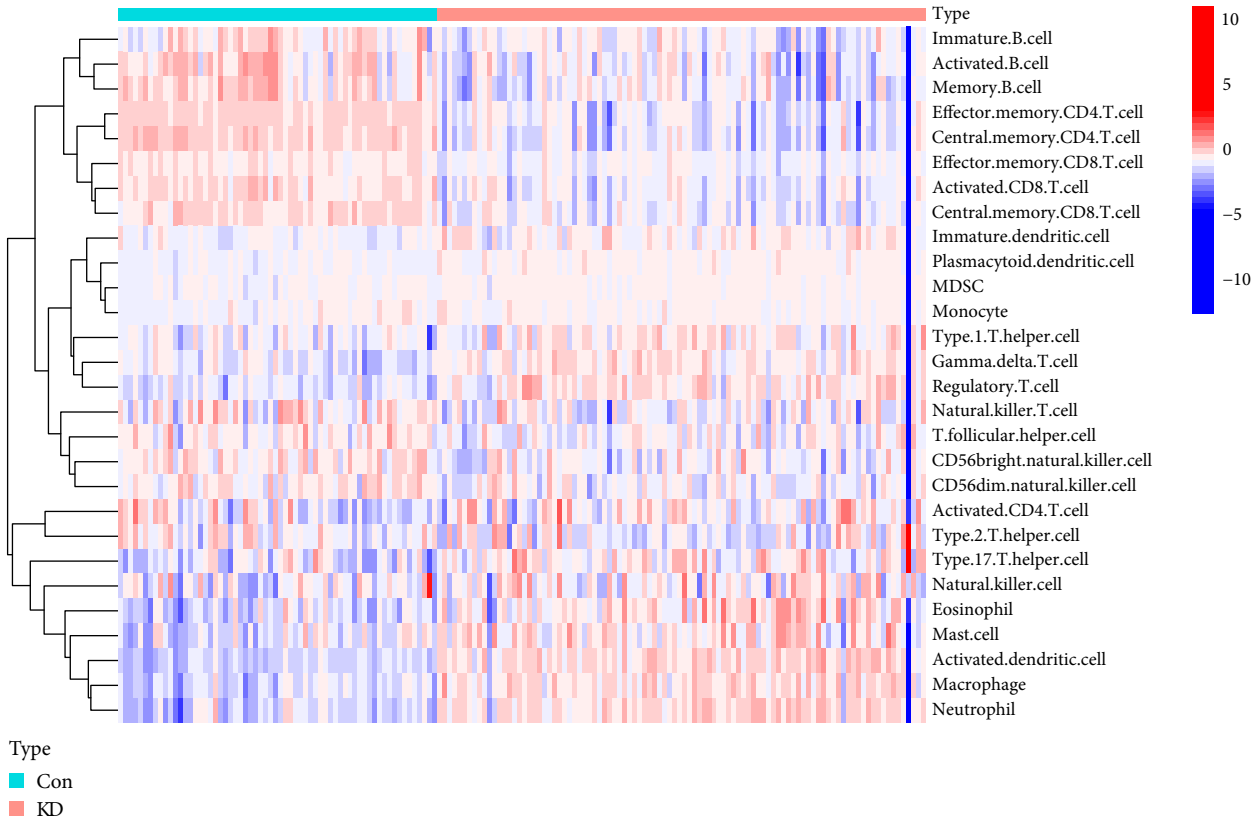

(a)

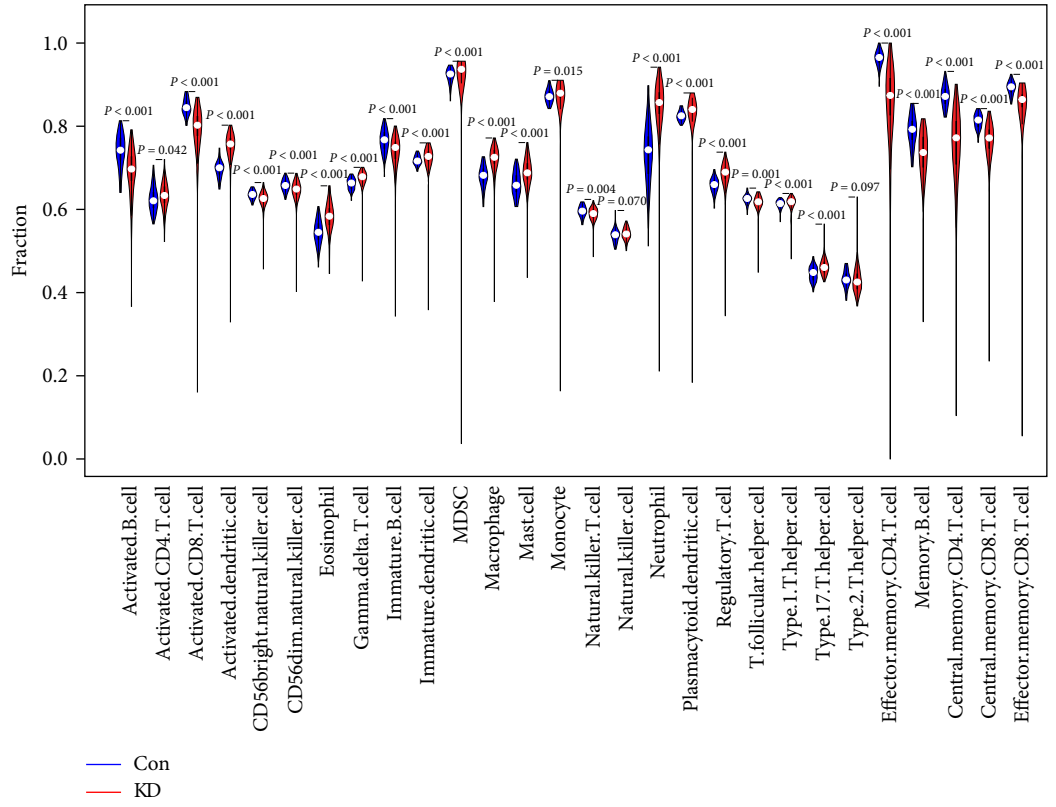

(b)

Figure 8: Continued.

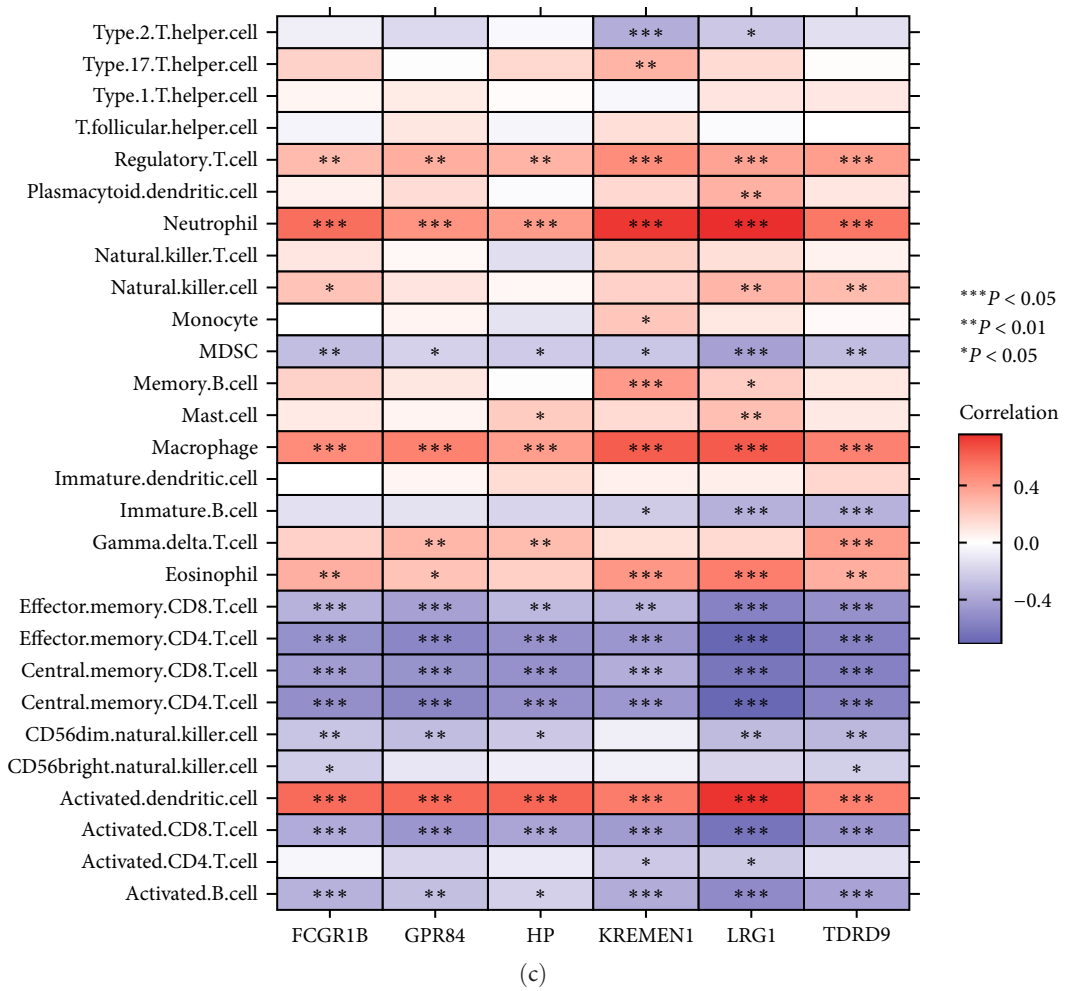

(c)

Figure 8: Examining the immune landscape associated with Kawasaki disease. A heat map (a) and a violin plot (b) graphically representing the distribution of the 28 different immune cells found in healthy control tissues and KD tissues, respectively. (c) the connection between immune cell infiltration and the activity of six hub genes found in the human genome. Abbreviation: KD, Kawasaki disease.

genes were identified through LASSO analysis: *FCGR1B*, *GPR84*, *HP*, *KREMEN1*, *LRG1*, and *TDRD9*. These six key genes were considerably overexpressed in the KD group compared to healthy controls.

FCGR1 is an immunoglobulin G receptor with a high affinity that three gene families encode in humans [28]. One of the subtypes is designated by the acronym *FCGR1B*. *FCGR1B* was upregulated in patients with active tuberculosis and was associated with interferon (IFN)-stimulated gene expression, IL-1 production, and the NOD-like receptor signaling pathway [29]. *GPR84* is expressed by myeloid cells of the innate immune system, including neutrophils, monocytes, and macrophages. This receptor is a G protein-coupled medium-chain fatty acid receptor [30]. *GPR84* has been shown to play a unique role in innate immune cells and intestinal inflammation and is closely related to inflammasome activation [31]. HP is a plasma glycoprotein that binds to free hemoglobin and plays a crucial role in tissue protection and prevention of oxidative damage [32]. *KREMEN1* inhibits *Wnt* signaling [33]. It plays an important part in the control of cell death as well as the development of cancer [34, 35]. *LRG1* is an adipocytokine related to insulin resistance and angiogenesis [36, 37]. *TDRD9* is a member of the Tudor domain-containing protein family, primarily expressed in germ cells and closely related to azoospermia [38, 39]. *FCGR1B*, *GPR84*, *HP*, and *KREMEN1* are four of the six discovered hub genes associated with inflammation and the immune system. While *LRG1* is strongly associated with vascular homeostasis, the biological role of *TDRD9* in inflammation has not been previously identified and deserves further investigation.

These data support the notion that DEGs are associated with immune system reactions and inflammation. In many earlier investigations, KD has also been associated with monocytes, $CD8^+$ T cells, and neutrophil infiltration [4, 5, 40]. This study is the first to use the ssGSEA methodology to investigate the infiltration by 28 different types of immune cells in KD tissues. KD tissue demonstrated considerably more infiltration of activated and effector memory $CD4^+$ T cells, monocytes, neutrophils, and macrophages than healthy tissue. The results highlight that these cells are crucial to the course of KD. In addition, it was demonstrated that neutrophils stimulate DCs, and strong positive correlations were discovered between

Table 1: Top 15 significant immunological signatures enriched by DEGs in GSEA.

Gene set name	NES	*P*-value	NOM p.adjust	FDR *q*-values
GSE22886 NAÏVE BCELL VS. NEUTROPHIL DN	3.221629	1.00E-10	2.93E-09	1.83E-09
GSE6269 HEALTHY VS. STAPH PNEUMO INF PBMC DN	3.19896	1.00E-10	2.93E-09	1.83E-09
GSE7400 CTRL VS. CSF3 IN VIVO TREATED PBMC DN	3.180609	1.00E-10	2.93E-09	1.83E-09
GSE6269 E COLI VS. STREP PNEUMO INF PBMC DN	3.135927	1.00E-10	2.93E-09	1.83E-09
GSE6269 FLU VS. STAPH AUREUS INF PBMC DN	3.102818	1.00E-10	2.93E-09	1.83E-09
GSE22886 NAÏVE TCELL VS. NEUTROPHIL DN	3.097563	1.00E-10	2.93E-09	1.83E-09
GSE4748 CYANOBACTERIUM LPSLIKE VS. LPS AND CYANOBACTERIUM LPSLIKE STIM DC 3 H DN	3.078676	1.00E-10	2.93E-09	1.83E-09
GSE29618 MONOCYTE VS. PDC UP	3.035813	1.00E-10	2.93E-09	1.83E-09
GSE22886 NAÏVE TCELL VS. MONOCYTE DN	3.030273	1.00E-10	2.93E-09	1.83E-09
GSE22886 NAÏVE CD4$^+$ TCELL VS. MONOCYTE DN	3.014044	1.00E-10	2.93E-09	1.83E-09
GSE4984 UNTREATED VS. GALECTIN1 TREATED DC UP	2.999805	1.00E-10	2.93E-09	1.83E-09
GSE29618 MONOCYTE VS. PDC DAY7 FLU VACCINE UP	2.998979	1.00E-10	2.93E-09	1.83E-09
GSE34205 HEALTHY VS. RSV INF INFANT PBMC DN	2.991961	1.00E-10	2.93E-09	1.83E-09
GSE29618 MONOCYTE VS. MDC UP	2.991289	1.00E-10	2.93E-09	1.83E-09
GSE22886 NAÏVE CD8$^+$ TCELL VS. MONOCYTE DN	2.976089	1.00E-10	2.93E-09	1.83E-09

DEGs, differentially expressed genes; GSEA, gene set enrichment analysis; NES, normalized enrichment score; NOM, nominal; FDR, false discovery rate.

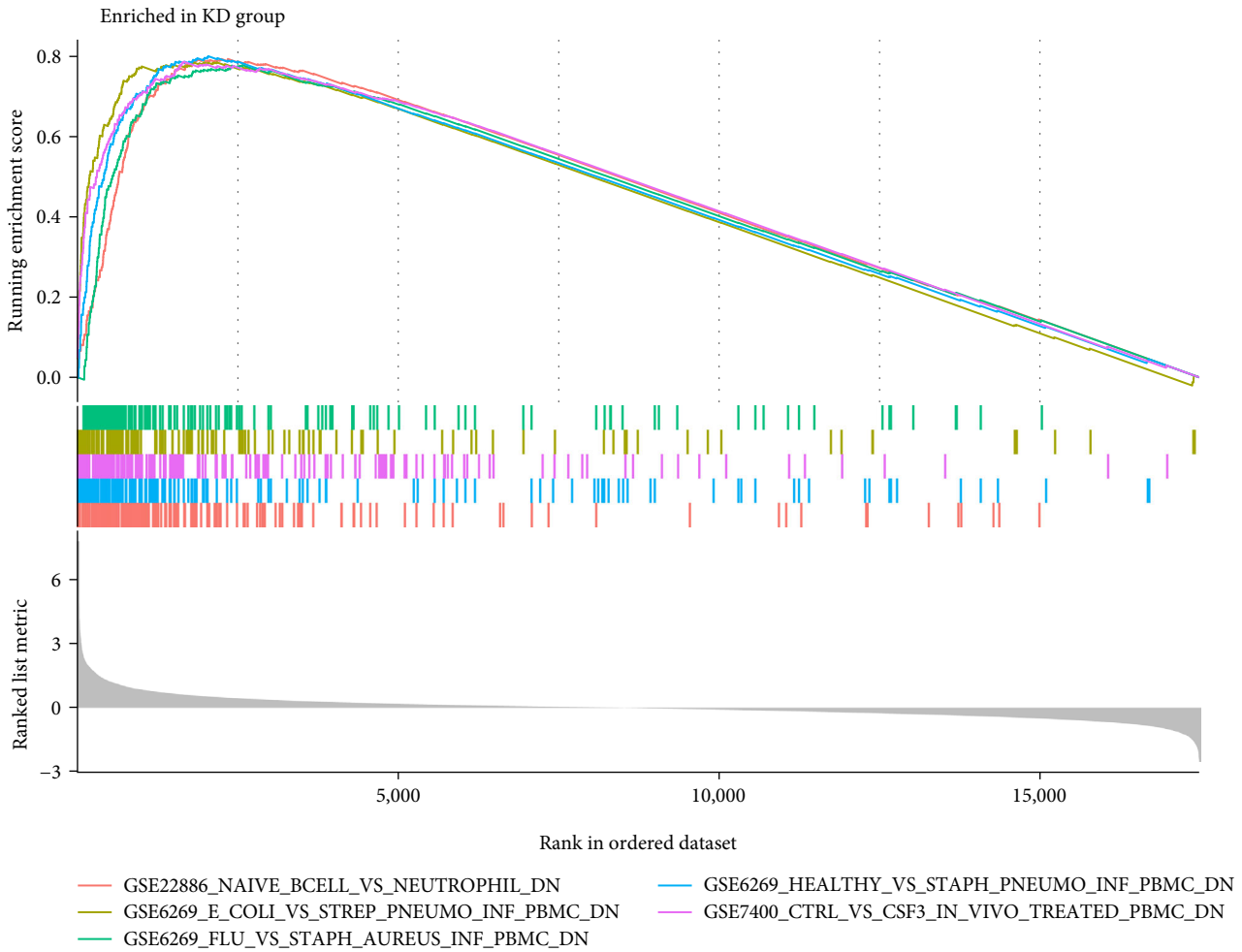

Figure 9: Enhancement diagram for the GSEA immunologic signature database.

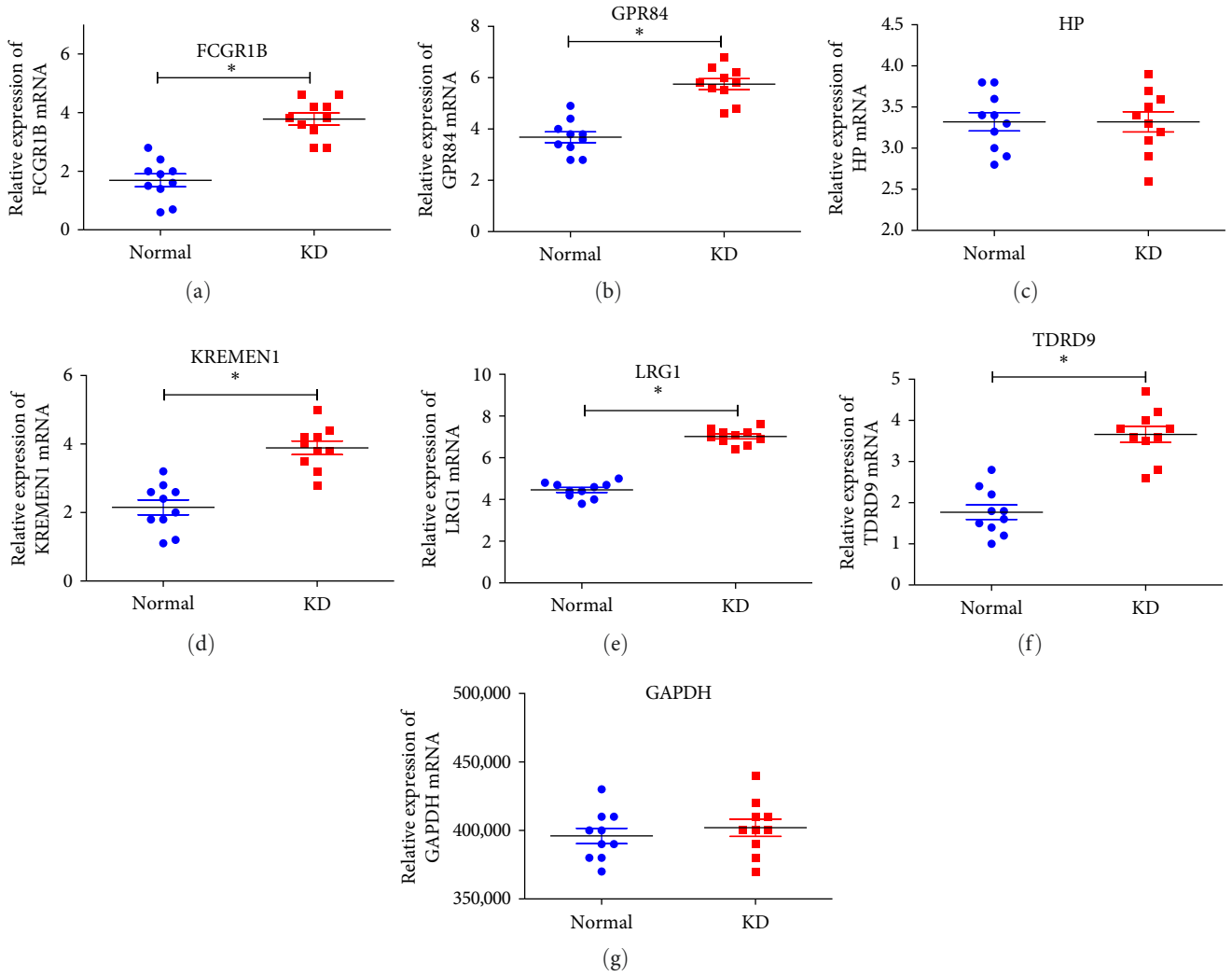

FIGURE 10: RT-qPCR validation of hub genes in KD patients: (a) expression level of *FCGR1B* gene; (b) expression level of *GPR84* gene; (c) expression level of *HP* gene; (d) expression level of *KREMEN1* gene; (e) expression level of *LRG1* gene; (f) expression level of *TDRD9* gene; (g) expression level of *GAPDH* gene. $^*P < 0.001$.

macrophages and the six hub genes. Six central and effector memory $CD4^+$ T cells and central and effector memory $CD8^+$ T cells were found to have an antagonistic interaction. Our results highlight the role of these immune cells and immunological regulatory genes in the development of KD [41, 42]. We utilized the MSigDB database of immunomarker genes as a reference for the GSEA of DEGs. This was done to investigate the likely mechanism by which immune function is maintained during the progression of KD. It was shown that neutrophils and peripheral blood mononuclear cells (PBMCs) have far more significant enrichment in DEGs. According to these studies, neutrophils and PBMCs are responsible for the onset and development of KD.

In this study, we screened for hub genes by analyzing the expression of differential genes in KD patients, and RT-qPCR further verified these results. The validated results indicated that the expression of *FCGR1B* ($P < 0.001$), *GPR84* ($P < 0.001$), *KREMEN1* ($P < 0.001$), *LRG1* ($P < 0.001$), and *TDRD9* ($P < 0.001$) was significantly upregulated in KD patients compared with the control group, while *HP* ($P > 0.05$) was not significantly upregulated in KD patients compared to the normal group (Figure 10). The results suggested that *FCGR1B*, *GPR84*, *KREMEN1*, *LRG1*, and *TDRD9* could be used as hub genes for screening KD. However, whether these hub genes are directly related to coronary artery damage in KD patients need further study.

In summary, using WGCNA and LASSO regression in conjunction with ssGSEA bioinformatic analysis, we found one hub module (blue module) and six hub genes (*FCGR1B*, *GPR84*, *HP*, *KREMEN1*, *LRG1*, and *TDRD9*) that may be associated with the development of KD. Five of the six hub genes (*FCGR1B*, *GPR84*, *KREMEN1*, *LRG1*, and *TDRD9*) were validated. This study gives early information on KD's immune infiltration pattern and immunomodulatory mechanisms. Prospective and large-sample follow-up studies should detect the diagnostic indicators of KD described here with high sensitivity and specificity, minimize misdiagnosis of KD, and serve as a guide for the early diagnosis and successful

pharmacological treatment of KD. The limitations of this study are as follows: first, as the study mainly relied on published RNA microarray datasets for analysis, key clinical data could not be obtained. Second, the mechanism of action of these identified hub genes needs to be further studied.

Abbreviations

KD: Kawasaki disease
WGCNA: Weighted gene coexpression network analysis
GEO: Gene Expression Omnibus
KEGG: Kyoto Encyclopedia of Genes and Genomes
GSEA: Gene set enrichment analysis
ssGSEA: Single sample of GSEA
DEGs: Differentially expressed genes
FCGR1: Fc gamma RI
GPR84: G protein-coupled medium-chain fatty acid receptor
Hp: Haptoglobin
KREMEN1: Kringle-containing transmembrane protein 1
LRG1: Leucine-rich α-2-glycoprotein 1
TDRD9: Tudor domain-containing protein 9
SVM-RFE: Support vector machine recursive feature elimination
LASSO: Least absolute shrinkage and selection operator
AUC: Area under the receiver operating characteristic curve
CALs: Coronary artery lesions
GO: Gene Ontology
MSigDB: Molecular Signatures Database.

Data Availability

This research evaluated public databases. All the source data applied in this research came from the GEO data platform, which is open to the public (https://www.ncbi.nlm.nih.gov/geo/; accession numbers: GSE18606, GSE73461, and GSE68004).

Conflicts of Interest

The authors declare that they have no conflicts of interest.

Authors' Contributions

HJB, YW, and XZ conceived and designed the research. HJB and LLZ managed the data and performed the bioinformatics analyses. The manuscript was rewritten and modified by HJB, LLZ, HMP, XFH, XZ, and YW. The final manuscript was reviewed and approved by all authors. HJB and LLZ have contributed equally to this work and share the first authorship.

Funding

The study was supported by the Guangdong Basic and Applied Basic Research Foundation (2020A1515010184).

Acknowledgments

The authors acknowledge the GEO database for granting them access to the KD data.

Supplementary Materials

Supplementary 1. The primers used for RT-qPCR with their sequence.

Supplementary 2. Weighted gene coexpression network analysis (WGCNA) establishes the effectiveness of the soft threshold. Analysis of the scale-free fit index and the average degree of connection for a range of soft-threshold powers (β). The red line denotes the position of the point when the correlation coefficient equals to 0.85, and the soft-thresholding power equals to 3.

Supplementary 3. Weighted gene coexpression network analysis (WGCNA) establishes the effectiveness of the soft threshold. A histogram depicts the distribution of connections and verification of scale-free topology for $\beta = 3$.

Supplementary 4. Dissolution curve of RT-qPCR experimental genes.

References

[1] T. Kawasaki, "Acute febrile mucocutaneous syndrome with lymphoid involvement with specific desquamation of the fingers and toes in children," *Arerugi = [Allergy]*, vol. 16, no. 3, pp. 178–222, 1967.

[2] U. K. Akca, S. Kesici, Y. Ozsurekci et al., "Kawasaki-like disease in children with COVID-19," *Rheumatology International*, vol. 40, pp. 2105–2115, 2020.

[3] B. W. McCrindle, A. H. Rowley, J. W. Newburger et al., "Diagnosis, treatment, and long-term management of Kawasaki disease: a scientific statement for health professionals from the American Heart Association," *Circulation*, vol. 135, no. 17, pp. e927–e999, 2017.

[4] Z. Geng, Y. Tao, F. Zheng et al., "Altered monocyte subsets in Kawasaki disease revealed by single-cell RNA-sequencing," *Journal of Inflammation Research*, vol. 14, pp. 885–896, 2021.

[5] Z. Wang, L. Xie, G. Ding et al., "Single-cell RNA sequencing of peripheral blood mononuclear cells from acute Kawasaki disease patients," *Nature Communications*, vol. 12, Article ID 5444, 2021.

[6] T. J. Brown, S. E. Crawford, M. L. Cornwall, F. Garcia, S. T. Shulman, and A. H. Rowley, "CD8 *T* lymphocytes and macrophages infiltrate coronary artery aneurysms in acute Kawasaki disease," *The Journal of Infectious Diseases*, vol. 184, no. 7, pp. 940–943, 2001.

[7] A. H. Rowley, C. A. Eckerley, H. M. Jäck, S. T. Shulman, and S. C. Baker, "IgA plasma cells in vascular tissue of patients with Kawasaki syndrome," *The Journal of Immunology*, vol. 159, no. 12, pp. 5946–5955, 1997.

[8] A. H. Rowley, S. T. Shulman, C. A. Mask et al., "IgA plasma cell infiltration of proximal respiratory tract, pancreas, kidney, and coronary artery in acute Kawasaki disease," *The Journal of Infectious Diseases*, vol. 182, no. 4, pp. 1183–1191, 2000.

[9] H. Nie, S. Wang, Q. Wu, D. Xue, and W. Zhou, "Five immune-gene-signatures participate in the development and pathogenesis of Kawasaki disease," *Immunity, Inflammation and Disease*, vol. 9, no. 1, pp. 157–166, 2021.

[10] P. Langfelder and S. Horvath, "WGCNA: an R package for weighted correlation network analysis," *BMC Bioinformatics*, vol. 9, Article ID 559, 2008.

[11] N. Simon, J. H. Friedman, T. Hastie, and R. Tibshirani, "Regularization paths for cox's proportional hazards model via coordinate descent," *Journal of Statistical Software*, vol. 39, no. 5, pp. 1–13, 2011.

[12] J. Duan, C. Soussen, D. Brie, J. Idier, M. Wan, and Y.-P. Wang, "Generalized LASSO with under-determined regularization matrices," *Signal Processing*, vol. 127, pp. 239–246, 2016.

[13] W. Fury, A. H. Tremoulet, V. E. Watson et al., "Transcript abundance patterns in Kawasaki disease patients with intravenous immunoglobulin resistance," *Human Immunology*, vol. 71, no. 9, pp. 865–873, 2010.

[14] V. J. Wright, J. A. Herberg, M. Kaforou et al., "Diagnosis of Kawasaki disease using a minimal whole-blood gene expression signature," *JAMA Pediatrics*, vol. 172, no. 10, Article ID e182293, 2018.

[15] P. Jaggi, A. Mejias, Z. Xu et al., "Whole blood transcriptional profiles as a prognostic tool in complete and incomplete Kawasaki disease," *PLOS ONE*, vol. 13, no. 5, Article ID e0197858, 2018.

[16] M. E. Ritchie, B. Phipson, D. Wu et al., "Limma powers differential expression analyses for RNA-sequencing and microarray studies," *Nucleic Acids Research*, vol. 43, no. 7, Article ID e47, 2015.

[17] S. Davis and P. S. Meltzer, "GEOquery: a bridge between the Gene Expression Omnibus (GEO) and bioconductor," *Bioinformatics*, vol. 23, no. 14, pp. 1846-1847, 2007.

[18] G. Bindea, B. Mlecnik, M. Tosolini et al., "Spatiotemporal dynamics of intratumoral immune cells reveal the immune landscape in human cancer," *Immunity*, vol. 39, no. 4, pp. 782–795, 2013.

[19] T. Wu, E. Hu, S. Xu et al., "Clusterprofiler 4.0: a universal enrichment tool for interpreting omics data," *The Innovation*, vol. 2, no. 3, Article ID 100141, 2021.

[20] Y. Xiao, Y. Yang, Y. Wang, X. Li, and W. Wang, "Five novel genes related to the pathogenesis and progression of pancreatic neuroendocrine tumors by bioinformatics analysis with RT-qPCR verification," *Frontiers in Neuroscience*, vol. 13, Article ID 937, 2019.

[21] M. N. Rivas and M. Arditi, "Kawasaki disease: pathophysiology and insights from mouse models," *Nature Reviews Rheumatology*, vol. 16, pp. 391–405, 2020.

[22] M. D. Hicar, "Antibodies and immunity during Kawasaki disease," *Frontiers in Cardiovascular Medicine*, vol. 7, Article ID 94, 2020.

[23] Z. Xie, Y. Huang, X. Li et al., "Atlas of circulating immune cells in Kawasaki disease," *International Immunopharmacology*, vol. 102, Article ID 108396, 2022.

[24] M. Matsui, Y. Okuma, J. Yamanaka et al., "Kawasaki disease refractory to standard treatments that responds to a combination of pulsed methylprednisolone and plasma exchange: cytokine profiling and literature review," *Cytokine*, vol. 74, no. 2, pp. 339–342, 2015.

[25] A. Jinkawa, M. Shimizu, K. Nishida et al., "Cytokine profile of macrophage activation syndrome associated with Kawasaki disease," *Cytokine*, vol. 119, pp. 52–56, 2019.

[26] M. J. Mason, G. Fan, K. Plath, Q. Zhou, and S. Horvath, "Signed weighted gene co-expression network analysis of transcriptional regulation in murine embryonic stem cells," *BMC Genomics*, vol. 10, Article ID 327, 2009.

[27] J. A. Botía, J. Vandrovcova, P. Forabosco et al., "An additional k-means clustering step improves the biological features of WGCNA gene co-expression networks," *BMC Systems Biology*, vol. 11, Article ID 47, 2017.

[28] D. L. Maresco, E. Chang, K. S. Theil, U. Francke, and C. L. Anderson, "The three genes of the human FCGR1 gene family encoding Fc_YRI flank the centromere of chromosome 1 at 1p12 and 1q21," *Cytogenetic and Genome Research*, vol. 73, no. 3, pp. 157–163, 1996.

[29] S. Natarajan, M. Ranganathan, L. E. Hanna, and S. Tripathy, "Transcriptional profiling and deriving a seven-gene signature that discriminates active and latent tuberculosis: an integrative bioinformatics approach," *Genes*, vol. 13, no. 4, Article ID 616, 2022.

[30] L.-H. Chen, Q. Zhang, X. Xie, and F.-J. Nan, "Modulation of the *G*-protein-coupled receptor 84 (GPR84) by agonists and antagonists," *Journal of Medicinal Chemistry*, vol. 63, no. 24, pp. 15399–15409, 2020.

[31] Q. Zhang, L.-H. Chen, H. Yang et al., "GPR84 signaling promotes intestinal mucosal inflammation via enhancing NLRP3 inflammasome activation in macrophages," *Acta Pharmacologica Sinica*, vol. 43, pp. 2042–2054, 2022.

[32] S. N. Naryzhny and O. K. Legina, "Haptoglobin as a biomarker," *Biomeditsinskaya Khimiya*, vol. 67, no. 2, pp. 105–118, 2021.

[33] M. Osada, E. Ito, H. A. Fermin et al., "The Wnt signaling antagonist Kremen1 is required for development of thymic architecture," *Journal of Immunology Research*, vol. 13, Article ID 602150, 21 pages, 2006.

[34] Y. Gu, J. Cao, X. Zhang et al., "Receptome profiling identifies KREMEN1 and ASGR1 as alternative functional receptors of SARS-CoV-2," *Cell Research*, vol. 32, pp. 24–37, 2022.

[35] F. Causeret, I. Sumia, and A. Pierani, "Kremen1 and Dickkopf1 control cell survival in a Wnt-independent manner," *Cell Death & Differentiation*, vol. 23, pp. 323–332, 2016.

[36] S. He, J. Ryu, J. Liu et al., "LRG1 is an adipokine that mediates obesity-induced hepatosteatosis and insulin resistance," *The Journal of Clinical Investigation*, vol. 131, no. 24, Article ID e148545, 2021.

[37] Q. Hong, L. Zhang, J. Fu et al., "LRG1 promotes diabetic kidney disease progression by enhancing TGF-β-induced angiogenesis," *Journal of the American Society of Nephrology*, vol. 30, no. 4, pp. 546–562, 2019.

[38] M. Shoji, T. Tanaka, M. Hosokawa et al., "The TDRD9-MIWI2 complex is essential for piRNA-mediated retrotransposon silencing in the mouse male germline," *Developmental Cell*, vol. 17, no. 6, pp. 775–787, 2009.

[39] E. Babakhanzadeh, A. Khodadadian, S. Rostami et al., "Testicular expression of *TDRD1*, *TDRD5*, *TDRD9* and *TDRD12* in azoospermia," *BMC Medical Genetics*, vol. 21, Article ID 33, 2020.

[40] C. Zhang, X. Zhang, J. Shen, X. Lu, J. Zhang, and S. Chen, "Changes in peripheral blood neutrophils, lymphocytes and IL-10 in children with Kawasaki disease from different age groups undergoing intravenous immunoglobulin: a retrospective study," *Mediators of Inflammation*, vol. 2020, Article ID 5213451, 9 pages, 2020.

[41] Y. P. Zhu, I. Shamie, J. C. Lee et al., "Immune response to intravenous immunoglobulin in patients with Kawasaki disease and MIS-C," *The Journal of Clinical Investigation*, vol. 131, no. 20, Article ID e147076, 2021.

[42] J. C. Burns, L. E. Hsieh, J. Kumar et al., "Characterization of circulating immune cells in acute Kawasaki disease suggests exposure to different antigens," *Clinical and Experimental Immunology*, vol. 202, no. 3, pp. 263–272, 2020.

Hindawi
Journal of Immunology Research
Volume 2023, Article ID 4319551, 19 pages
https://doi.org/10.1155/2023/4319551

Research Article

The Efficacy and Mechanism of Qinghua Jianpi Recipe in Inhibiting Canceration of Colorectal Adenoma Based on Inflammatory Cancer Transformation

Ting Liu[1], **Juping You**[1], **Qingjian Gao**[1], **Yufeng Zhang**[1], **Wei Xu**[1], **Desong Kong**[2], **Li Chen**[3], **Bao Yuan**[1], **and Haibing Hua**[1]

[1]*Department of Gastroenterology, Jiangyin Hospital of Traditional Chinese Medicine, Jiangyin Hospital Affiliated to Nanjing University of Chinese Medicine, Jiangyin, 214400 Jiangsu Province, China*
[2]*Chinese Medicine Modernization and Big Data Research Center, Nanjing Hospital of Chinese Medicine Affiliated to Nanjing University of Chinese Medicine, Nanjing University of Chinese Medicine, Nanjing, 210022 Jiangsu Province, China*
[3]*Department of Pharmacology, School of Pharmacy, Nanjing University of Chinese Medicine, Nanjing, 210023 Jiangsu Province, China*

Correspondence should be addressed to Bao Yuan; doctoryuan1985@gmail.com and Haibing Hua; jyzy3288@163.com

Received 16 July 2022; Revised 6 October 2022; Accepted 12 October 2022; Published 15 February 2023

Academic Editor: Xiaojiaoyang Li

Objective. This study is aimed at exploring the effect of Qinghua Jianpi Recipe on preventing colon polyp recurrence and inhibiting the progress of "inflammatory cancer transformation." And another goal is to explore the changes of intestinal flora structure and intestinal inflammatory (immune) microenvironment of mice with colon polyps treated by Qinghua Jianpi Recipe and to clarify its mechanism. *Methods*. Clinical trials were conducted to confirm the therapeutic effect of Qinghua Jianpi Recipe on patients with inflammatory bowel disease. The inhibitory effect of Qinghua Jianpi Recipe on "inflammatory cancer transformation" of colon cancer was confirmed by an adenoma canceration mouse model. Histopathological examination was used to evaluate the effects of Qinghua Jianpi Recipe on intestinal inflammatory state, adenoma number, and pathological changes of adenoma model mice. The changes of inflammatory indexes in intestinal tissue were tested by ELISA. Intestinal flora was detected by 16S rRNA high-throughput sequencing. Short-chain fatty acid metabolism in the intestine was analyzed by targeted metabolomics. Network pharmacology analysis of possible mechanism of Qinghua Jianpi Recipe on colorectal cancer was performed. Western blot was used to detect the protein expression of the related signaling pathways. *Results*. Qinghua Jianpi Recipe can significantly improve intestinal inflammation status and function in patients with inflammatory bowel disease. Qinghua Jianpi Recipe could significantly improve the intestinal inflammatory activity and pathological damage of adenoma model mice and reduce the number of adenoma. Qinghua Jianpi Recipe significantly increased the levels of Peptostreptococcales_Tissierellales, NK4A214_group, Romboutsia, and other intestinal flora after intervention. Meanwhile, the treatment group of Qinghua Jianpi Recipe could reverse the changes of short-chain fatty acids. Network pharmacology analysis and experimental studies showed that Qinghua Jianpi Recipe inhibited the "inflammatory cancer transformation" of colon cancer by regulating intestinal barrier function-related proteins, inflammatory and immune-related signaling pathways, and free fatty acid receptor 2 (FFAR2). *Conclusion*. Qinghua Jianpi Recipe can improve the intestinal inflammatory activity and pathological damage of patient and adenoma cancer model mice. And its mechanism is related to the regulation of intestinal flora structure and abundance, short-chain fatty acid metabolism, intestinal barrier function, and inflammatory pathways.

1. Introduction

Colorectal cancer (CRC) is a malignant tumor originating in the colorectal mucosal epithelium. And it is one of the common malignant tumors in clinic. It is the third most common malignancy in the world. There are more than one million new cases of CRC in the world every year, and the number of deaths caused by CRC is as high as 500,000 [1, 2]. With the improvement of Chinese people's living standard, the change of life style, and diet structure, the incidence of CRC is increasing year by year, which seriously harms human health. Inflammatory bowel diseases (IBD) such as ulcerative colitis (UC) are considered major risk factors for CRC, and the degree of colon injury, lesion extent, duration, and activity of intestinal inflammation are closely related to prognosis and outcome [3, 4]. Studies have found that there is a certain correlation between the progression of UC to CRC and the lesion site. Compared with normal people, the risk of tumor development in total colitis, left colitis, and proctitis is 14.8, 2.8, and 1.7 times, respectively. Current studies suggest that IBD is related to genetic, environmental, immune, intestinal flora, and psychological factors, among which the role of intestinal flora in the occurrence and development of IBD cannot be ignored [5–7]. There is a very complex relationship between intestinal dysbiosis and IBD. The dysbiosis of intestinal flora may be the inducing factor of IBD, and IBD may aggravate the dysbiosis of intestinal flora, but the mechanism of interaction is still not very clear [8]. There is evidence that certain medications for UC may reduce the risk of CRC, while the risk of stationary disease is lower than that of chronic active disease. Therefore, it is of great value to seek therapeutic methods that can control intestinal inflammation, promote intestinal mucosal repair, and maintain intestinal homeostasis for the prevention and treatment of "inflammatory cancer transformation" of CRC.

There is no disease name of colonic polyps in traditional Chinese medicine (TCM) literature, but related clinical symptoms are described, such as diarrhea, hematochezia, and enterogastritis. Studies have shown that abnormal intestinal immune response is an important link in the occurrence and development of IBD and CRC, as well as one of the inducing factors for the persistence and recurrence of intestinal inflammation [5]. In patients with active UC or CRC, one of the most important changes of intestinal immune barrier dysfunction is the abnormal increase of inflammatory factors and the excessive activation of mucosal lamina propria immune system, especially the destruction of intestinal mucosal immune barrier by proinflammatory factors such as TNF-α, INF-γ, IL-13, IL-6, and IL-10, which leads to the increase of intestinal mucosal permeability [7, 8]. It is extremely important in the pathophysiology of CRC. A large number of studies have found that some effective components of TCM can significantly inhibit the expression of inflammatory factors in the intestinal mucosa of UC or CRC animal models or patients and reduce the intestinal inflammatory response, so as to promote the balance of intestinal mucosal immune regulation and improve the intestinal barrier function [9, 10]. Common therapeutic recipes include Shenling Baizhu powder, Lizhong decoction, Wumei pill, Sishen pill, and Pingwei powder [11]. According to the TCM, treatment based on syndrome differentiation can regulate the internal environment of the patient, enhance the immune function of the body, and adjust the anticancer ability of the body from a macro perspective. However, the adverse reactions of TCM are mild, because Chinese medicine is taken from natural animals, plants, and minerals.

Qinghua Jianpi Recipe is composed of Dangshen (Codonopsis pilosula (Franch.) Nannf), Huangqin (Scutellaria baicalensis Georgi), Baizhu (Atractylodes macrocephala Koidz), Fuling (Wolfiporia cocos (F.A. Wolf) Ryvarden & Gilb), Huangqi (Astragalus membranaceus (Fisch.) Bunge), Yiyiren (Semen Coicis), Wumei (Fructus Mume), Fangfeng (Saposhnikovia divaricata (Turcz.) Schischk), Chenpi (Citrus reticulata Blanco), Niuxi (Achyranthes bidentata Blume), and Gancao (Glycyrrhiza uralensis Fisch). It is a recipe created by Professor Zhu Bingyi, a famous Chinese doctor of TCM, for preventing recurrence after colon polyp removal. It is suitable for the pathogenesis of colorectal polyp and has achieved good clinical effect in clinical use. However, its therapeutic mechanism needs to be further clarified to provide a scientific basis for clinical medication and lay a theoretical foundation for the development of new drugs for the prevention and treatment of postoperative recurrence of colon polyps in colon cancer.

Therefore, based on the above points, this study is aimed at exploring the effect of Qinghua Jianpi Recipe on blocking the process of "inflammation-cancer transformation" and preventing the recurrence of colorectal polyps and CRC. And whether the above effects are caused by Qinghua Jianpi Recipe through regulating intestinal flora and improving intestinal the inflammatory (immune) microenvironment. Moreover, the effects of Qinghua Jianpi Recipe on s intestinal immune microenvironment and inflammatory process and the role of intestinal flora in the pathogenesis of colon polyps were systematically observed in the study.

2. Materials and Methods

2.1. Clinical Trial Scheme. All clinic participants in this study were screened and collected from the Department of Gastroenterology and Colorectal Surgery of Jiangyin Hospital of Chinese Medicine Affiliated to Nanjing University of Chinese Medicine from January 2021 to August 2022. Participants were diagnosed with ulcerative colitis (active stage) and randomly divided into 2 groups according to the order of treatment. There were 30 cases in the therapeutic group and 30 cases in the control group, including 35 male patients and 25 female patients. The study was approved by the Ethics Committee of Jiangyin Hospital of Chinese Medicine Affiliated to Nanjing University of Chinese Medicine (Approval No. 2020102) and carried out under the supervision and guidance of the committee. In the therapeutic group, Qinghua Jianpi Recipe granule was taken with warm water, one dose a day, three times a day. The Chinese medicine granule was dissolved in 300 mL boiling water after each meal, and the medicine was taken after the water temperature was moderate. Two weeks was the course of

Table 1: The modified Mayo index.

Project	The score			
	0 points	1 points	2 points	3 points
Diarrhea	Normal	Over the normal period for 1 to 2 times/d	Over the normal period for 3 to 4 times/d	More than normal 5 times/d or more
Hematochezia	No bleeding	Less than half of the time for the blood mixed in the excrement	Most of the time for the blood mixed in the excrement	There has always been the blood mixed in the excrement
Endoscopic detection	Normal or no active lesions occurred	Mild lesions (reduced vascular texture of colon mucosa, visible mild erosion)	Moderate lesions (moderate mucosal erosion)	Severe lesions (spontaneous bleeding, scattered dotted ulcers)
The physician evaluation	Normal	Mild lesions	Moderate lesion	Severe lesions

During the quantification of the score, each subject was compared with himself to judge the grade of stool frequency. The hematochezia score represents the most severe hematochezia in one day. The overall evaluation included three criteria: the subjects' feeling of abdominal discomfort, the degree of impact of the disease on their life and work, and other manifestations.

treatment, and two courses of treatment were taken continuously. The control group was given mesalazine enteric-coated tablet 1.0 g alone, three times a day, for 30 days. During the treatment, the enrolled patients did not use intestinal probiotics, prebiotics, broad-spectrum antibiotics, and other drugs, and other nutritional support treatment plans were consistent between the two groups. All participants were tested for the following indicators before and after treatment:

IBD activity was graded and converted to a quantitative score (2 endoscopist scores) according to the degree of grading by Baron endoscopic review: 0: grade 0, normal mucosa; 1: grade I, mucosal congestion and blurred blood vessels; 2 points: grade II, mucosal contact bleeding; 3: grade III, spontaneous hemorrhage of mucosa; and 4 points: grade IV. Ulcers of varying sizes were seen in the mucosa.

The standard modified Mayo index was used to rate the disease activity index. The score directly reflects the severity grade of the disease and the microscopic inflammatory activity grade for clinical treatment (Table 1).

Clinical efficacy was evaluated with the modified rating scale. Clinical efficacy: A decrease of ≥ 30% or ≥3 from baseline in the total Mayo score, accompanied with a decrease of ≥1 in the hematostoecium subscore or an absolute hematostoecium subscore of 0 or 1. Clinical remission: The total Mayo score ≤ 2 and no single item subscore > 1. Endoscopic response: Mayo score endoscopic subscore decreased by at least 1 from baseline. Mucosal healing: the absolute Mayo score of 0 or 1 on the endoscopic subscore.

2.2. Animal Grouping, Feeding, and Sampling. All animal experiments were performed according to the guidelines of Animal Experimentation at Nanjing University of Chinese Medicine (Nanjing, China). The research has been reviewed by the Ethics Committee of Animal Experiments at Nanjing University of Chinese Medicine (Approval No. 202111A041). All animals were kept in a pathogen-free environment and fed ad lib. The procedures for the care and use of animals were approved by the Ethics Committee, and all applicable institutional and governmental regulations concerning the ethical use of animals were followed.

According to the literature and previous experimental results, five cycles of AOM combined with DSS were selected to establish the mouse adenoma canceration model. Except for the blank group, all mice were intraperitoneally injected with AOM at a dose of 10 mg/kg on the first day. After a week's rest, they were given drinking water containing 2% DSS for 5 days and then, it was changed to ordinary drinking water for 14 days as a cycle. The experiment was completed at the 15th week. Based on the reported time point at which the adenoma appeared in this model mouse, three mice were randomly selected from the fifth week to be put to execution every week (except the blank group). At the time point of adenoma appearance, different concentrations of Qinghua Jianpi Recipe were given through intragastric administration. Sixty C57BL/6 mice were randomly divided into 4 groups: blank group, model group (AOM/DSS), Qinghua Jianpi Recipe low-dose group ($15.6\,g{\cdot}kg^{-1}$), and Qinghua Jianpi Recipe high-dose group ($31.2\,g{\cdot}kg^{-1}$).

After 16 weeks of feeding, blood was taken from the eyeballs, and the animals were sacrificed by neck removal. Tissue samples of the liver, spleen, colon, and intestinal contents were collected. The colon tissue was longitudinally cut to collect intestinal contents and then flattened to count the number of adenomas.

2.3. Intestinal Histopathology and Collagen Deposition Examination. Intestinal tissues were sampled in a fume cupboard. Tissue samples with appropriate target location and size were carefully separated with sampling instruments and fixed with 10% formalin solution. After fixation and washing, the specimen was dehydrated, which was completed by an automatic dehydrator. Paraffin is immersed in the tissue, and the wax-soaked tissue is placed in melted solid paraffin, which is solidified to form tissue wax blocks. Then, the paraffin slicer was used to cut the wax block into slices about 4 μm thick. Use ophthalmic tweezers to gently spread the wax tape on the slide to fix the tissue, and put the slide into the slide baking machine at 60°C for 15-30 minutes to remove the paraffin wax that dissolved the tissue space. The slides were taken out, and the tissue sections were stained with hematoxylin-eosin (HE). And the pathological

changes of intestinal tissues were observed under the microscope. The statistical analysis was performed using the analysis software ImageJ.

2.4. General Situation Assessment and Disease Activity Index (DAI) Scores. After administration, hair luster, mental activity, body weight change, food intake and water intake, stool characteristics, whether there is blood in the stool, and the degree of blood in the stool were observed and recorded at the same time every day (if there is no visible blood in stool, fecal occult blood test kit was used to determine whether there is blood in the stool). After weighing the body weight of mice at a regular time every day, the rate of change in body weight was calculated, and the changes in fecal traits, occult blood, and hematochezia of mice were comprehensively observed by naked eye. The DAI score of rats in each group was calculated according to the computational formula, DAI = (weight loss fraction + stool trait fraction + hematochezia fraction)/3, to evaluating the changes of inflammatory activity in mice.

2.5. ELISA Detection. MPO levels in intestinal tissue and IL-1β, IL-6, IL-18, and TNF-α levels in serum were detected by ELISA. After balancing at room temperature for 20 min, take out the lath, set the standard well and sample well, and add standard 50 μL of different concentrations to the standard well. Add sample 10 μL to the test sample well; then, add sample dilution 40 μL; do not add to the blank well. In addition to the blank well, add 100 μL horseradish peroxidase-labeled detection antibody to each well of standard and sample wells, seal the reaction well with seal plate membrane, and incubate at 37°C for 60 min. Discard liquid, dry with washing solution, add washing solution to each well, rest for 1 min, swing the washing solution, dry with washing solution, and repeat washing plate 5 times. Add substrates A and B 50 μL to each well, and incubate at 37°C for 15 min away from light. Add the stop solution 50 μL to each well, and measure the OD value of each well at 450 nm wavelength within 15 min.

2.6. High-Throughput Sequencing of 16S rRNA in Mouse Feces. E.Z.N.A.® Soil DNA Kit was used to extract microbial DNA from feces samples of mice. The specific steps were in accordance with the instructions. Primers for v4-V5 region of the 16S rRNA gene were used in this study. The upstream primers were 515F 5′-GTGCCAGCMGCCGCGG-3′, and the downstream primers were 907R 5′-CCGTCAattCMTTTRAGTTT-3′. PCR reaction system contains 5× FastPfu Buffer 4 μL, (2.5 mM) dNTPs 2 μL, (5 μM) upstream and downstream primers 0.8 μL, FastPfu Polymerase 0.4 μL, DNA template 10 ng, and ddH_2O to the total volume of 20 μL. After the PCR reaction system was fully mixed, the amplification was carried out by the machine after heating up and the reaction procedure was as follows: predenaturation at 95°C for 2 min, denaturation at 95°C for 30 s, annealing at 55°C for 30 s, extension at 72°C for 30 s, cycle 25 times, and extension at 72°C for 10 min. All PCR products were detected by 2% agarose Gel electrophoresis and recovered and purified by AxyPrep DNA Gel Extraction Kit according to the instructions.

The purified PCR products were quantified using Qubit®3.0, and Illumina genomic DNA library was constructed based on Illumina genomic DNA library preparation program. The amplicon library was paired and sequenced on Illumina MiSeq platform according to the standard protocol (2 × 250).

2.7. Targeted Metabolomics Analysis of Short-Chain Fatty Acids. 20 mg of feces samples was taken from each group; 120 μL methanol was added, homogenized for 1 min, and centrifuged at 4°C for 14000 r/min for 10 min; 100 μL was absorbed. The supernatant is extracted for 14000 r/min for 10 min at 4°C; 50 μL supernatant was absorbed to prepare a liquid injection flask for UPLC-QTOF-MS analysis. For quality control sample (QC), weigh 10 mg of each stool sample and use it as QC sample after treatment in accordance with the above method. Before analysis, continuous sample injection 3 times is performed to ensure good stability of the instrument, and QC sample injection after every 8-needle sample during analysis. GC-MS instrument (2030/TQ-8040NX), Agilent DB-Wax capillary column (30 m × 0.25 mm, 0.5 μm), was used for detection and analysis. The heating procedure is as follows: the initial temperature was 80°C and maintained for 2 min; then, the temperature was raised to 180°C at 10°C/min and maintained for 3 min; then, the temperature was raised to 230°C at 40°C/min and maintained for 2 min; injection temperature 230°C; split ratio 5 : 1; injection volume: 1 μL; carrier gas: high purity helium (He); flow rate: 1 ml/min; electron bombardment source (EI); interface temperature: 240°C; ion source temperature: 230°C; select the ion monitoring (MRM) mode. For data processing and analysis, MarkView 1.3.1 software was used to preprocess the original data, such as peak identification, alignment, noise filtering, and peak area normalization, to obtain the data matrix file containing information, such as metabolite retention time, mass-to-charge ratio, and intensity. It was imported into SIMCA-P 14.0 software for principal component analysis (PCA) and orthogonal partial least squares discriminant analysis (OPLS-DA). Variables that meet variable importance projection value (VIP) > 1.0 and $P < 0.05$ is considered a differential variable. HMDB (http://www.hmdb.ca/) and KEGG (http://www.kegg.ca/) were used to identify the difference variables, and the error margin was set as 0.1 Da. MetaboAnalyst 5.0 database (http://www.metaboanalyst.ca/) was used for analysis of metabolic pathways. And if impact value which is greater than 0.10, metabolic pathway is considered to be a potential target path.

2.8. Network Pharmacology Analysis. Compound chemical composition and drug targets were collected and predicted. Dangshen (Codonopsis pilosula (Franch.) Nannf), Huangqin (Scutellaria baicalensis Georgi), Baizhu (Atractylodes macrocephala Koidz), Fuling (Wolfiporia cocos (F.A. Wolf) Ryvarden & Gilb), Huangqi (Astragalus membranaceus (Fisch.) Bunge), Yiyiren (Semen Coicis), Wumei (Fructus Mume), Fangfeng (Saposhnikovia divaricata (Turcz.)

Schischk), Chenpi (Citrus reticulata Blanco), Niuxi (Achyranthes bidentata Blume), and Gancao (Glycyrrhiza uralensis Fisch) were inputted to the TCMSP database (https://old.tcmsp-e.com/tcmsp.php), to collect all compounds [12]. Then, according to the pharmacokinetic principle, the suitable compounds are screened based on oral bioavailability (OB) $\geq 30\%$ and drug-like index (DL) ≥ 0.18. Drug target data were obtained from DrugBank (https://go.drugbank.com/) and standardized using the UniProt (https://www.Uniprot.org/) database [13]. Based on GeneCards (https://www.genecards.org/) and OMIM-NCBI databases (https://www.ncbi.nlm.nih.gov/omim), IBD as keyword was used to screen disease targets, while for species selection "Homosapiens" was used. Draw Venn Diagrams tool in R software is used to process drug targets and disease targets obtained in the above steps to obtain the intersection gene targets and output Venn Diagram for display.

PPI network interaction analysis was performed on the active chemical components and core targets of Qinghua Jianpi Recipe by using the STRING database and Cytoscape3.7.1 software. According to the requirements of Cytoscape, the "source-target" data table was constructed, and the NetworkAnalyzer plug-in was used to construct the regulation network of TCM, active component, and target. In the generated regulation network, nodes represent the interaction between TCM, active component, and target, and edges represent the interaction between active the component and target disease. Furthermore, MCC algorithm of CytoHubba plug-in was used to calculate and construct PPI network of each target. Based on Bioconductor (https://www.bioconductor.org/) in the R package (https://www.r-project.org/) and clusterProfiler 3.12.0 to GO (gene ontology) core target function and KEGG pathway enrichment analysis (KEGG pathway analysis), Homo sapiens was selected and a threshold $P < 0.05$ was set. According to the results, the core target-critical pathway network was conducted in Cytoscape 3.7.1 software.

2.9. Western Blot Analysis. After tissue sample fragmentation, precooled RIPA lysate was added; then, PMSF and phosphatase inhibitors were immediately added, incubated on ice for 30 minutes, then transferred into a tube, and centrifuged at 4°C, 15 000 $r \cdot min^{-1}$ for 15 minutes; and supernatant was obtained as the cell lysate. The protein concentration was determined by the BCA method. Electrophoresis buffer was added and incubated in boiling water for 10 minutes. Proteins (50 g per sample) were resolved on SDS-PAGE gel at 100 V and transferred to a blotting membrane for 1.5 h, using skim milk powder as a blocking agent. Then, the membranes were incubated with the first antibody. Membranes were washed, and then, the secondary antibody was incubated and the chemiluminescent agent ECL was used for visualization.

2.10. Statistical Methods. The experimental data were processed by SPASS 23.0, and the parameter values were expressed as mean + standard deviation, ANOVA, and T-test were used to compare the differences between groups, and the comparison between groups was analyzed by one-way ANOVA. $P < 0.05$ means the difference is statistically significant.

3. Results

3.1. Qinghua Jianpi Recipe Has a Significant Clinical Effect on Ulcerative Colitis. A total of 60 patients with UC were included, including 35 males and 25 females. Patients were randomly divided into 2 groups according to the order of visit. There were 30 cases in the therapeutic group and 30 cases in the control group. Pearson's chi-square test showed that there was no significant difference in age composition between the two groups, so the influence of gender could be excluded (Figure 1(a)). Among the 60 patients with UC, the age distribution was between 18 and 55 years old. The rank-sum test was used to analyze the age of the two groups, and the results were not statistically significant. Therefore, the influence of age factor was excluded, and the two groups could be compared (Figure 1(b)). In the therapeutic group, the shortest disease duration was 3 months and the longest disease duration was 41 months. The rank-sum test was also applied to rank variables of the two groups to exclude the influence of disease duration factors, indicating that the two groups could be compared (Figure 1(c)).

Paired sample t-test was used for pairwise comparison of individual items and overall mean scores before and after treatment in the two groups, and P values were much less than 0.05, indicating significant statistical differences. The results showed that the Qinghua Jianpi Recipe therapeutic group and mesalazine treatment control group were effective in treating the clinical manifestations of UC patients in terms of diarrhea, hematochezia, endoscopic manifestations (including Baron endoscopic grading score), physician evaluation, and activity index (Figures 1(d) and 1(e)). There was no significant difference in clinical efficacy, endoscopic response rate, and mucosal healing rate between the two groups after treatment ($P > 0.05$). There is no significant difference in the clinical effective rate, clinical remission rate, endoscopic response rate, and mucosal healing rate between the therapeutic group and the control group (Figure 1(f)). It indicates that the Qinghua Jianpi Recipe treatment group has achieved the same effect as the mesalazine treatment group in the single disease evaluation index.

No special discomfort or other serious adverse reactions were reported in the two groups. After 8 weeks of treatment, the electrocardiogram and liver and kidney function of all patients were reviewed and compared, and no obvious abnormalities were found, indicating that the Qinghua Jianpi Recipe group and mesalazine have greater safety in the treatment of ulcerative colitis patients.

3.2. Effect of Qinghua Jianpi Recipe on the Changes of Signs of Colorectal Adenoma Model Mice. Before the experiment, mice in each group had normal development, bright hair color, good spirit, active activity, normal feeding, and granular stool. During the first DSS cycle, the general situation of blank group is normal activity. But mice activity of other groups decreased, a series of reactions occuring simultaneously including deformed feces, looking glazed, food intake reduction. However, change of ordinary drinking

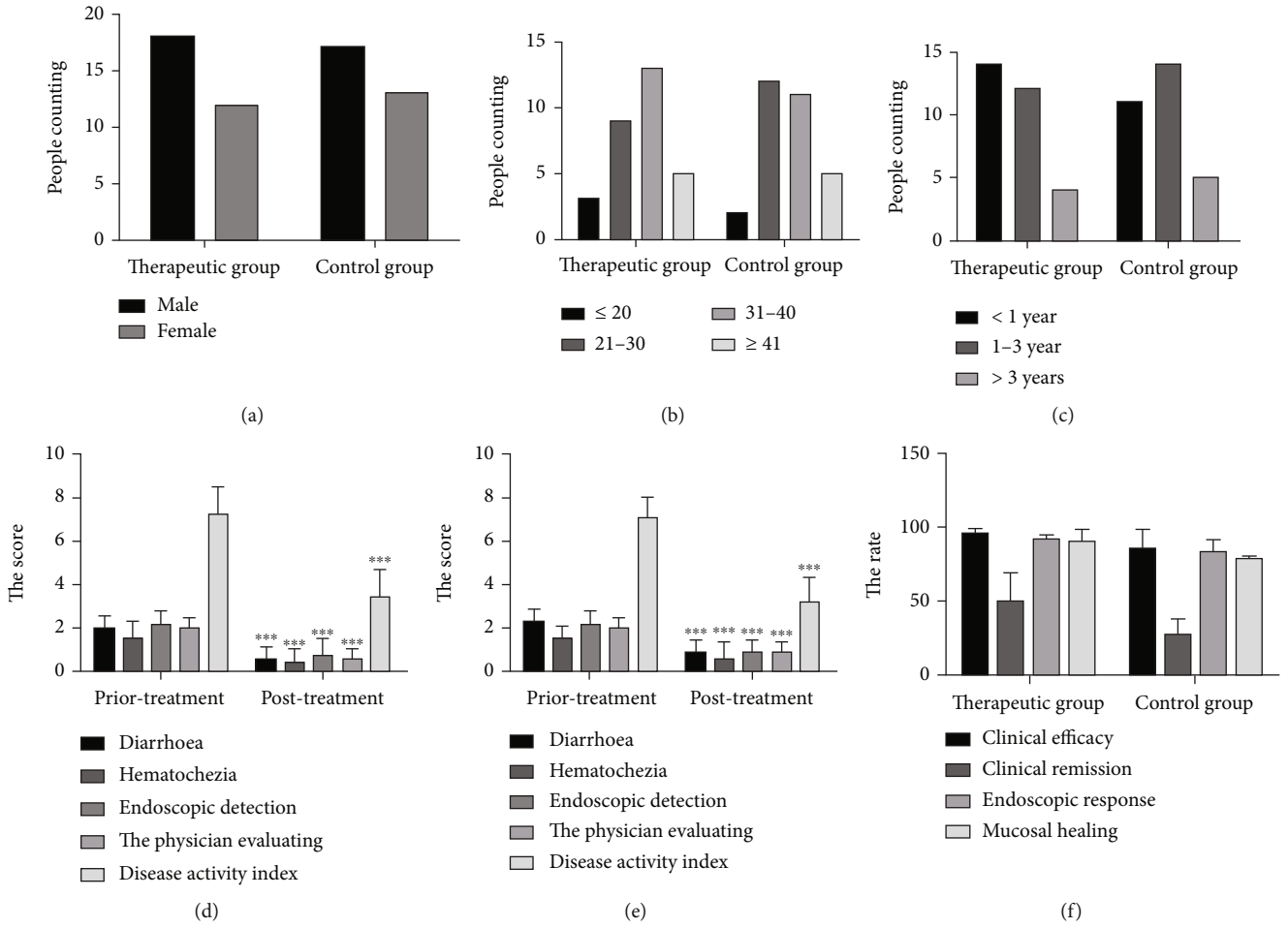

Figure 1: Qinghua Jianpi Recipe has a significant clinical effect on ulcerative colitis. The figure shows the gender (a), age (b), and disease duration (c) of the enrolled patients. The therapeutic group and control group patients, in the application of Qinghua Jianpi Recipe before (e) and after (d) treatment, get diarrhea, hematochezia, endoscopic detection, physician evaluation, and disease activity score. The clinical effective rate, clinical remission rate, endoscopic response rate, and experience healing rate of the therapeutic group and the control group were analyzed (f). $^{***}P < 0.001$, the difference was statistically significant.

water can alleviate the symptoms. After 2 to 4 weeks' time DSS loop, the blank group is in good condition. And the other groups mice have the color dark and dry coat, depressed, and tired. They have diarrhea, bloody stools, and weight gain after replacement of ordinary water. In subsequent experiments, the general situation of mice in the blank group remained normal all time, while the situation of mice in the model group gradually intensified with the increase of subsequent DSS circulation, presenting dry hair, emaciation, perianal redness and swelling, anal prolapse, and large amount of bloody stools. Compared with the model group, the Qinghua Jianpi Recipe treatment group has improved hair gloss, mental state, and relatively increased physical activity. Similarly, diarrhea and blood stool symptoms were relieved. Experiments were made to start each group about the same weight. Giving DSS cycle period, except the blank group of mice, each weight was significantly decreased in mice. After the treatment with Qinghua Jianpi Recipe, compared with the model group, the low- and high-dose group mouse body weights have a rising trend (Figure 2(a)).

3.3. Qinghua Jianpi Recipe Significantly Increased Colon Length and Decreased DAI Score in Colorectal Adenoma Model Mice. Colon lengths reflect the degree of intestinal inflammatory response in mice with colitis to a certain extent [14]. Therefore, to clarify the inhibitory effect of Qinghua Jianpi Recipe on intestinal inflammatory activity in the mice with adenoma cancer model, the colon length of mice in each group was observed. In this study, we found that, compared with the model group, Qinghua Jianpi Recipe significantly increased the length of colon in mice, while reducing DAI score (Figures 2(b), 2(c), and 2(f)). This means that the intervention of Qinghua Jianpi Recipe can effectively inhibit the systemic inflammatory response, thus helping to improve the prognosis of patients with high levels of inflammation such as IBD.

3.4. Effect of Qinghua Jianpi Recipe on the Number and Size of Intestinal Tumor Formation in Adenoma Model Mice. The mice were dissected after death in each group, and the intestinal tubes were cut longitudinally and laid flat on the plate. The intestinal conditions of mice and the location, number,

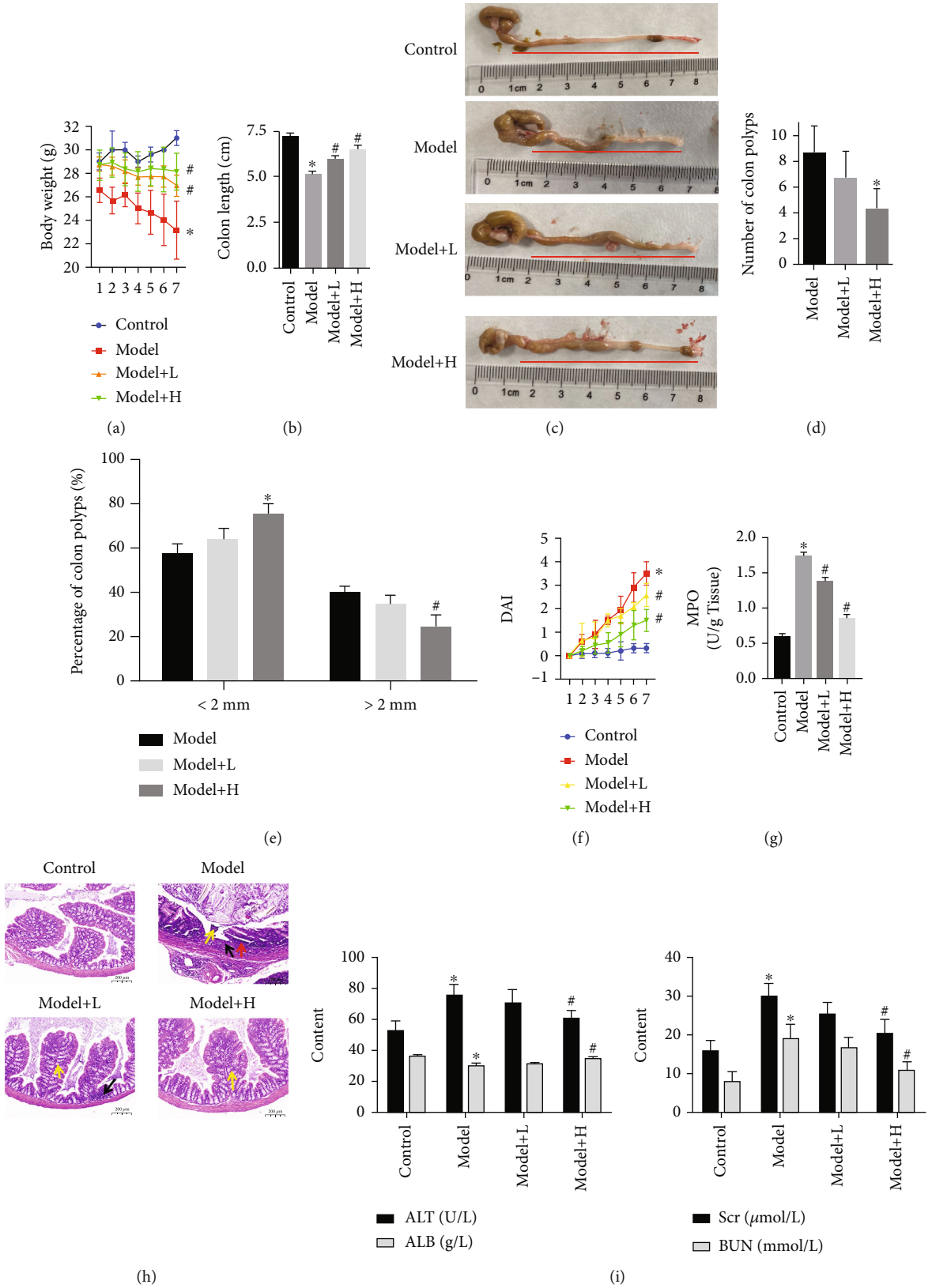

Figure 2: Effect of Qinghua Jianpi Recipe on intestinal inflammation, tumorigenesis, and pathological changes. (a) Body weight change in mice in seven weeks; (b, c) colon length of mice in each group and statistical results; (d) the number of intestinal tumor formation in adenoma model mice; (e) the size of intestinal tumor formation in adenoma model mice (<2 mm or >2 mm); (f) DAI score of rats in each group; (g) levels of MPO of intestinal tissues in each group; (h) HE staining of intestinal tissues. (i) Liver and kidney function indexes were analyzed in each group. $^{*}P < 0.05$ and $^{\#}P < 0.05$, the difference was statistically significant.

and size of tumors were observed by naked eye and recorded. The results showed that the colon of mice in the blank group was soft in texture, and the intestinal mucosa was smooth and flat, without hyperemia and edema or obvious hyperplasia. In the model group, the flexibility of the colon was decreased, the intestinal mucosa surface was rough, hyperemia and edema were obvious, hemorrhages were visible locally, and multiple bulges were observed in the mucosa of the middle and lower segment of the colon and near the anus, with the maximum diameter of 5 mm, and the number of tumors was 10.75 + 2.98. Compared with the model group, mice in the Qinghua Jianpi Recipe low-dose group had less colorectal hyperemia and edema, and mucosal neoplasm was mostly in the lower segment of the colorectum, with the number of tumors being 7.75 + 1.99, which was statistically different from that in the model group. The intestinal condition of the Qinghua Jianpi Recipe high-dose group was similar to that of the low-dose group, and the number of tumors was 5 + 1.91, which was significantly different from that of the model group. According to the tumor volume analysis, 41.9% of the mice in the model group had tumors larger than 2 mm in diameter, while 25.4% of the mice in the Qinghua Jianpi Recipe high-dose group had tumors larger than 2 mm in diameter, showing a significant difference compared with the model group. In summary, it indicates that Qinghua Jianpi Recipe can alleviate the intestinal injury induced by the molding agent and inhibit the number and size of intestinal adenoma formation (Figures 2(d) and 2(e)).

3.5. Qinghua Jianpi Recipe Significantly Improved the Colorectal Pathological Changes in Colorectal Adenoma Model Mice. After paraffin embedding, sectioning, and HE staining, the nucleus was purplish blue, and the cytoplasm was red. The pathological conditions of tissues and cells were determined by staining. HE staining results of intestinal tissues of mice in each group showed that the colon glands in the blank group were arranged regularly, with flat or cubic nuclei at the base and mild morphology, and a few lymphocytes infiltrated in the interstitium. In the model group, the epithelial cells showed no polarity and fused with each other, presenting nests and mesopores. Necrosis was observed in the center, the epithelial mucus layer disappeared, the nucleoplasma ratio increased, the nuclei were stained deeply, nucleoli were obvious, and mitosis was easy to see. In the Qinghua Jianpi Recipe low-dose group, goblet cells disappeared, proliferation, crowding, columnar or pseudostratified structure, thick nuclear chromatin, small nucleoli, and increased mitosis in colonic epithelial cells were noted. In the high-dose Qinghua Jianpi Recipe group, the gland arrangement was orderly, the number of goblet cells decreased, some crypts and epithelial mucus layer disappeared, epithelial nuclei slightly enlarged, small nucleoli were seen, and mitosis was occasionally seen. It was found that Qinghua Jianpi Recipe intervention could significantly reduce the incidence of adenoma in CRC and the state of colon inflammation, significantly improve the pathological damage of the colon in adenoma canceration model mice, and reduce inflammatory cell infiltration (Figure 2(h)). At the same time, we observed that the expression level of myeloperoxidase (MPO) in colon tissue could be significantly reduced by Qinghua Jianpi Recipe intervention compared with the adenoma cancer model mice (Figure 2(g)). We also found that the corresponding modeling reagents produced toxic effects on the liver and kidney of mice. However, Qinghua Jianpi Recipe plays the role of reducing the toxicity and increasing the effect (Figure 2(i)). It was not toxic to the liver or kidney at the doses in this study.

3.6. Qinghua Jianpi Recipe Significantly Improved the Intestinal Microflora Structure of Colorectal Adenoma Canceration Model Mice. With the increase of intestinal flora 16S RAN sequencing depth, the trend of species increase slowed down, indicating that this sequencing has covered the dominant flora in the sample, suggesting that the sequencing data of this time is qualified (Figure 3(a)). Compared with the normal control group, the Simpson index of the model group has an increasing trend, while that in the Qinghua Jianpi Recipe intervention group had a similar trend. This suggests that the modeling of the colorectal adenoma canceration model reduced the diversity of intestinal flora, while the Qinghua Jianpi Recipe intervention restored the diversity of intestinal flora. Compared with the normal control group, the Shannon and Chaos indexes of the model group showed a decreasing trend. This suggests that the diversity of intestinal flora was reduced after modeling, while the Shannon and Chaos indexes of the Qinghua Jianpi Recipe intervention group showed a rising trend compared with the model group (Figure 3(b)). All the above results indicated that the intestinal microflora diversity of the Qinghua Jianpi Recipe intervention group was closer to that of the normal control group.

Beta diversity analysis (PCoA results) showed that the first principal component PCoA1 could explain 68.64% of the difference between groups, and the second principal component PCoA2 could explain 12.73% of the difference between groups. The distance between the normal control group, the model group, and Qinghua Jianpi Recipe intervention group was far (Figure 3(c)).

Analysis of the intestinal flora structure revealed that at the phylum level, the top 6 phyla in abundance were Firmicutes, Bacteroidota, Verrucomicrobiota, Actinobacteriota, Proteobacteria, and Patescibacteria. In terms of the composition and structure of bacteria, the model group and the Qinghua Jianpi Recipe intervention group were similar. However, on the whole, the dominant bacteria in the three groups were Firmicutes, Bacteroidota, and Verrucomicrobiota. At the genus level, the top 10 genera in relative abundance were Muribaculaceae_norank, Lactobacillus, Akkermansia, Clostridia UCG−014_norank, Dubosiella and Prevotellaceae UCG−001, Lachnospiraceae_uncultured, Clostridium sensu stricto 1, Lachnospiraceae NK4A136 group, and Ligilactobacillus. The three groups have significantly different structural changes at the genus level. The model group and the Qinghua Jianpi Recipe intervention group have relatively high Lactobacillus and Akkermansia, while the normal control group has relatively high Muribaculaceae_norank (Figures 3(d) and 3(e)).

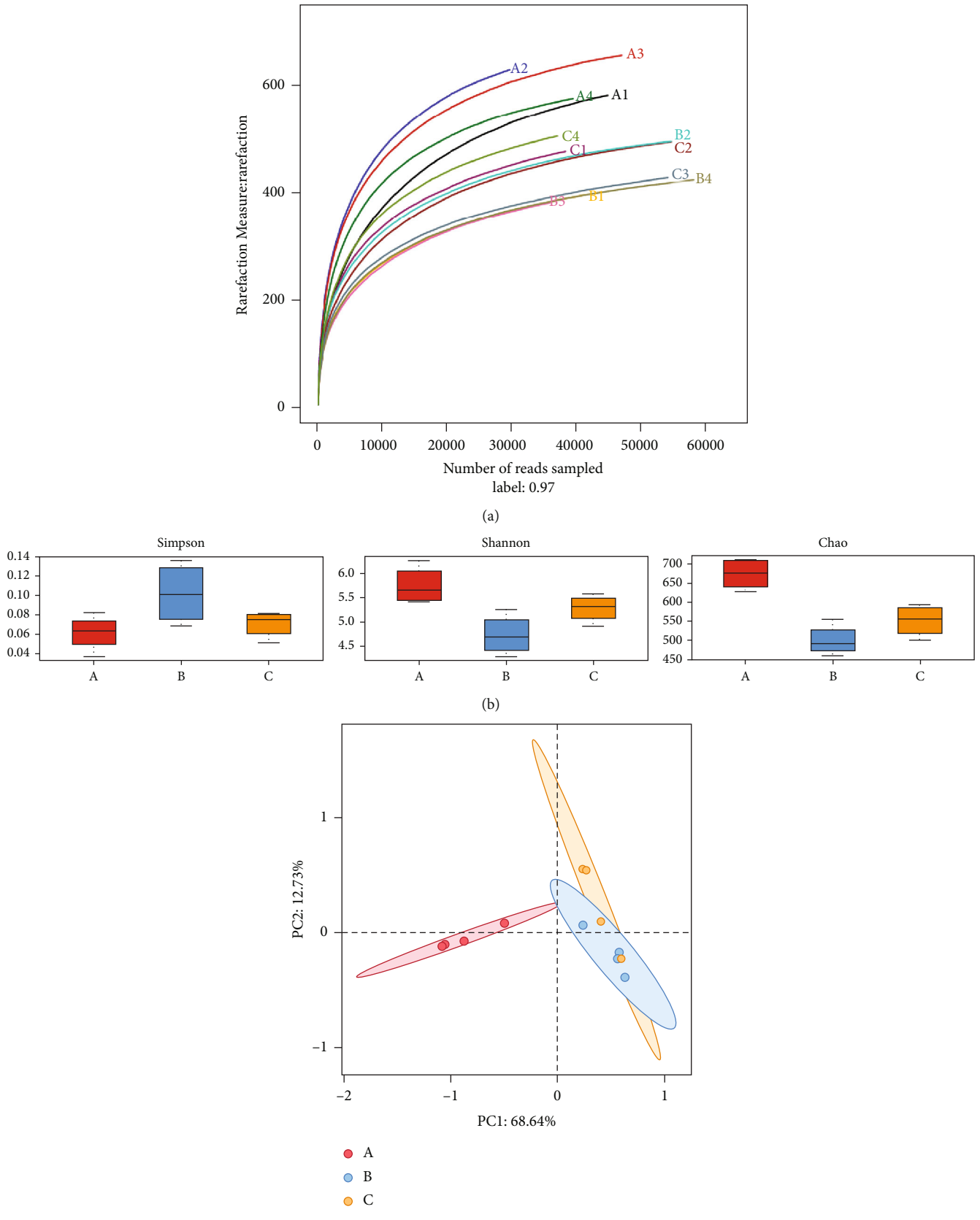

(a)

(b)

(c)

Figure 3: Continued.

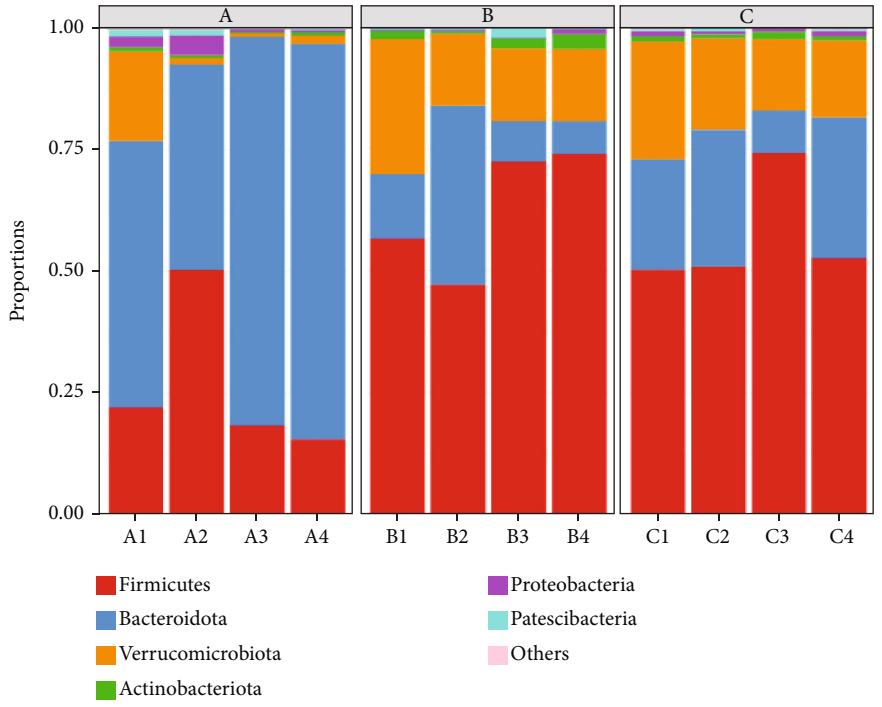

(d)

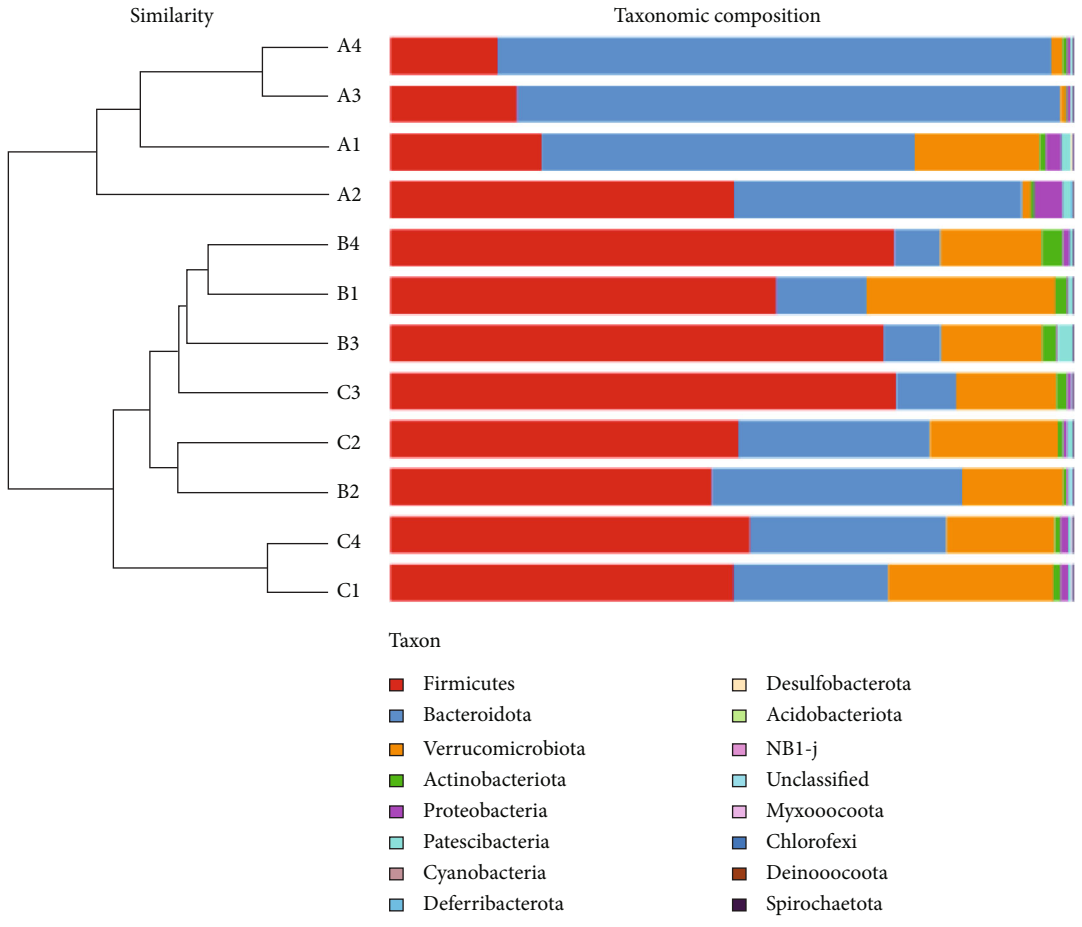

(e)

Figure 3: Continued.

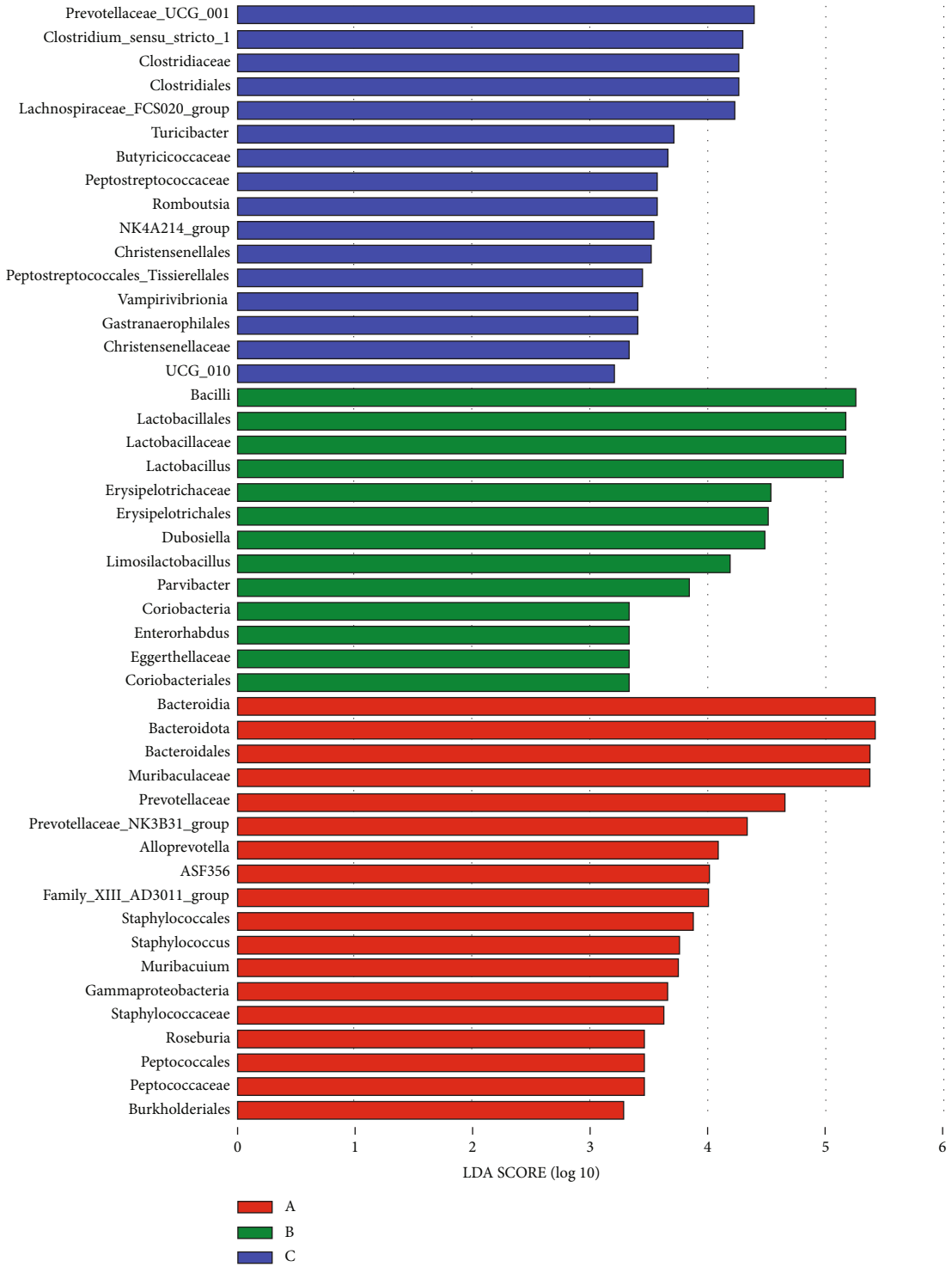

(f)

Figure 3: Effect of Qinghua Jianpi Recipe on the intestinal microflora structure of colorectal adenoma canceration model mice. (a) Rarefaction curve, the depth of sample sequencing can be obtained by making dilution curve; (b) alpha-diversity, the abundance and diversity of microbial communities can be reflected by single-sample diversity analysis (alpha diversity), including Simpson, Shannon, and Chao indexes; (c) beta diversity analysis, used to study similarities or differences in the composition of sample communities; (d, e) diversity analysis of intestinal microbiota of rats in each group; (F) LEfSe analysis, the figure shows the LDA scores obtained by LDA (linear regression analysis) for the microorganisms with significant effects in the two groups.

LEfSe analysis was performed on fecal microbiome sequence data to explore the potential biomarker flora of related organisms. The results showed that after modeling, at the genus level, the levels of Coriobacteriia, Parvibacter, Limosilactobacillus, Dubosiella, Lactobacillus, Bacilli, and UCG_010 were significantly increased. The prognosis of Qinghua Jianpi Recipe was significantly increased levels of the genera Peptostreptococcales_Tissierellales, NK4A214_group, Romboutsia, Peptostreptococcaceae (Streptococcus mutans), Turicibacter (genus), Lachnospiraceae_FCS020_group, Clostridium_sensu_stricto_1, and Prevotellaceae_UCG_001. Compared with the model group and Qinghua Jianpi Recipe intervention group, Bacteroidota (Bacteroidetes) was specific in the phylum level in the normal control group. At the genus level, the specific bacterial communities include Peptococcales, Roseburia (Roche), Muribaculum (genus), Staphylococcus (Staphylococcus), Family_XIII_AD3011_group, ASF356, Alloprevotella, and Prevotellaceae_NK3B31_group (Figure 3(f)).

3.7. Qinghua Jianpi Recipe Can Regulate Short-Chain Fatty Acid Metabolism of Intestinal Bacteria in Mice with Colorectal Adenoma Cancer Model. In this study, acetic acid, propionic acid, isobutyric acid, butyric acid, isovaleric acid, valeric acid, and caproic acid in feces were analyzed based on GC-MS. It was found that the content of short-chain fatty acids in the model group was significantly changed, especially isobutyric acid and propionic acid (Figures 4(a) and 4(c)). It was also found that the Qinghua Jianpi Recipe intervention group could reverse the changes of short-chain fatty acids (Figures 4(a) and 4(c)). PCA based on the determination results of 7 kinds of short-chain fatty acids showed that the normal group, the model group, and the drug treatment group could be clearly distinguished. This indicated that the content of short-chain fatty acids among the three groups had significant overall differences (Figure 4(b)).

3.8. Network Pharmacology Analysis Found That Qinghua Jianpi Recipe May Inhibit Inflammatory Cancer Transformation of the Station and the Occurrence and Development of Colorectal Tumor through Regulatory Pathways. OB ≥ 30% and DL ≥ 0.18 were set in the TCMSP database to screen the effective components of Atractylodes macrocephala, Tangerine peel, Radix Paeoniae, Codonopsis pilosula, parsnip, Poria cocos, Glycyrrhiza, Astragalus membranaceus, Scutellaria baicalensis, Achyranthes bidentata, and coix seed. A total of 236 potential active components were obtained. 1036 drug targets were screened out using the Swiss Target Prediction database. Based on the keywords "colorectal carcinoma", we searched OMIM, DisGeNet, and GeneCards databases and obtained 1011 disease targets. Venny2.1 online software mapping tool platform was used to input 1036 drug targets and 1011 disease targets to draw a Venn diagram, and 137 drug-disease common targets were obtained after the intersection of the two. The 236 potential active components and 137 drug-disease common targets in TCM compounds were input into Cytoscape software, and isolated components without intersection with targets were deleted to draw the network diagram of "drug-component-target-disease" interaction (Figures 5(a) and 5(b) and Supplementary materials 1-2).

The above 137 common targets were input into the STRING database for retrieval. The protein type was set as "Homo sapiens," and the minimum interaction threshold was 0.4. The network relationship data of the target interaction was obtained and imported into Cytoscape software. Protein interaction network diagram was drawn. The biological process, cell components, and molecular functions of 137 common targets were selected by GO analysis after R language operation. GO results showed that the set of intersected genes was enriched into 2435 biological process pathways. It mainly includes regulation of MAP kinase activity, response to oxidative stress, and epithelial cell proliferation. The intersection gene sets were enriched with 59 cell components, which mainly involved cell-substrate adherens junctions, membrane region, and so on. The set of intersected genes was enriched with 129 genes related to molecular function. There are mainly protein serine/threonine kinase activity, protein tyrosine kinase activity, etc. (Figures 5(c)–5(e) and Supplementary materials 3-8).

151 KEGG pathways were obtained by running 137 common targets in R language, and the first 20 results formed a bar graph with KEGG enrichment. The results showed that Qinghua Jianpi Recipe may inhibit intestinal inflammation and the process of "inflammatory cancer transformation" through multiple pathways and multiple targets, mainly through regulating PI3K-Akt, JAK-Stat, nod-like receptor, and other signaling pathways (Figure 5(f) and Supplementary materials 9).

3.9. Qinghua Jianpi Recipe May Regulate the Expression of Pathway-Related Proteins and Inhibit the Expression of Inflammatory Factors in Intestinal Tissue. Based on the network pharmacology analysis and related experimental results, we further confirmed the specific molecular mechanism of Qinghua Jianpi Recipe inhibiting intestinal inflammation and "inflammatory cancer transformation." First, Qinghua Jianpi Recipe could inhibit the expression of inflammatory factors in colon tissues, including IL-1β, IL-6, IL-18, and TNF-α (Figure 6(a)). In the inflammatory state, intestinal barrier function was impaired, and the expression of intestinal barrier function-related proteins claudin-1, Occludin, and ZO-1 decreased. And the expression of the above proteins increased in the Qinghua Jianpi Recipe intervention group (Figure 6(b)). In the inflammatory state, the expression of pattern recognition receptor-related genes Nod1, Nod2, and Ripk2 increased, initiating the immune response; inflammatory factors NF-κB and STAT3 and inflammatory factors IL-6, IL-23, and IL-17A increased. The expression of the above proteins decreased in the Qinghua Jianpi Recipe intervention group (Figures 6(b) and 6(c)). Intestinal flora is involved in many links of intestinal inflammation, among which metabolites play an important role. In the inflammatory state, the expression of free fatty acid receptor 2 (FFAR2) is decreased, and the protein expression is increased after the treatment of Qinghua Jianpi Recipe (Figure 6(b)).

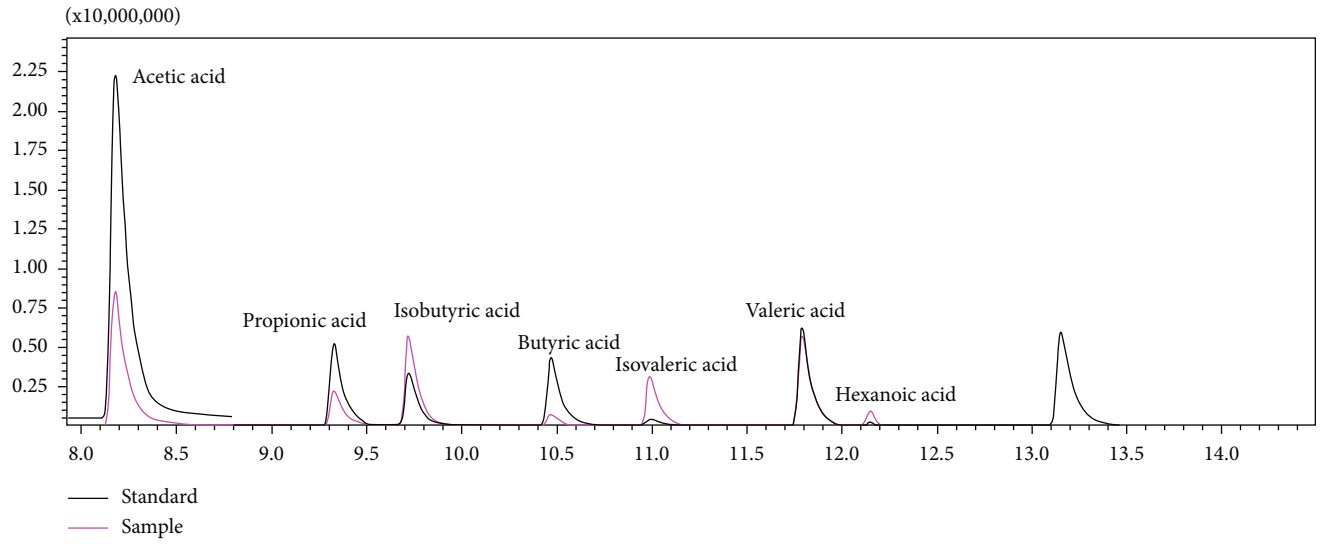

(a)

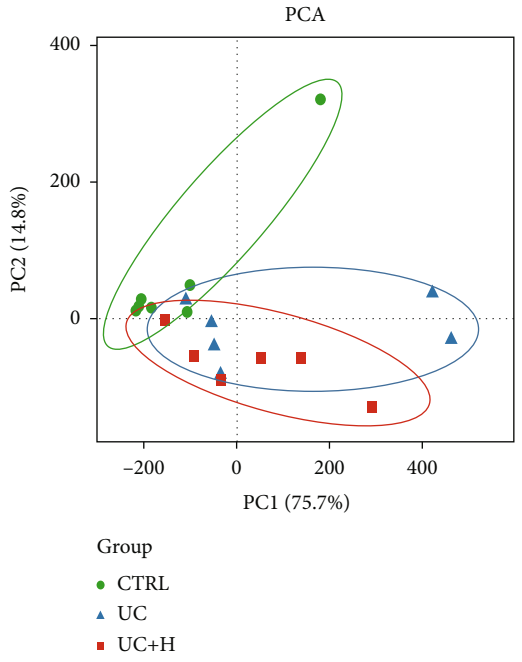

(b)

Figure 4: Continued.

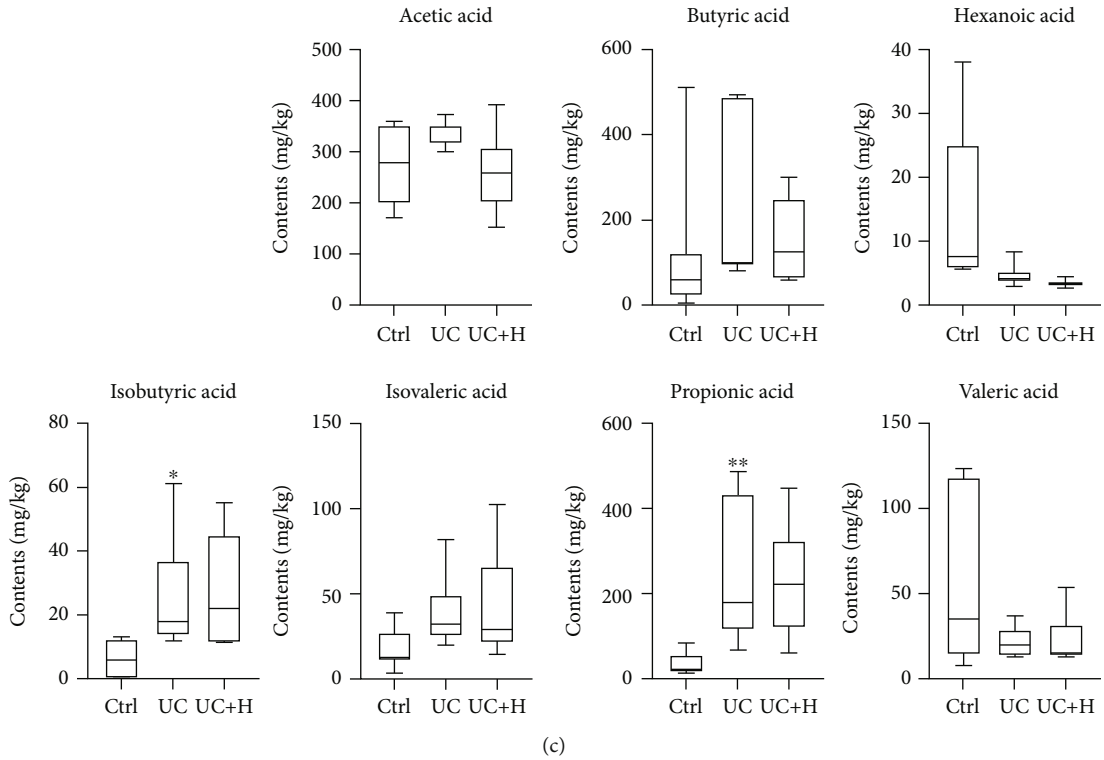

Figure 4: Qinghua Jianpi Recipe can regulate short-chain fatty acid metabolism of intestinal bacteria in mice with colorectal adenoma cancer model. The TIC chromatograms (a), PCA (b) and concentration (c) of the short-chain fatty acids in fecal samples. $^{*}P < 0.05$ and $^{**}P < 0.05$, the difference was statistically significant.

4. Discussion

CRC is a disease with high morbidity and mortality due to the interaction of multiple factors, such as genes and environment, and its specific mechanism is unknown. CRC with genetic predisposition accounts for only a small proportion, including familial adenomatous polyposis (FAP), hereditary nonpolyposis colorectal cancer (HNPCC), and hamartomatous polyposis syndrome. Among them, chronic inflammation is the main environmental factor for the occurrence and development of CRC. Studies have shown that patients with Crohn's disease (CD) and UC have a higher risk of developing CRC [15, 16].

In this study, our goal was to confirm the inhibitory effect of Qinghua Jianpi Recipe on the "transformation" of inflammatory carcinoma. We first confirmed the efficacy of Qinghua Jianpi Recipe in improving colonic inflammatory status and function in patients with UC. And then, the influence of Qinghua Jianpi Recipe on adenoma canceration model mouse was observed, including intestinal inflammation state, number of adenoma, and pathological changes. Qinghua Jianpi Recipe can significantly improve the intestinal inflammatory state of adenoma cancer model mice, reduce the number of 1-3 mm adenoma, reduce intestinal inflammatory activity and pathological intestinal damage, and reduce the expression of proinflammatory cytokine MPO in colon tissue. Previous studies and network pharmacology studies have confirmed that the occurrence of colon polyps and colorectal tumors is closely related to intestinal barrier function, intestinal flora metabolism, and intestinal inflammation [17, 18]. Increased tumorigenesis was observed in mice lacking free fatty acid receptor 2 (FFAR2), which is considered due to reduced intestinal epithelial cell (IEC) integrity and an influx of bacteria [19]. We found that after modeling, at the genus level, the levels of Coriobacteriia, Parvibacter, Limosilactobacillus, Dubosiella, Lactobacillus, Bacilli, and UCG_010 were significantly increased. The prognosis of Qinghua Jianpi Recipe was significantly increased the genus level of Peptostreptococcales_Tissierellales, NK4A214_group, Romboutsia, Peptostreptococcaceae (Streptococcus mutans), Turicibacter, Lachnospiraceae_FCS020_group, Clostridium_sensu_stricto_1, and Prevotellaceae_UCG_001. The concentration of short-chain fatty acids in the feces of mice in each group was detected by GC-MS, and it was observed that the content of short-chain fatty acids in the model group was significantly changed, especially isobutyric acid and propionic acid, while the change of short-chain fatty acids in the Qinghua Jianpi Recipe group was reversed. Further experimental studies confirmed that intestinal barrier function-related proteins, inflammatory and immune-related signaling pathways (STAT3 and Nod pathways), and free fatty acid receptor 2 (FFAR2) inhibited the "inflammatory transformation" of colon cancer.

In this study, the effects of Qinghua Jianpi Recipe on preventing colon polyp recurrence and inhibiting the progress of "inflammatory cancer transformation" were observed. And the changes of the structure of intestinal flora

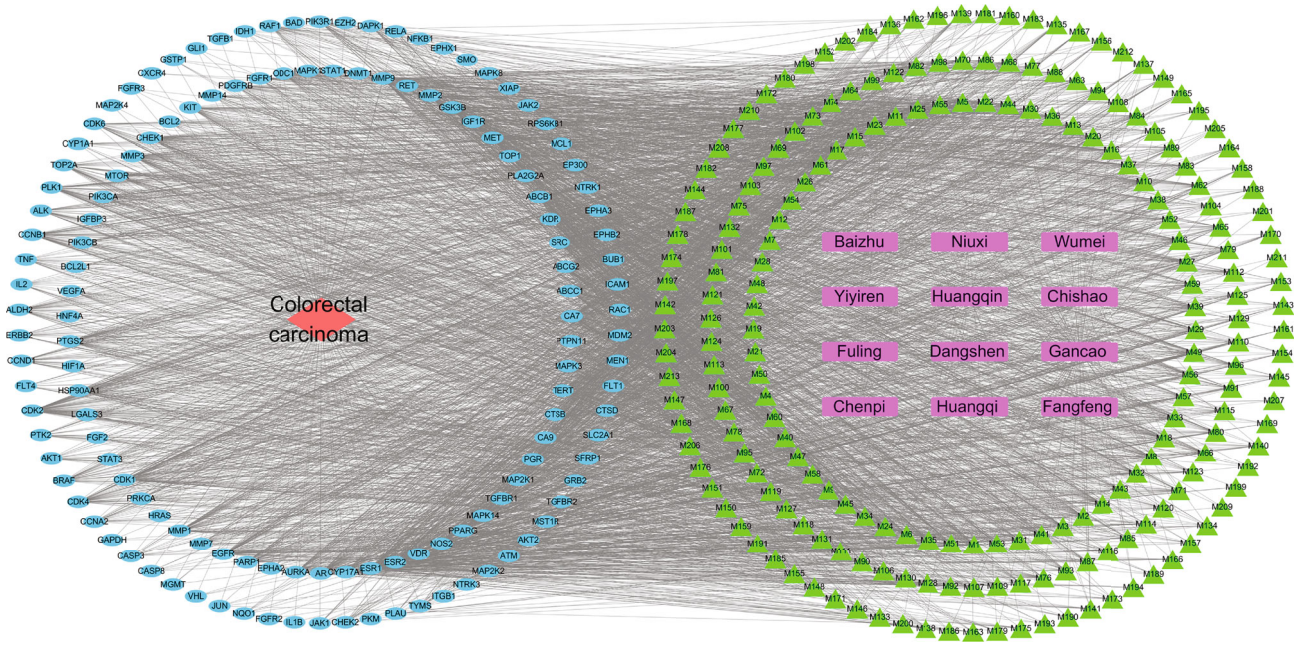

(a)

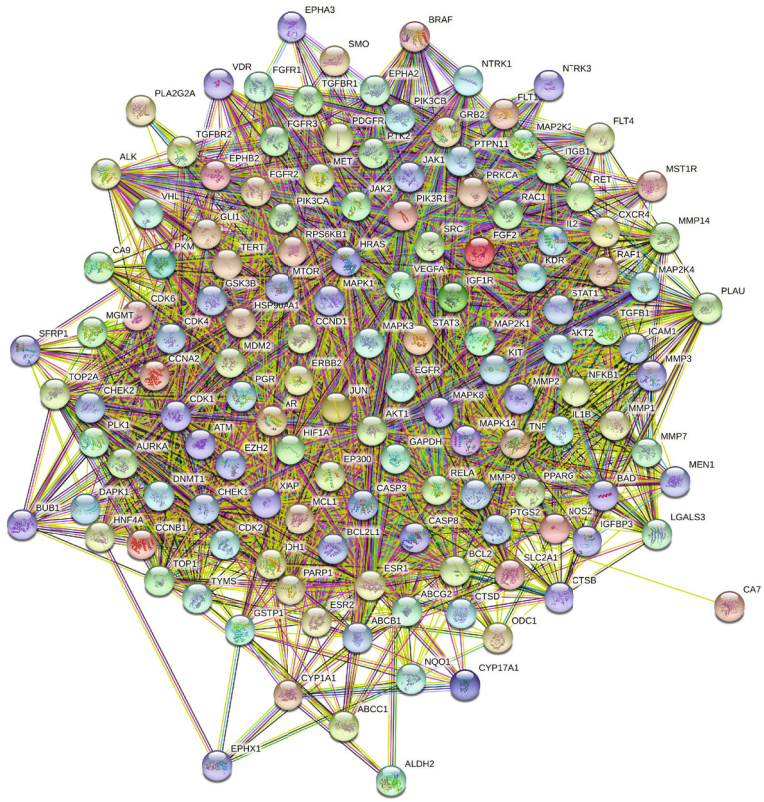

(b)

Figure 5: Continued.

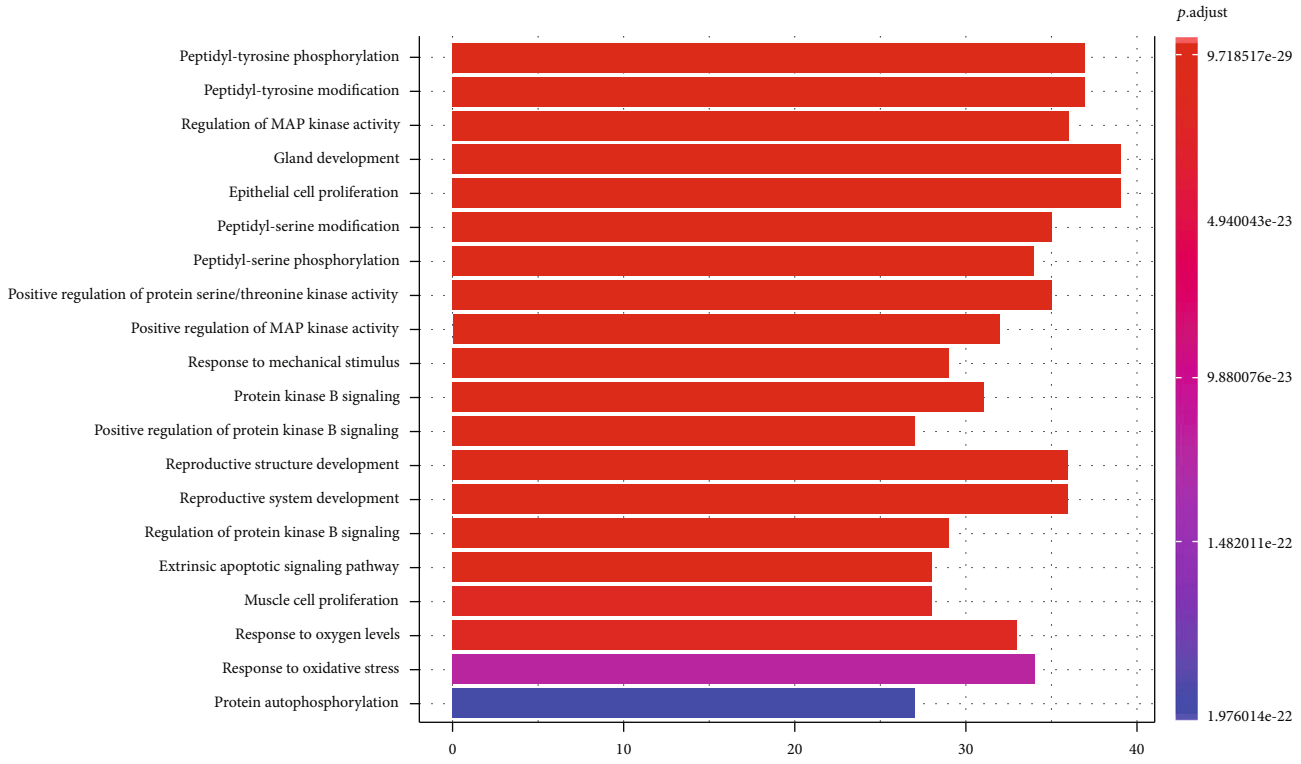

(c)

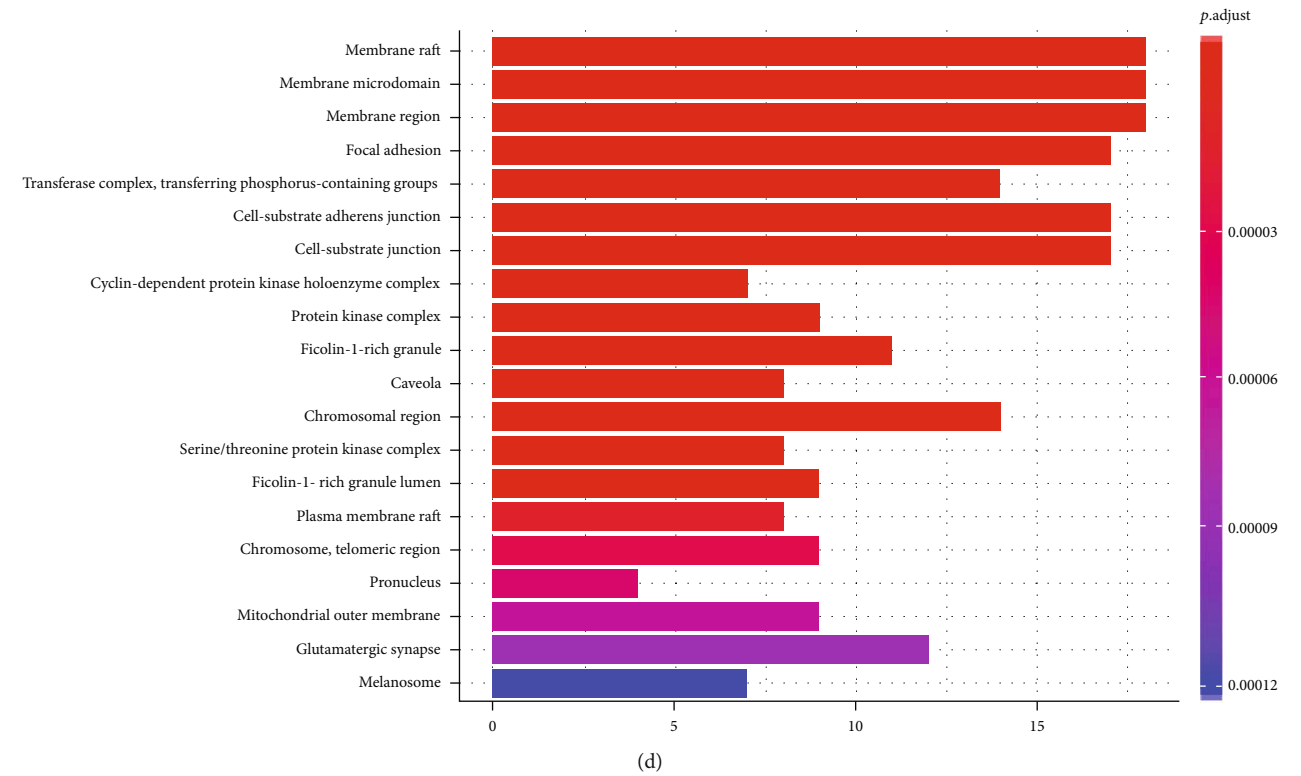

(d)

Figure 5: Continued.

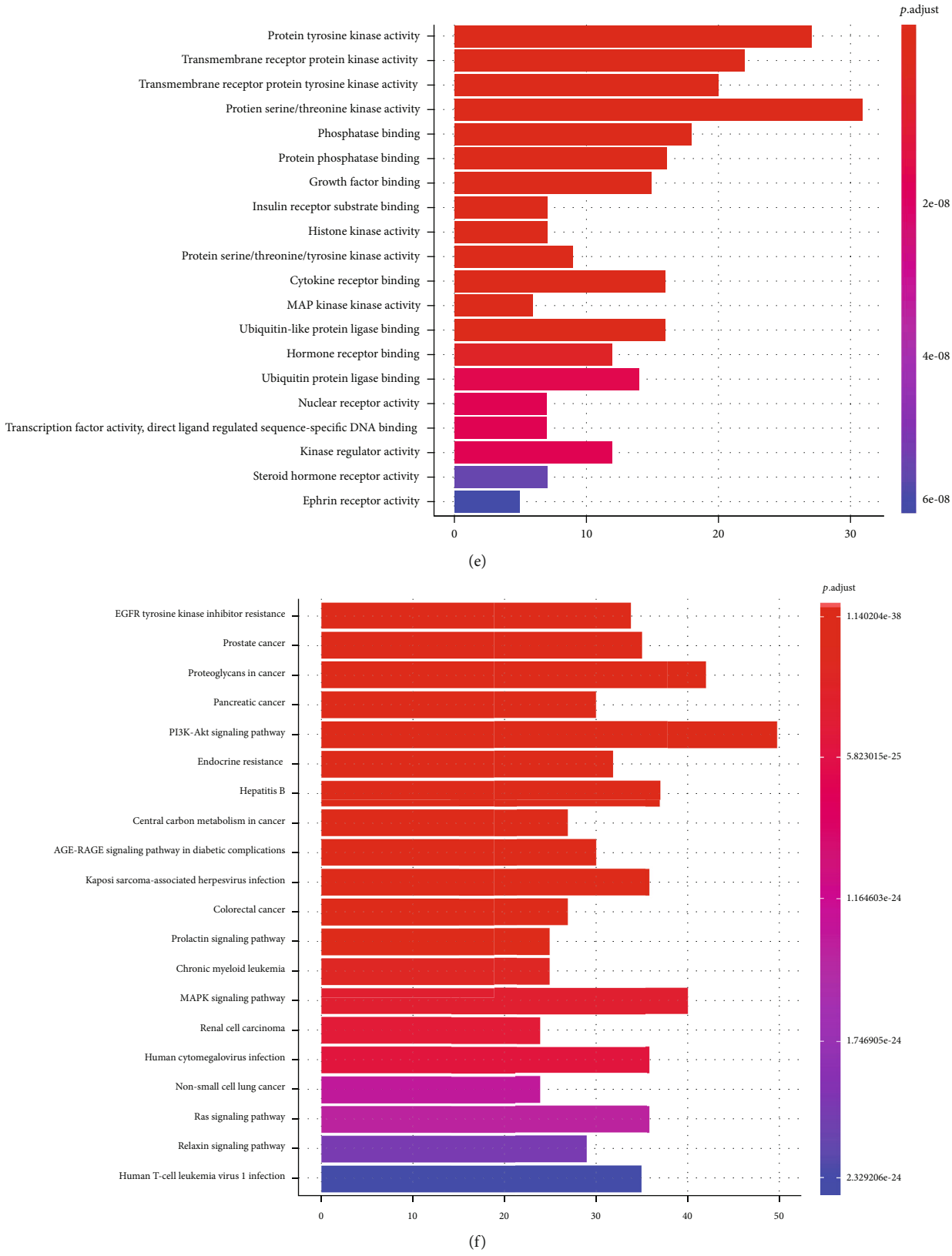

Figure 5: Network pharmacology analysis of the molecular mechanism of Qinghua Jianpi Recipe in preventing the transformation process of inflammatory cancer. Network diagram of drug-component-target-disease interactions (a); PPI network of protein interaction (b); the biological processes, cell components, and molecular functions of 137 common targets were selected by GO analysis after R language operation (c–e). The first 20 results formed a bar graph (f) of KEGG functional enrichment, with *P* value representing the significance of enrichment, and the redder the color, the higher the significance.

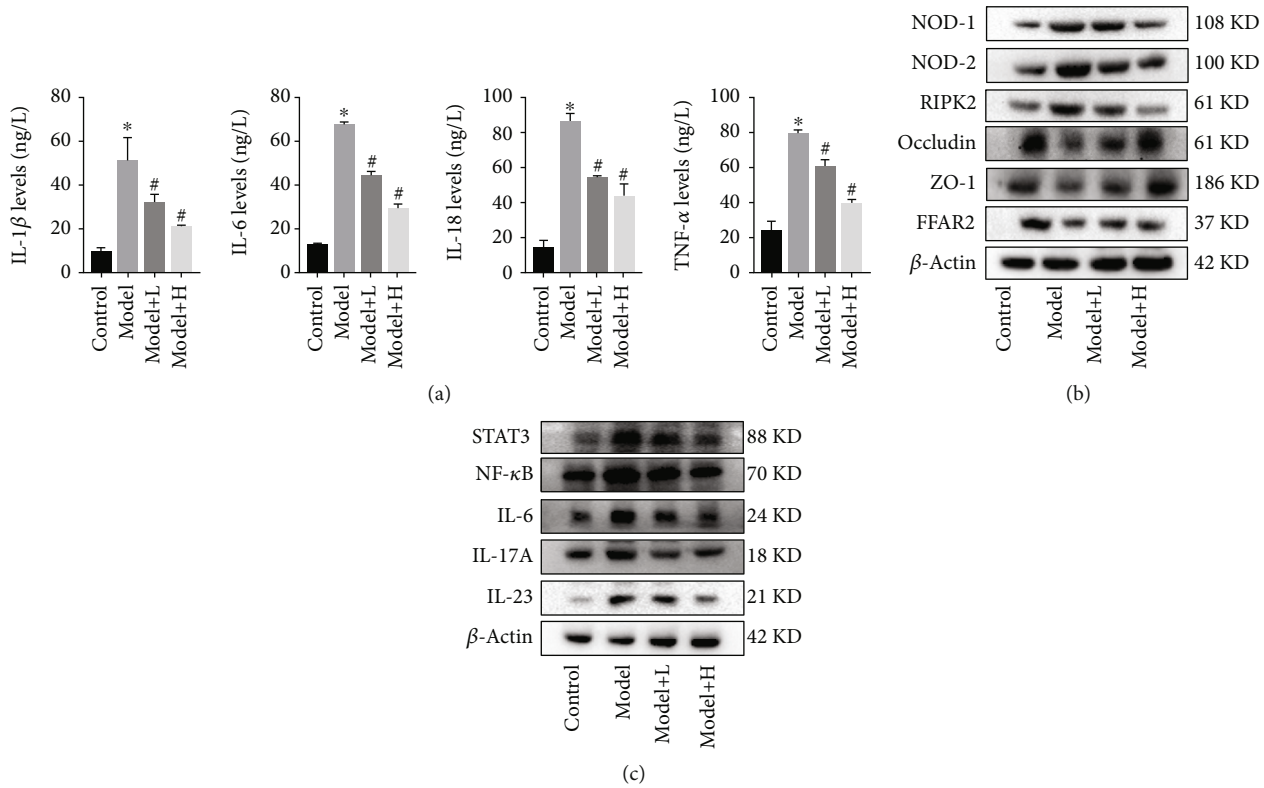

Figure 6: Qinghua Jianpi Recipe regulated the expression of pathway-related proteins and inhibited the expression of inflammatory factors in intestinal tissue. ELISA was used in testing the expression of inflammatory factors in intestinal tissue (a); Western blot analysis was used to detect related protein ($x \pm s$, $n \geq 3$) (b, c). β-Actin was used as an invariant control for equal loading. $^{*}P < 0.05$ and $^{\#}P < 0.05$, the difference was statistically significant.

and inflammatory (immune) microenvironment in mice with colon polyp were investigated by taking the intestinal flora as the core. However, there is still a lack of studies on the mutated genes in adenoma carcinoma sequence by Qinghua Jianpi Recipe, as well as the related signal pathways. It is believed that with the further development of Qinghua Jianpi Recipe, its mechanism of preventing adenoma canceration will be further clarified. That will provide a new strategy for preventing precancerous lesions of CRC. The research results of this project will further supplement the occurrence mechanism of colon polyps and CRC, provide an objective basis for TCM to prevent polyp recurrence and cancer, and lay a scientific foundation for the development of new TCM to prevent colorectal polyp recurrence and cancer.

Data Availability

We can provide additional methods and data if needed.

Conflicts of Interest

The authors declare no conflict of interest.

Acknowledgments

This research was supported by Jiangsu Province "333" Talent Project, Chinese Medicine Science and Technology Key Special Project (ZT202113), Major Health Risks and Chinese Medicine Intervention Technology Platform (JKFXFK-006), Natural Science Foundation of Nanjing University of Chinese Medicine (XZR2020076).

Supplementary Materials

The analysis data of the network pharmacology. Active ingredients in traditional Chinese medicine (1); 1011 targets in colorectal cancer (2); PPI topological analysis (3); topological analysis of 213 active components in the network diagram (4); MCODE analysis (5); biological processes (BP, GO enrichment analysis) (6); cell components (CC, GO enrichment analysis) (7); molecular function (MF, GO enrichment analysis) (8); KEGG analysis (9). *(Supplementary Materials)*

References

[1] R. L. Siegel, K. D. Miller, and A. Jemal, "Cancer statistics, 2020," *CA: a Cancer Journal for Clinicians*, vol. 70, no. 1, pp. 7–30, 2020.

[2] F. Bray, J. Ferlay, I. Soerjomataram, R. L. Siegel, L. A. Torre, and A. Jemal, "Global cancer statistics 2018: GLOBOCAN estimates of incidence and mortality worldwide for 36 cancers in 185 countries," *CA: a Cancer Journal for Clinicians*, vol. 68, no. 6, pp. 394–424, 2018.

[3] T. A. Ullman and S. H. Itzkowitz, "Intestinal inflammation and cancer," *Gastroenterology*, vol. 140, no. 6, pp. 1807–1816.e1, 2011.

[4] I. S. Reynolds, A. O'Toole, J. Deasy, D. A. McNamara, and J. P. Burke, "A meta-analysis of the clinicopathological characteristics and survival outcomes of inflammatory bowel disease associated colorectal cancer," *International Journal of Colorectal Disease*, vol. 32, no. 4, pp. 443–451, 2017.

[5] J. W. Windsor and G. G. Kaplan, "Evolving epidemiology of IBD," *Current Gastroenterology Reports*, vol. 21, no. 8, p. 40, 2019.

[6] H. Tilg, T. E. Adolph, R. R. Gerner, and A. R. Moschen, "The intestinal microbiota in colorectal cancer," *Cancer Cell*, vol. 33, no. 6, pp. 954–964, 2018.

[7] A. I. Robles, G. Traverso, M. Zhang et al., "Whole-exome sequencing analyses of inflammatory bowel disease–associated colorectal cancers," *Gastroenterology*, vol. 150, no. 4, pp. 931–943, 2016.

[8] K. Makki, E. C. Deehan, J. Walter, and F. Bäckhed, "The impact of dietary fiber on gut microbiota in host health and disease," *Cell Host & Microbe*, vol. 23, no. 6, pp. 705–715, 2018.

[9] Q. Zhou, Y. G. Chen, J. Xiao et al., "Traditional Chinese medicine (*Xiaoai Jiedu Decoction*) as an adjuvant treatment for prevention new colorectal adenomatous polyp occurrence in post-polypectomy: study protocol for a randomized controlled trial," *Medicine (Baltimore)*, vol. 98, no. 31, article e16680, 2019.

[10] X. G. Sun, X. C. Lin, J. X. Diao, Z. L. Yu, and K. Li, "Pi (Spleen)-deficiency syndrome in tumor microenvironment is the pivotal pathogenesis of colorectal cancer immune escape," *Chinese Journal of Integrative Medicine*, vol. 22, no. 10, pp. 789–794, 2016.

[11] C. Zhong, S. Wu, C. Chen et al., "Tiaochang Xiaoliu Decoction Granules prevent the recurrence of colorectal adenoma: a study protocol for a randomized controlled trial," *Annals of Palliative Medicine*, vol. 10, no. 4, pp. 4897–4905, 2021.

[12] J. L. Ru, P. Li, J. Wang et al., "TCMSP: a database of systems pharmacology for drug discovery from herbal medicines," *Journal of Cheminformatics*, vol. 6, no. 1, p. 13, 2014.

[13] Y. Qu, X. Yang, J. Li et al., "Network pharmacology and molecular docking study of Zhishi-Baizhu herb pair in the treatment of gastric cancer," *Evidence-based Complementary and Alternative Medicine*, vol. 2021, Article ID 2311486, 18 pages, 2021.

[14] V. M. Fazio, M. D. Robertis, E. Massi et al., "The AOM/DSS murine model for the study of colon carcinogenesis: from pathways to diagnosis and therapy studies," *Journal of Carcinogenesis*, vol. 10, no. 1, p. 9, 2011.

[15] R. Dienstmann, L. Vermeulen, J. Guinney, S. Kopetz, S. Tejpar, and J. Tabernero, "Consensus molecular subtypes and the evolution of precision medicine in colorectal cancer," *Nature Reviews Cancer*, vol. 17, no. 2, pp. 79–92, 2017.

[16] S. Din, K. Wong, M. F. Mueller et al., "Mutational analysis identifies therapeutic biomarkers in inflammatory bowel disease-associated colorectal cancers," *Clinical Cancer Research*, vol. 24, no. 20, pp. 5133–5142, 2018.

[17] F. Chen, X. Dai, C. C. Zhou et al., "Integrated analysis of the faecal metagenome and serum metabolome reveals the role of gut microbiome-associated metabolites in the detection of colorectal cancer and adenoma," *Gut*, vol. 71, no. 7, pp. 1315–1325, 2022.

[18] A. D. Kostic, E. Chun, L. Robertson et al., "*Fusobacterium nucleatum* potentiates intestinal tumorigenesis and modulates the tumor-immune microenvironment," *Cell Host & Microbe*, vol. 14, no. 2, pp. 207–215, 2013.

[19] Y. W. Huang, C. W. Lin, P. Pan et al., "Dysregulated free fatty acid receptor 2 exacerbates colonic adenoma formation in $Apc^{min/+}$ mice: relation to metabolism and gut microbiota composition," *Journal of Cancer Prevention*, vol. 26, no. 1, pp. 32–40, 2021.

Hindawi
Journal of Immunology Research
Volume 2023, Article ID 7040113, 19 pages
https://doi.org/10.1155/2023/7040113

Research Article

Pyroptosis-Related Signature Predicts the Progression of Ulcerative Colitis and Colitis-Associated Colorectal Cancer as well as the Anti-TNF Therapeutic Response

Yumei Ning,[1,2] Kun Lin,[1,2] Jun Fang,[1,3] Xiaojia Chen,[1,2] Xinyi Hu,[1,2] Lan Liu,[1,2] Qiu Zhao ,[1,2] Haizhou Wang ,[1,2] and Fan Wang [1,2]

[1]*Department of Gastroenterology, Zhongnan Hospital of Wuhan University, Wuhan, China*
[2]*Hubei Clinical Center and Key Lab of Intestinal and Colorectal Diseases, Wuhan, China*
[3]*Renmin Hospital of Huangmei County, Huanggang, China*

Correspondence should be addressed to Qiu Zhao; zhaoqiuwhu@163.com, Haizhou Wang; whzcj@outlook.com, and Fan Wang; fanndywang@foxmail.com

Yumei Ning, Kun Lin, and Jun Fang contributed equally to this work.

Received 25 April 2022; Revised 22 July 2022; Accepted 26 November 2022; Published 27 January 2023

Academic Editor: Quanwen Liu

Ulcerative colitis (UC) is a complex intestinal inflammation with an increasing risk of colitis-associated colorectal cancer (CAC). However, the pathogenesis is still unclear between active UC and inactive UC. Recently, it has been reported that pyroptosis-related genes (PRGs) are closely associated with inflammatory disease activity. Nevertheless, the specific roles of PRGs in the progression and treatment of UC and CAC remain unclear. In this study, we identified 30 differentially expressed PRGs based on the immune landscape of active and inactive UC samples. Meanwhile, weighted gene coexpression network analysis was applied to explore important genes associated with active UC. By intersecting with the differentially expressed PRGs, CASP5, GBP1, GZMB, IL1B, and IRF1 were selected as key PRGs to construct a pyroptosis-related signature (PR-signature). Then, logistic regression analysis was performed to validate the PR-signature and establish a pyroptosis-related score (PR-Score). We demonstrated that PR-Score had a powerful ability to distinguish active UC from inactive UC in multiple datasets. Besides, PR-Score was positively correlated with immune cell infiltration and inflammatory microenvironment in UC. Lower PR-Score was associated with a better response to anti-TNF therapy for patients with UC. Additionally, high-PR-Score was found to suppress CAC and improve the survival outcomes of patients with colorectal cancer. Finally, the levels of the PR-signature genes were validated both in vitro and in vivo. These findings can improve our understanding of PRGs in UC and provide new markers for predicting the occurrence of active UC or CAC and the treatment of UC.

1. Introduction

Ulcerative colitis (UC), a subcategory of inflammatory bowel disease (IBD), is a complex, chronic, and recurrent inflammation [1], with an increasing risk of colitis-associated colorectal cancer (CAC) occurring after 8 to 10 years of disease [2]. UC can be further divided into inactive and active states, the latter of which is known to be associated with a stronger immune response. However, the differences of immune cell infiltration between active UC and inactive UC remain unclear, and recent studies have pointed out that there are significant differences between UC and normal mucosa in this regard [3, 4]. Currently, antitumor necrosis factor (TNF) therapy is the first-line treatment for patients with moderate to severe UC [5]. Nevertheless, only two-third of the patients respond to the treatment [6]. Genetic markers are urgently needed to predict individual response to anti-TNF therapy.

Pyroptosis, an inflammatory form of programmed cell death, plays an important role in both tissue homeostasis

and immune response [7]. The gasdermin (GSDM) family proteins serve as the main mediators of pyroptosis, which can be activated by caspase (CASP) family (CASP1/4/5/11) via proteolysis, and induce the formation of GSDM-N, resulting in swelling and lysis [8]. Triggered by certain inflammasomes, pyroptosis releases a large number of inflammatory factors, leading to immune disorders such as autoimmune disease [9]. Pyroptosis also plays a complex role in cancers: on the one hand, pyroptosis can inhibit the oncogenesis and progression of tumors; on the other hand, the inflammatory microenvironment formed by pyroptosis provides suitable conditions for tumor growth [10]. Previous studies have shown that pyroptosis is more associated with the cancers that develop as a result of inflammation, such as liver cancer [11], esophageal cancer [12], and colorectal cancer (CRC) [12]. Accounted for approximately 5% of CRC cases, CAC is developed from chronic UC [13]. Given the existing findings, pyroptosis plays a potentially important role in the inflammatory processes; however, the mechanism of pyroptosis in UC, the relationship between pyroptosis and CAC, and the clinical value of pyroptosis-related genes (PRGs) remain unknown.

The prognostic value of PRGs in cancers (such as breast cancer [14], lung cancer [15], and glioma [16]) has been extensively studied in recent years, whereas the value of PRGs remains unclear in UC. Biomarkers or gene signatures are of great importance in predicting disease, and more and more studies applied various methods to explore the significant biomarkers. For example, weighted gene coexpression network analysis (WGCNA) can search gene modules with coexpression and identify the correlations between the modules and phenotypes [17]. Logistic regression is often used to explore the risk factors that cause disease and predict the probability of disease occurrence based on the risk factors [18].

In this study, we comprehensively evaluated the expression profiles of PRGs and obtained the immune landscape between active and inactive UC. WGCNA and logistic regression analysis were applied to generate the pyroptosis-related signature (PR-signature) and PR-Score, which were significantly associated with active UC. We demonstrated that the PR-Score had a powerful diagnostic capability for active UC. Also, we reported the associations of the PR-signature with the anti-TNF therapy response and the occurrence of CAC. The levels of the PR-signature genes were validated in cell and animal models that mimic UC/CAC pathologies in vitro and in vivo. Our study will help clarify the role of pyroptosis in the progression and treatment of UC, thus optimizing personalized treatment.

2. Materials and Methods

2.1. Dataset Collection. The workflow of our study is shown in Figure 1. The Gene Expression Omnibus (GEO) database (http://www.ncbi.nlm.nih.gov/geo/) was used to download the microarray datasets. Detailed information of all datasets and included samples is shown in Table S1. Briefly, GSE13367, GSE38713, GSE48958, and GSE53306 were consisted of the training set, including 53 normal, 54 active UC, and 44 inactive UC colon mucosa samples. The "sva" R package was used to remove batch effects between different datasets. Principal component analysis (PCA) was used to detect the results by "prcomp" R function (Figure S1). Additionally, GSE75214 and GSE94648 were selected as validation sets. The GSE75214 contained 22 normal, 74 active UC, and 23 inactive UC mucosa samples, and the GSE94648 included 17 active UC and 8 inactive UC blood samples. Moreover, GSE111889 was obtained for clustering validation, including 73 UC mucosa samples.

To analyze the correlation between the PR-Score and therapy response, we searched several datasets with UC patients treated with anti-TNF agents, including GSE92415 (golimumab), GSE16879 (infliximab), and GSE23597 (infliximab).

Furthermore, to analyze the relationships of the PR-signature with CAC and CRC, two CAC datasets (GSE4183 and GSE47908) from human tissues and a mouse model of colitis-cancer (GSE31106) were collected. And two CRC cohorts with survival information of patients, GSE39582 and TCGA-COAD (The Cancer Genome Atlas—colon adenocarcinoma, https://portal.gdc.cancer.gov/), were also included.

2.2. Single-Sample Gene-Set Enrichment Analysis (ssGSEA). The relative abundances of 28 immune cells in the colon mucosa tissue of normal control and active/inactive UC were calculated by ssGSEA. Besides, we selected some representative gene sets for inflammatory pathways from MSigDB (http://www.broad.mit.edu/gsea/msigdb/). The signatures of tumor immune-related pathways were collected from previous research [19]. The ssGSEA algorithm was also used to calculate the enrichment scores of these gene sets or signatures via the "GSVA" R package.

2.3. Identification of Differentially Expressed PRGs. Seventy-five PRGs were retrieved from previous publications [20, 21], and they were presented in Table S2. The "limma" R package was used to identify differentially expressed genes between active UC samples and inactive UC samples from PRGs. Those genes with the threshold adjusted P value $(\text{adj}.P) < 0.05$ and $|\log 2\,(\text{fold change})| \geq 1.0$ were selected as differentially expressed PRGs.

2.4. Construction of WGCNA and Identification of PR-Signature. The training set was used to a coexpression network via the "WGCNA" R package. At first, Pearson's correlation matrices were calculated for all paired genes and a weighted adjacency matrix was constructed. A value of $\beta = 5$ scale ($R^2 = 0.88$) was applied to build a scale-free network (Figure S2). Then, the adjacency matrix was converted to a topological overlap matrix (TOM) to prepare for hierarchical clustering analysis [22]. The gene modules were identified using a dynamic tree cut algorithm with a minimum size of 30, and gene modules were clustered according to the cutoff value of 0.32. The key module was identified by both the highest absolute value of module significance (MS), and the correlation between active UC and module eigengene (ME). Meanwhile, the hub genes in the key module were selected by a cutoff of the absolute value of Pearson's correlation $(|\text{cor.Standard}|) > 0.55$. By intersecting with the differentially expressed PRGs, the

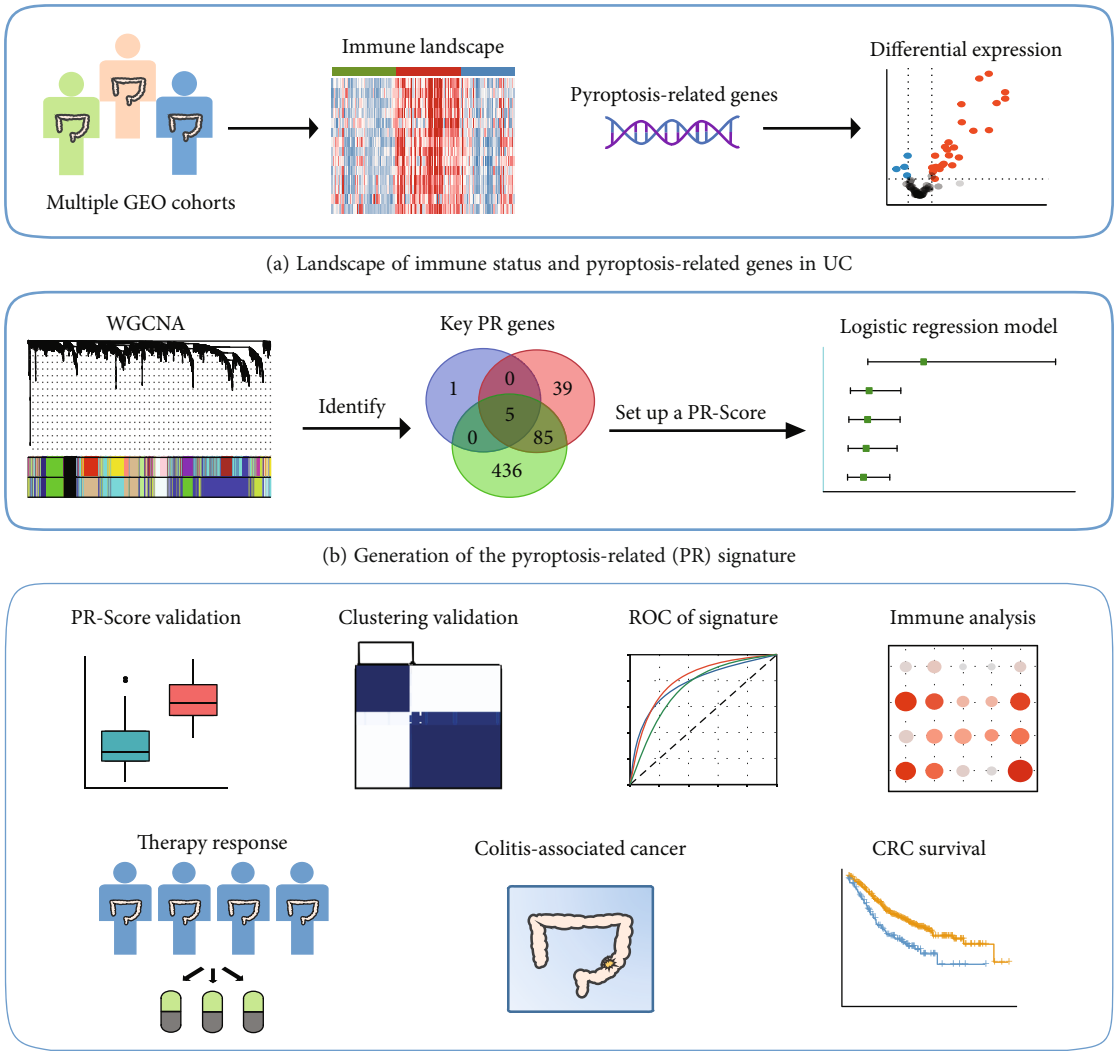

Figure 1: Research flow chart of this study. UC: ulcerative colitis; GEO: Gene Expression Omnibus; PR: pyroptosis-related; WGCNA: weighted gene coexpression network analysis; ROC: receiver operating characteristic; CRC: colorectal cancer.

overlapping genes were identified as key PRGs and composed a pyroptosis-related signature (PR-signature).

2.5. Generation of Logistic Regression Model and Pyroptosis-Related Score (PR-Score). Univariate logistic regression analysis was used to validate the diagnostic abilities of the PRGs in the PR-signature for active UC. Based on the PR-signature genes, multivariate logistic regression model was constructed to establish a PR-Score using the training set.

The PR-Score was calculated as follows:

$$\mathrm{PR-Score} = \Sigma\left(\mathrm{Expi} * \mathrm{Coefi}\right) + b, \tag{1}$$

where Expi, Coefi, and b denote expression of each gene, the risk coefficient, and the constant term in the logistic regression equation, respectively.

Based on the median of PR-Score, patients with UC could be separated into high- and low-PR-Score groups for further analysis.

2.6. Consensus Clustering Analysis of UC Samples. Based on the expressions of the PR-signature genes, we used consensus unsupervised clustering to classify UC patients into clusters to investigate whether the PR-signature can distinguish active UC from inactive UC. The "ConsensusClusterPlus" package was used to perform the above steps [23]. The key operating parameters included 80% item resampling, a maximum evaluated k of 9, and 1000 repetitions for guaranteeing the stability of classification.

2.7. Cell Line and Treatment. Normal colon mucosal epithelial cell line NCM460 was purchased from the China Center for Type Culture Collection (Wuhan, China), and cells had been authenticated for STR profiling and tested for mycoplasma by the vendor. All the cells were cultured in RPMI 1640 medium (HyClone, USA) containing 10% fetal bovine serum (FBS, HyClone, USA), 100 U/ml penicillin, and 100 mg/ml streptomycin (Genom, China), at 37°C with 5% CO_2. 50 ng/ml TNF-α (PeproTech, USA) treated cells for

24 h to construct a cell model that mimics the active UC pathology in vitro.

2.8. Quantitative Reverse Transcription Polymerase Chain Reaction (qRT-PCR) Assays. Total RNA was extracted from NCM460 using TRIzol reagent (Invitrogen, Carlsbad, CA, USA). RNA quantity was determined by NanoDrop 2000c (Thermo Scientific, Waltham, MA, USA). For qRT-PCR, 1 μg RNA was reverse transcribed to cDNA using a Reverse Transcription Kit (Toyobo, Osaka, Japan). The qRT-PCR assays were conducted on LightCycler® 96. Target gene expression was normalized against GAPDH. The expression levels of mRNA were calculated using the comparative CT (2-$\Delta\Delta$CT), and all experiments were performed with three biological replicates. The primer sequences are listed in Table S3.

2.9. The Models of DSS-Induced Colitis and AOM/DSS CAC. Nine male C57BL/6 mice, aged 8 weeks, were purchased from the Beijing Vital River Laboratory Animal Technology Company (Beijing, China). All mice were housed in specific pathogen-free conditions at the Animal Experimental Center of Zhongnan Hospital of Wuhan University. Mice were grouped into DSS- (dextran sulfate sodium-) induced colitis model and AOM (azoxymethane)/DSS-induced CAC model. The detailed processes of establishing the models were carried out as previously described [24–26]. Briefly, 3% DSS was added to the drinking water to induce colitis for 7 consecutive days. On day 8, the mice were sacrificed, and colon samples were collected. To establish an AOM/DSS model, 8-week-old male mice were administered with a single intraperitoneal injection (i.p.) of 10 mg/kg AOM (Sigma-Aldrich, MO, USA), followed by seven days of regular diet and water ad libitum. Mice were then administered with three cycles of 1.5% DSS (Sigma-Aldrich, MO, USA) for seven days and drinking water for 14 days. After three cycles, they were sacrificed, and colon samples were collected.

All animals received humane care, and the study protocol was approved by the Animal Ethics Committee of Wuhan University (Animal Use Protocol Number: 2019157).

2.10. Mouse Tissue Processing and Immunohistochemistry (IHC). Colon tissues were fixed in 10% neutral-buffered formalin (Sigma-Aldrich, USA) and embedded in paraffin. Tissue sections were sliced from paraffin blocks into 4 μm thick slices. The slices were further used for IHC test.

IHC was used to measure the levels of CASP5, GZMB, GBP1, IL1B, and IRF1 in colonic tissues as previously described [27]. The primary antibodies applied were CASP 5 (1 : 400, Boster, A05259-4), GZMB (1 : 3000, abcam, ab255598), GBP1 (1 : 300; Proteintech, 15303-1-AP), IL1B (1 : 500; abcam, ab283818), and IRF-1 (1 : 400, Cell Signaling Technology, 8478). CASP 5, IL1B, and IRF1 were performed heat-mediated antigen retrieval with Tris/EDTA buffer pH 9.0; others were with citrate buffer pH 6.0. We semiquantified the expression levels of the PR-signature genes using an immune-reactive score (IRS) method [28]. Briefly, the proportion of positively stained cells was graded as 0 (0%), 1 (0-5%), 2 (6-10%), 3 (11-50%), or 4 (51-100%), and the staining intensity was expressed as 0 (none), 1 (weak), 2 (intermediate), or 3 (strong). Both values were multiplied to obtain an IRS between 0 and 12. The evaluation was carried out independently by two observers.

2.11. Statistical Analyses. Receiver operating characteristic (ROC) curve was used to show the diagnostic ability of PR-Score and the clustering ability of PR-signature for distinguishing active UC from inactive UC. The "pROC" R package was used to plot the ROC curve. The "survival" R package was used to investigate the correlation of PR-Score and CRC survival outcomes, and the optimal cutoff point of PR-Score was determined using the "survminer" R package. The correlation between PR-Score and clinicopathologic features was analyzed using the χ^2 test. Unpaired two-tailed Student's t-test or one-way ANOVA was used for more than two comparison groups. The results are expressed as the mean ± SEM at least three replicates. IBM SPSS version 25.0 was used to conduct logistic regression analyses, and other statistical analyses were performed using R version 4.1.0 and GraphPad Prism 9. All results were considered to be statistically significant at $P < 0.05$.

3. Results

3.1. Landscape of Immune Status and Differential Expression of PRGs in UC. We first explored the differences of the immune microenvironment of UC and normal samples. As shown in the heat map (Figure 2(a)), both in the training set and GSE75214, active UC samples had more abundant immune cell infiltration than normal control, while inactive UC was more similar to the normal, showing a status of immune desert. Meanwhile, the enrichment scores of the inflammatory-related pathways showed similar distributions in normal and active/inactive samples as the immune cell infiltration (Figure 2(b)). Active UC was not only active in the pathways of inflammatory response as well known, but also in IL6-JAK-STAT3 signaling, interferon-α/γ response, and TNF-α signaling via NF-κB. In contrast, these pathways were silent in the inactive UC, similar to the status of normal tissues.

Next, to investigate the relationship of pyroptosis and the occurrence of active UC, there were 75 PRGs involved in the study. Differentially expressed analysis (active UC vs. inactive UC) identified 30 PRGs with altered expression in the training set, where only a few genes were downregulated while a large proportion of them was upregulated (Figure 2(c) and Table S4), indicating upregulation of the pyroptosis regulators was more related to active UC. The levels of the altered PRGs in normal and inactive UC were similar, but significantly different from the active UC (Figure 2(d)). In GSE75214, these altered PRGs also showed consistent regulatory trends (Figures 2(e) and 2(f) and Table S5). Together, we found that the trends of PRG alteration were similar to the trends of immune status in UC, suggesting pyroptosis was correlated with the progression of UC.

3.2. Generation of PR-Signature and PR-Score. A WGCNA was then constructed to explore the crucial genes related to active UC. We identified ten modules in the module

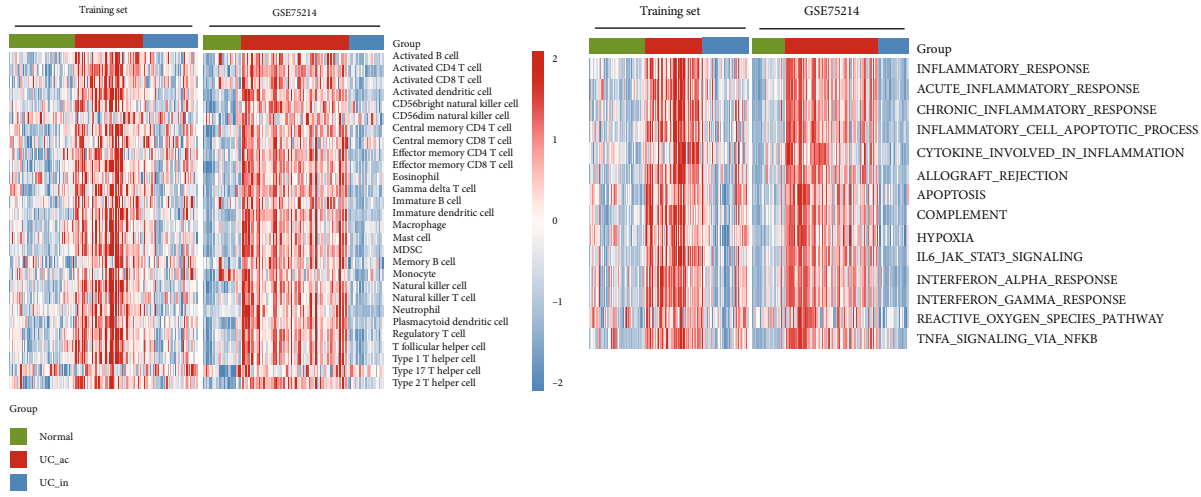

Figure 2: Continued.

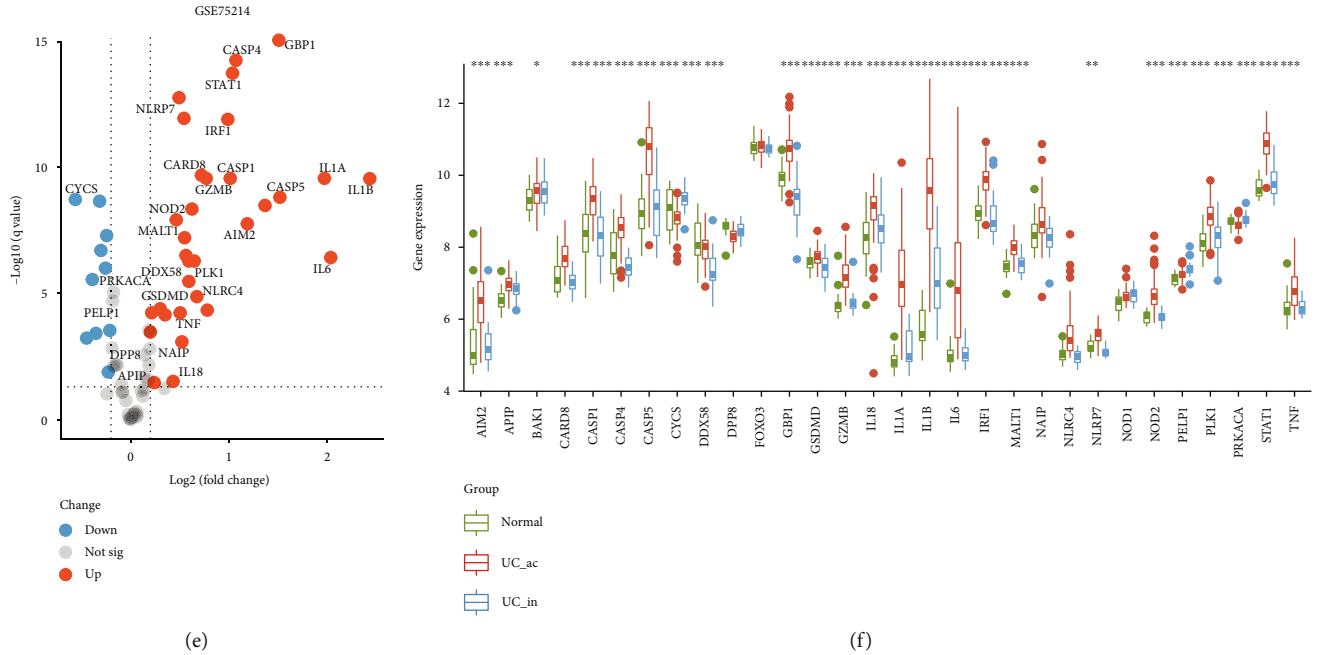

(e) (f)

Figure 2: Landscape of immune status and pyroptosis-related genes (PRGs) in UC. (a) The distributions of 28 immune cells in normal and active/inactive UC samples. Red represents abundant infiltration and blue represents immune cell desert. (b) GSVA showed the distributions of the inflammation-related pathways in normal and active/inactive UC samples. Red represents activation of biological pathways and blue represents inhibition of biological pathways. (c) The volcano plot displayed the expression changing information of 75 PRGs between active UC and inactive UC samples in the training set. (d) Expression distributions of the 30 altered PRGs in normal and active/inactive UC samples in the training set. (e) The volcano plot showed the expression changing information of 75 PRGs between active UC and inactive UC samples in GSE75214. The marked genes are the 30 altered PRGs in the training set. (f) Expression distributions of the 30 altered PRGs in normal and active/inactive UC samples in GSE75214. UC: ulcerative colitis; ac: active; in: inactive. $^{*}P < .05$, $^{**}P < .01$, $^{***}P < .001$, and $^{****}P < .0001$. ns: not significant.

classification through WGCNA (Figure 3(a)). The ME showed the greenyellow module was most positively relevant to the active UC ($r = 0.73$, $P = 2e - 17$) (Figure 3(b)). In addition, the MS of the greenyellow module was higher than other modules (Figure 3(c)). Thus, our data indicated that the greenyellow module was the most associated with the occurrence of active UC. Meanwhile, under the absolute value of Pearson's correlation coefficients (|cor. Standard|) higher than 0.55 (Table S6) and $|\log 2\,(\text{fold change})| \geq 1.0$ of differential expression analysis for PRGs as mentioned above, a Venn diagram identified CASP5 (caspase 5), GBP1 (guanylate binding protein 1), GZMB (granzyme B), IL1B (interleukin 1 beta), and IRF1 (interferon regulatory factor 1) (Figure 3(d)) as key PRGs to compose a PR-signature.

Then, to confirm the PR-signature has a remarkable positive correlation with active UC, univariate logistic regression analysis was conducted for the PR-signature genes both in the training set and GSE75214 (Figures 3(e) and 3(f) and Table S7). Results showed that all 5 PR-signature genes could predict active UC well. Based on the PR-signature genes, multivariate logistic regression model was constructed to develop a PR-Score to distinguish active UC and inactive UC samples using the training set. The PR − Score = CASP5* (0.562) + IL1B* (0.956) + GZMB* (0.419) + IRF1* (0.885) + GBP1* (0.650) − 19.461.

3.3. Validation of the Performances of the PR-Score in UC. In order to validate the performance of PR-Score in UC, several datasets were used for analysis. Both in the training set and GSE75214, PR-Scores were significantly higher in the group of active UC than the inactive UC (Figures 4(a) and 4(b)). Interestingly, in GSE94648, a set with blood samples, PR-Score was also significantly high in the active UC, indicating PR-Score in blood also can distinguish the samples with active UC from the inactive UC (Figure 4(c)). The ROC curve showed that PR-Score had a great power in diagnosing active UC in three datasets, all with AUC > 0.8 (Figure 4(d)). In addition, PR-Score had a strong positive correlation with the Mayo score in GSE92415 (Figure 4(e)) and GSE94648 (Figure S3(a)). The Mayo score is an indicator of the severity of UC based on the endoscopic presentation, and higher score indicates severer disease [29]. As for other clinicopathologic features, PR-Score was associated with the lesion location of UC (Table S8-9).

Since the GSDM family genes play important roles in pyroptosis [8], we next analyzed the correlations of PR-Score and the GSDM family members. As shown in Figure 4(f), we observed that PR-Score was most positively associated with the expression of GSDMD, which was identified as the most important pyroptosis executioner among the GSDM genes [30].

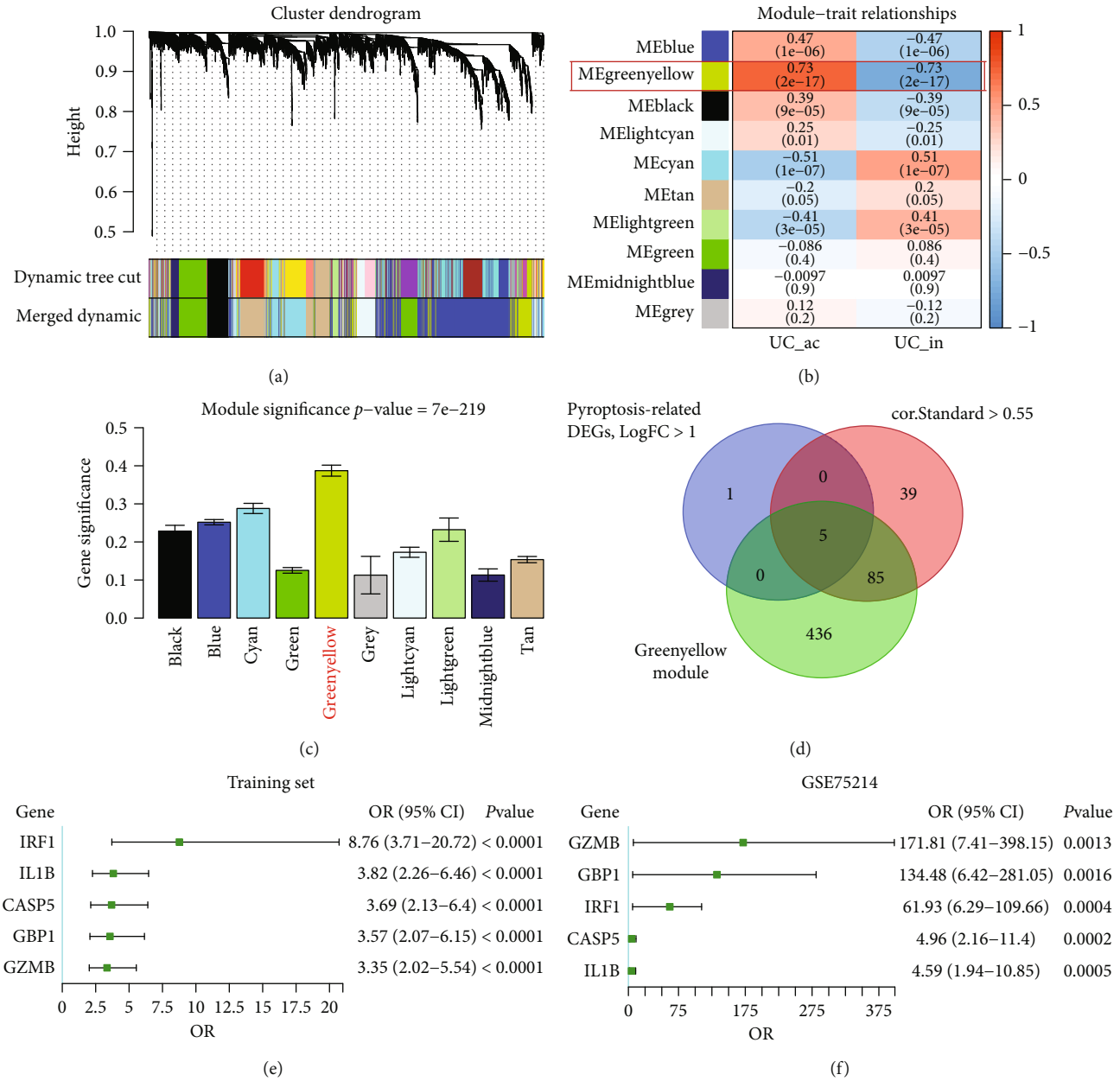

Figure 3: Identify the key PRGs and establish the PR-Score. (a) Module clustering dendrogram based on a dissimilarity measure (1-TOM). (b) Heat map of the correlations between MEs and active/inactive UC. (c) Distributions of average gene significance and errors in the modules related to active ulcerative colitis. (d) Venn diagram showed the overlapping genes between differentially expressed PRGs, the genes of greenyellow module, and the genes with |cor.Standard| >o.55 in WGCNA. Logistic regression analysis for the key PRGs in the training set (e) and GSE75214 (f). ME: module eigengene; UC: ulcerative colitis; ac: active; in: inactive; DEGs: differentially expressed genes; OR: odds ratio.

In terms of affecting immune status, we found that PR-Score was significantly positively related to immune cell infiltration, including neutrophils, myeloid-derived suppressor cells, activated CD4 T cells, and regulatory T cells (Figure 4(g)), which indicated that PR-signature genes could be involved in the inflammation of UC by regulating pyroptosis of these cells. Meanwhile, PR-Score had positive correlations with multiple inflammatory pathways (Figure 4(h)), among which the IL6-JAK-STAT3 signaling, interferon-α/γ, and chronic inflammatory response were most significant.

3.4. PR-Signature Was an Effective Classifier for Active/Inactive UC and Inflamed/Uninflamed Immune Status. By means of unsupervised clustering, we validated the classification ability of PR-signature for active and inactive UC patients. Based on the PR-signature genes, UC patients were reclassified into two clusters (Figure 5(a) and Figure S3 (b, d)). Notably, we found that the major proportion of cluster 2 (C2) was active UC, while the major proportion of cluster 1 (C1) was inactive UC (Figure 5(b) and Figure S3(e)). As the heat map shows (Figure 5(c)), active UC, higher PR-

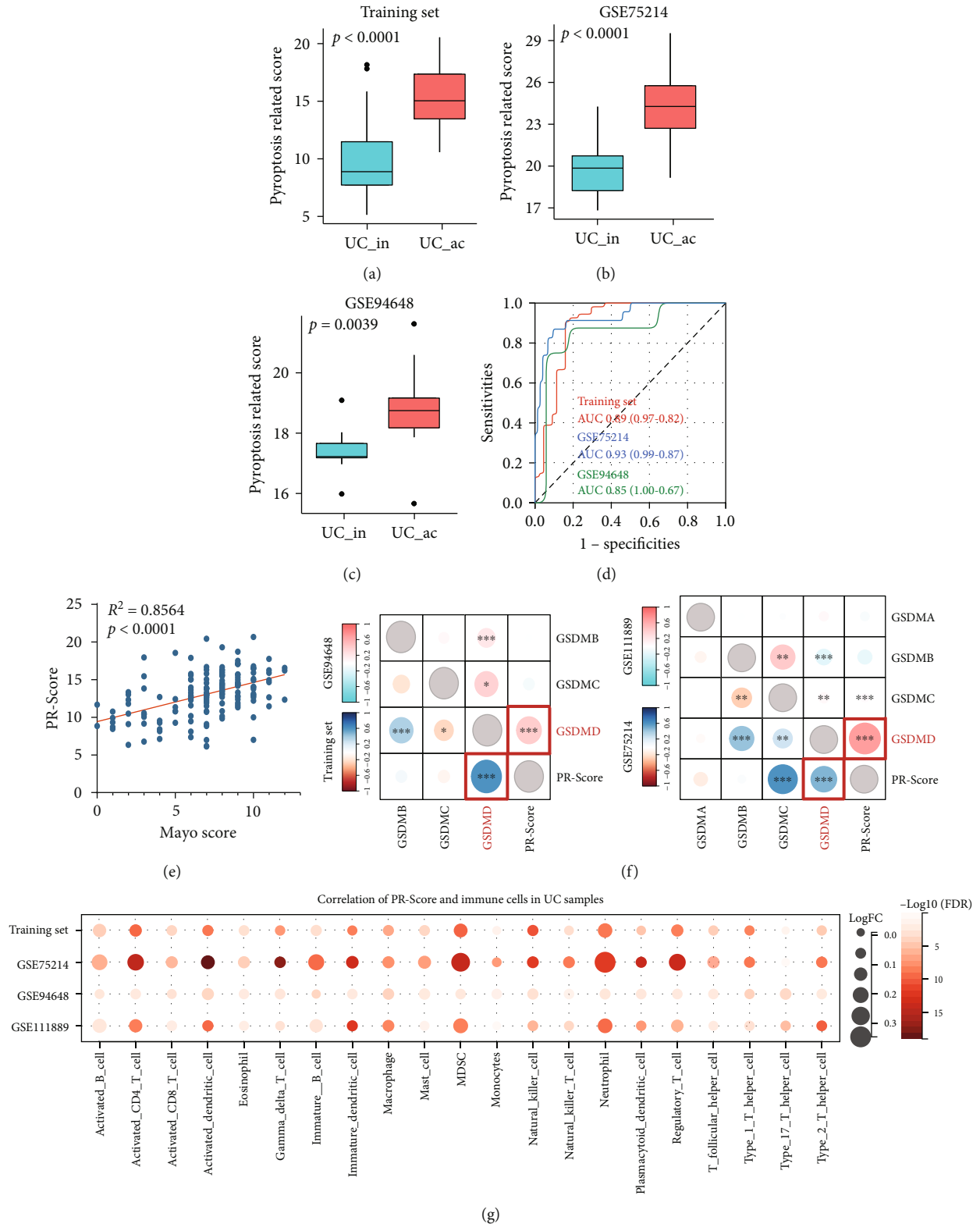

Figure 4: Continued.

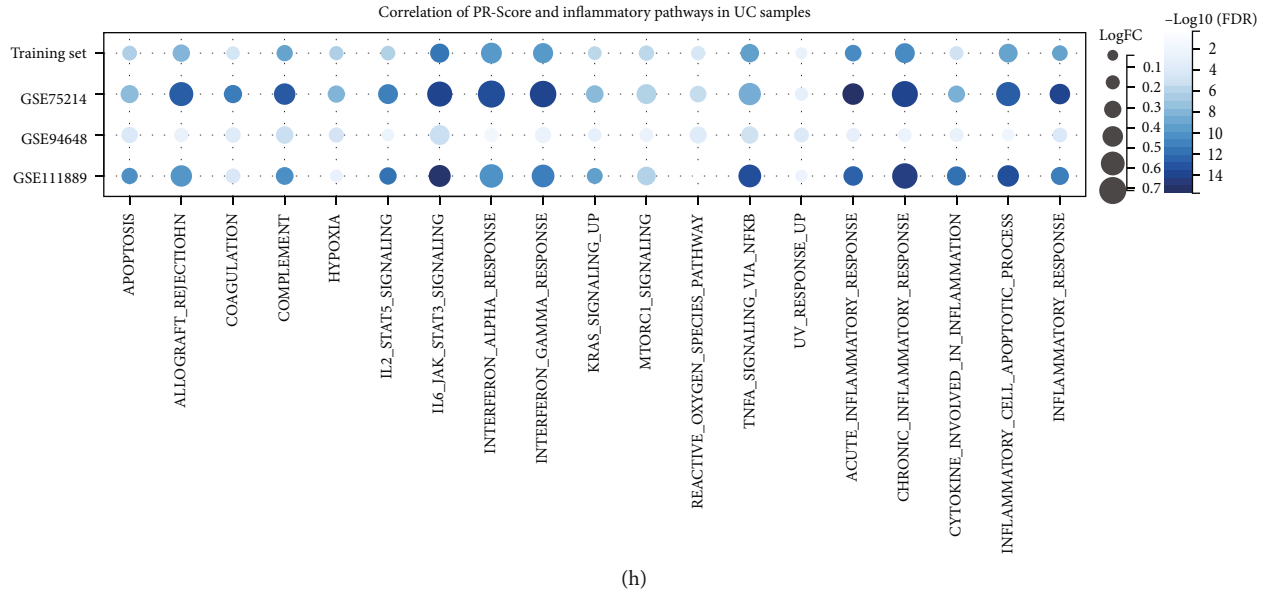

(h)

Figure 4: Correlation between PR-Score, expression of GSDM family members, and immune status. Differences of the PR-Score in active UC and inactive UC samples in the training set (a), GSE75214 (b), and GSE94648 (c). (d) The ROC curve showed the diagnostic efficiency of the PR-Score in three datasets. (e) The correlation of the PR-Score and Mayo score in GSE92415. (f) PR-Score was most positively associated with the expression of GSDMD in all datasets (left: the training set and GSE94648; right: GSE75214 and GSE111889). (g) Correlations of PR-Score and immune cells in UC samples in four datasets. (h) Correlations of PR-Score and inflammation-related pathways in UC samples in four datasets. UC: ulcerative colitis; ac: active; in: inactive; AUC: area under the curve. $^{*}P < .05$, $^{**}P < .01$, $^{***}P < .001$, and $^{****}P < .0001$. ns: not significant.

Score, and higher expressions of the PR-signature genes were more likely to concentrate in C2 than C1, so we suggested C2 might represent the samples with active UC in the clustering. The ROC curve revealed that the PR-signature also had good diagnostic capability for active UC (Figure 5(d)), but it was slightly inferior to PR-Score (Figure 4(d)). As shown in Figures 5(e) and 5(f), the samples in C2 had more abundant infiltration of immune cells and higher enrichment scores of the inflammation-related pathways than C1 across three datasets, so we defined C2 as the inflamed class while C1 as the uninflamed class in UC. Also, this finding further confirmed the differences of immune status between active and inactive UC.

Likewise, the patients in GSE111889 were not distinguished between active and inactive UC, but we found that the UC samples could also be well classified into two clusters based on the PR-signature (Figure 5(g) and Figure S3(f)). The UC samples in C2 had higher expressions of the PR-signature genes and higher PR-Scores than C1 (Figures 5(h) and 5(j)). Based on the knowledge from the results above, this C2 was closer to active UC. Besides, compared with C1, C2 had more abundant infiltration of immune cells and higher enrichment scores of inflammation-related pathways at the same time (Figures 5(k) and 5(l)). Therefore, C2 was reasonably identified as the inflamed class while C1 was the uninflamed class. Collectively, the clustering of C2 and C1 was likely equivalent to the classification of active and inactive UC, respectively. And the ROC curve showed that PR-Score could distinguish C1 and C2 well (Figure 5(m)). Collectively, the PR-signature could serve as an effective classifier for active/inactive UC and inflamed/uninflamed status.

3.5. Lower PR-Score Was Associated with a Better Response to Anti-TNF Therapy for Patients with UC. Anti-TNF agents are widely used to treat UC, but the effects vary from person to person [31]. We next investigated the relationship of PR-Score with the anti-TNF therapeutic response. Based on the GSE92415 dataset, PR-Score did not differ between placebo groups (Figure 6(a)) but was lower in the responders than in the nonresponders after 6 weeks of golimumab treatment (Figure 6(b)). Similarly, in GSE16879, both before and after infliximab (IFX) treatment, PR-Score was lower in the responders but higher in the nonresponders (Figure 6(c)). And interestingly, PR-Score was decreased after IFX treatment compared with before treatment, which was more significant in the responders (Figure 6(d)). Importantly, in GSE23597, PR-Score was significantly lower in the responders than the nonresponders, despite of dose or time administration (Figures 6(e) and 6(f)). In summary, the responders in anti-TNF treatment had lower PR-Score and PR-Score showed a decline after anti-TNF treatment. These findings suggested that the PR-signature genes were connected to the anti-TNF therapy and PR-Score could predict the anti-TNF therapeutic responses.

3.6. High PR-Score Suppressed the Occurrence of CAC and Improved the Survival Outcomes for Patients with CRC. We

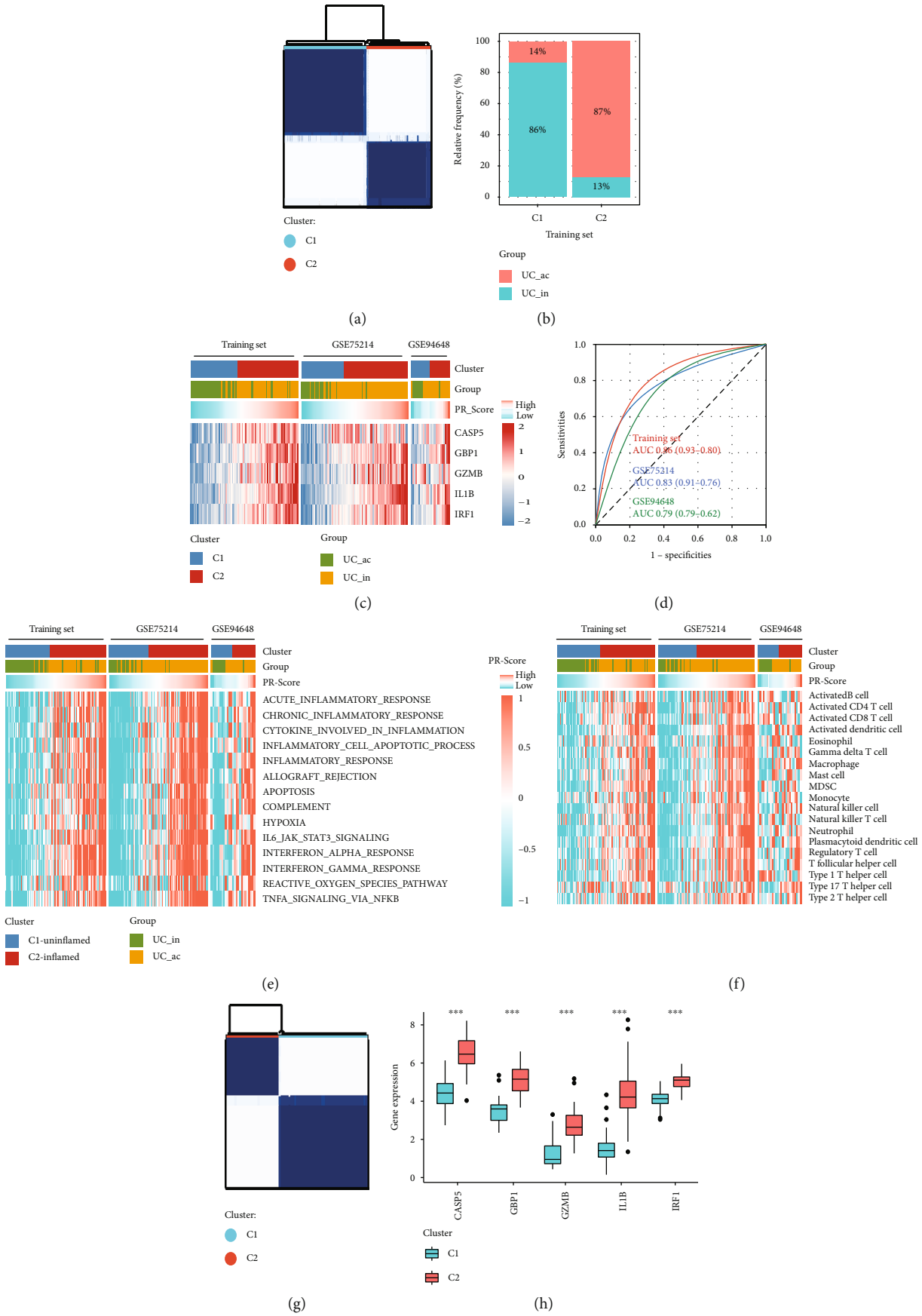

Figure 5: Continued.

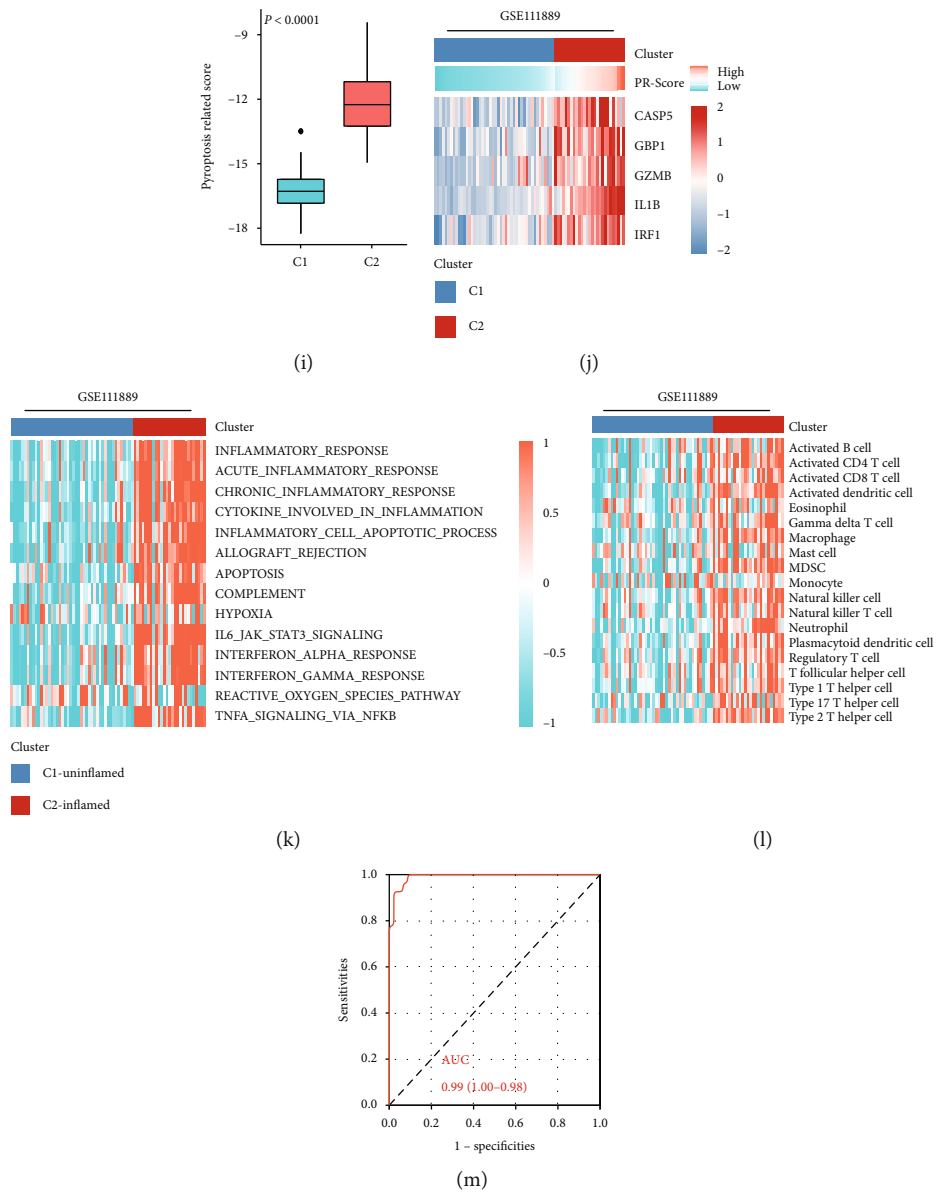

Figure 5: The capacity of PR-signature in classifying active/inactive UC and inflamed/uninflamed immune status. (a) Based on the PR-signature, UC samples of the training set were reclassified into two clusters using unsupervised consensus clustering. (b) Distributions of two clusters in active UC and inactive UC. (c) Distributions of active/inactive UC samples, PR-Score, and expression of the five key PRGs in two clusters. (d) The ROC curve showed the diagnostic efficiency of the PR-signature in three datasets. (e) Differences of activation of inflammatory-related pathways in two clusters. (f) Differences of immune cell infiltration in two clusters. (g) UC samples of GSE111889 were classified into two clusters based on the PR-signature using unsupervised consensus clustering. (h) Expression differences of the five key PRGs in two clusters. (i) Differences of the PR-Score in two clusters. (j) Distributions of PR-Score and expression of the five key PRGs in two clusters. (k) GSVA showed the distributions of the inflammatory-related pathways in two clusters. Orange represents activation of biological pathways and blue represents inhibition of biological pathways. (l) The distributions of immune cells in two clusters. Orange represents abundant infiltration and blue represents immune cell desert. (m) The ROC curve showed the diagnostic efficiency of the PR-signature for two clusters. UC: ulcerative colitis; ac: active; in: inactive; AUC: area under the curve.

next analyzed the associations of PR-Score with occurrence of CAC and tumor immunity of CRC. Notably, PR-Score was lower in adenoma and CRC compared with IBD tissues in GSE4183 (Figure 7(a)). Consistently, in GSE47908, PR-Score was also lower in UC-dysplasia than colitis samples (Figure 7(b)). In addition to these findings, in GSE31106, a mouse model, PR-Score was negatively correlated with the progressions from inflamed dysplasia to adenocarcinoma (Figure 7(c)). In brief, PR-Score was decreased in the samples with UC-related CRC, inferring the PR-signature genes might protect body from UC-associated cancer occurring. Meanwhile, PR-Score was positively correlated with the expressions of the molecules that suppress CAC/CRC but had no significant correlations with the tumor-promoting

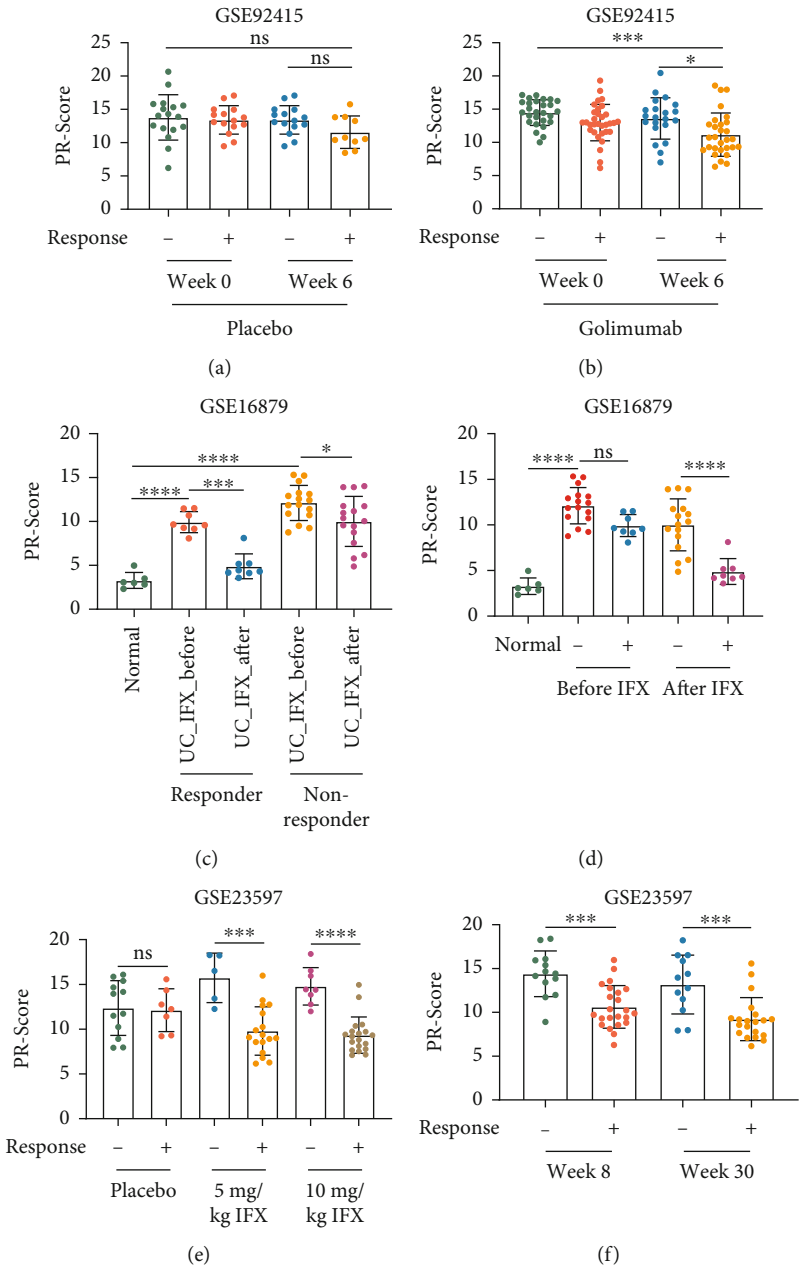

Figure 6: Differences of the PR-Score in responders/nonresponders with anti-TNF treatment. Based on the GSE92415 dataset, UC patients were treated with placebo (a) and golimumab (b) for 6 weeks, respectively. The PR-Score was compared. According to the GSE16879 dataset, the PR-Score was compared between UC patients before and after IFX treatment (c), or between responders and nonresponders (d). Based on the GSE23597 dataset, compare the effects of IFX doses (e) and the time of IFX administration (f) on the PR-Score in patients with IFX response. UC: ulcerative colitis; IFX: infliximab. $^{*}P < .05$, $^{**}P < .01$, $^{***}P < .001$, and $^{****}P < .0001$. ns: not significant.

molecules (Figures 7(d) and 7(e)). AIM2 was the most significant among the molecules both in UC and CRC samples. These data provided further evidences that PR-signature could inhibit tumorigenesis. In the patients with CRC, PR-Score was associated with the clinicopathologic features such as tumor stage, lymphatic invasion, and KRAS mutation (Table S10-11). Additionally, it is worth noting that higher PR-Score inferred better overall survival (OS) and disease-free survival (DFS) outcomes, which were consistent in the TCGA and GSE39582 cohorts (Figures 7(f) and 7(g)), also indicating that the PR-signature genes tended to play roles in suppressing CRC. The PR-Score had no significant difference between normal and tumor tissues (Figure 7(h)). By analyzing tumor immune-related pathways, we found that the pathways including "expanded immune," "APC costimulation," and "T cell costimulation" were significantly active in the high-PR-Score group; and the immune molecules including HLA, checkpoint, and CD8 T cell effector were also more active in the high-PR-Score group (Figure 7(i)). Together, the PR-signature played a potential

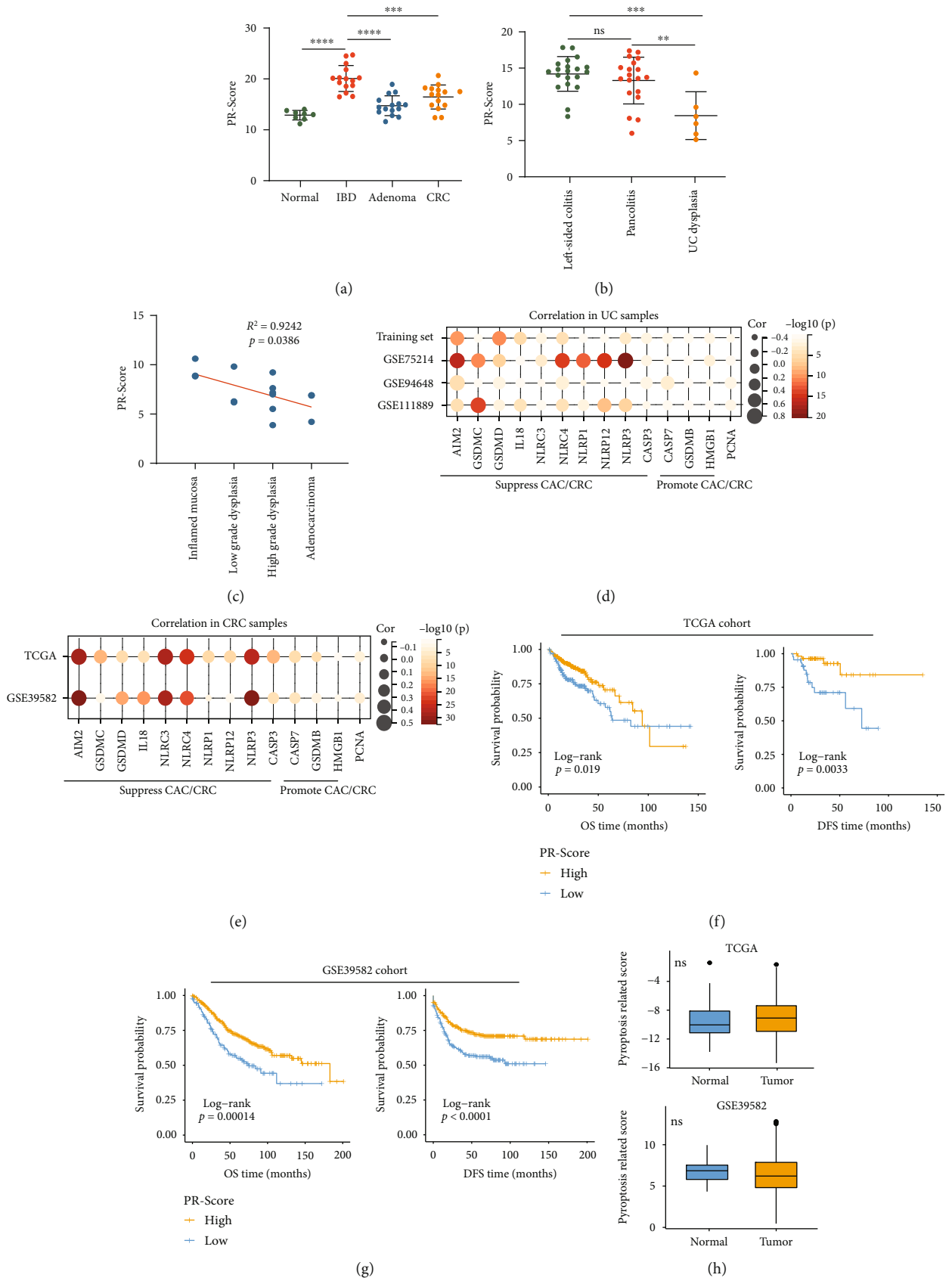

Figure 7: Continued.

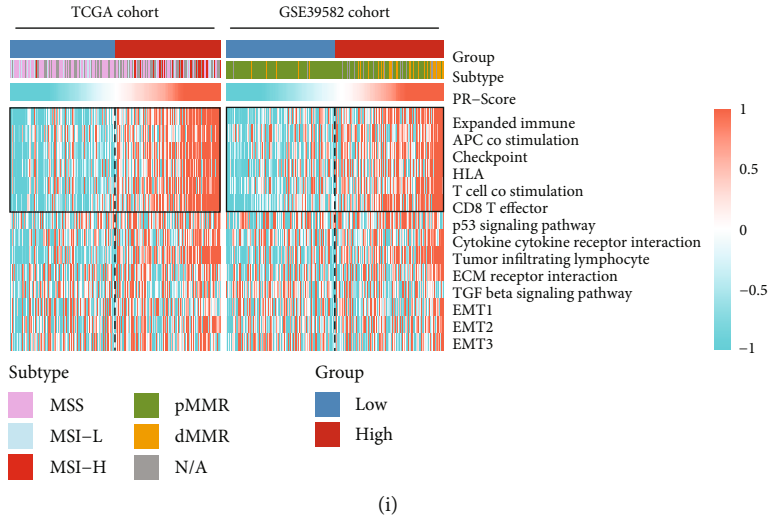

(i)

Figure 7: Relationships between the PR-Score/PR-signature, colitis-associated colorectal cancer (CAC), and colorectal cancer (CRC). (a) Comparison of the PR-Score in normal, IBD, adenoma, and CRC tissues using GSE4183. (b) Comparison of the PR-Score in colitis and UC-dysplasia tissues using GSE47908. (c) Correlation of the PR-Score and the progression from inflamed dysplasia to adenocarcinoma. Correlation of the PR-Score and the molecules that suppress/promote tumors in UC samples (d) and CRC samples (e). The effect of PR-Score on the OS and DFS of CRC in TCGA (f) and GSE39582 (g). (h) Differences of PR-Score between normal and tumor in TCGA and GSE39582. (i) Correlations of the PR-Score and the tumor immune-related pathways and CRC subtypes in TCGA and GSE39582. IBD: inflammatory bowel disease; CAC: colitis-associated colorectal cancer; CRC: colorectal cancer; UC: ulcerative colitis; OS: overall survival; DFS: disease-free survival; MSS: microsatellite stability; MSI-H: high microsatellite instability; MSI-L: low microsatellite instability; pMMR: proficient-mismatch-repair; dMMR: deficient-mismatch-repair; N/A: not applicable. $^{*}P < .05$, $^{**}P < .01$, $^{***}P < .001$, and $^{****}P < .0001$. ns: not significant.

antitumor role in CRC progression. The heat map also displayed the distribution of the subtypes of CRC between the high- and low-PR-Score groups (Figure 7(i)). The MSI-H/dMMR (high microsatellite instability/deficient-mismatch-repair) CRC was more likely to concentrate in the high-PR-Score group, while the MSS/pMMR (microsatellite stability/proficient-mismatch-repair) was more likely to concentrate in the low-PR-Score group, indicating the PR-signature was related to the microsatellite instability.

3.7. Validation of the Levels of the PR-Signature Genes In Vitro and In Vivo. Since the above conclusions were based on bioinformatics analysis, further validation was required to provide sufficient proof that the PR-signature was positively associated with the occurrence of the active UC but negatively correlated with the development of CAC. Thus, we validated these results in vitro and in vivo experiments. As shown in Figure 8(a), the expressions of CASP5, GBP1, GZMB, IL1B, and IRF1 were significantly upregulated in the TNF-α-stimulated NCM460 cells. Meanwhile, we also compared the associations of the PR-signature genes and the occurrence of UC and CAC in mouse models. The results showed that the protein levels of CASP5, GBP1, GZMB, IL1B, and IRF1 were significantly increased in the active UC tissues compared with normal controls while markedly reduced in CAC tissues compared to UC (Figures 8(b) and 8(c) and Figure S4). These data confirmed that the high level of PR-signature was associated with the occurrence of UC and suppression of CAC.

4. Discussion

Active UC and inactive UC are two different clinical stages of disease, and our study revealed the distinctions in the immune microenvironment between them. As a proinflammatory cell death, pyroptosis was potentially involved in the progression of inactive UC to the active stage. In this study, we generated a PR-Score/PR-signature that was associated with the occurrence of active UC and could distinguish active UC from inactive UC well. The PR-Score/PR-signature consisting of CASP5, GBP1, GZMB, IL1B, and IRF1 was closely related to the immune status, anti-TNF therapy response, and CAC suppression. Our findings may provide new markers for predicting the development of active UC and CAC and new targets for individualized treatment of UC patients.

One of the PR-signature genes identified by our study, IL1B, is a proinflammatory cytokine that plays an important role in many physiological and pathological processes [32, 33]. Pro-IL1B and GSDMD can be proteolytic processed by activated CASP1, which leads to the formation of the GSDMD pore, the release of mature IL1B, and eventually pyroptosis [34]. Li et al. clarified that activation of NF-κB signaling can exacerbate colonic inflammation in UC by releasing IL1B and inducing intestinal epithelial cell pyroptosis [35]. Therefore, the role of IL1B in active UC is relatively clear, and our study provides consistent and further evidences. Like CASP1, CASP5 is a member of the caspase family. CASP1 is an important signaling molecule in promoting inflammation in UC [34], but the role of CASP5 in

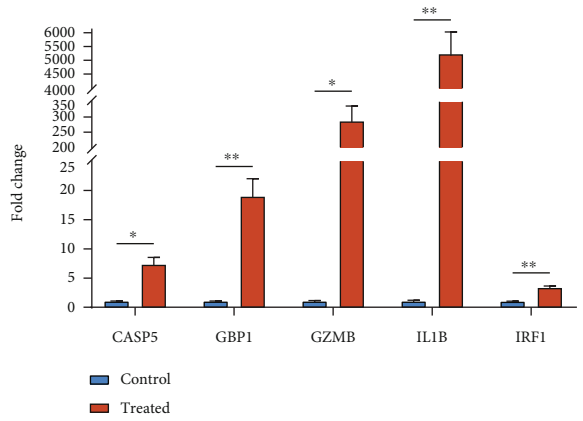

(a)

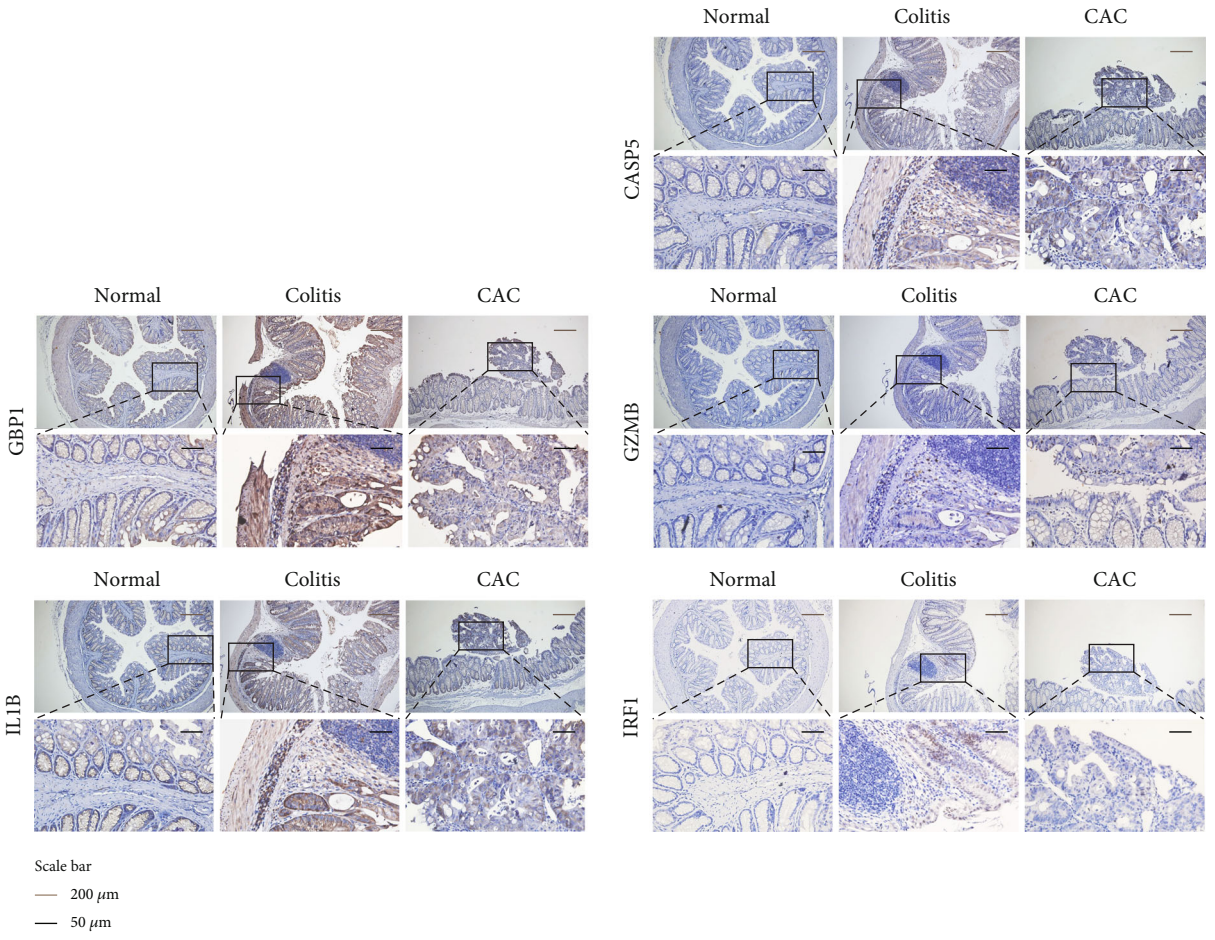

(b)

Figure 8: Continued.

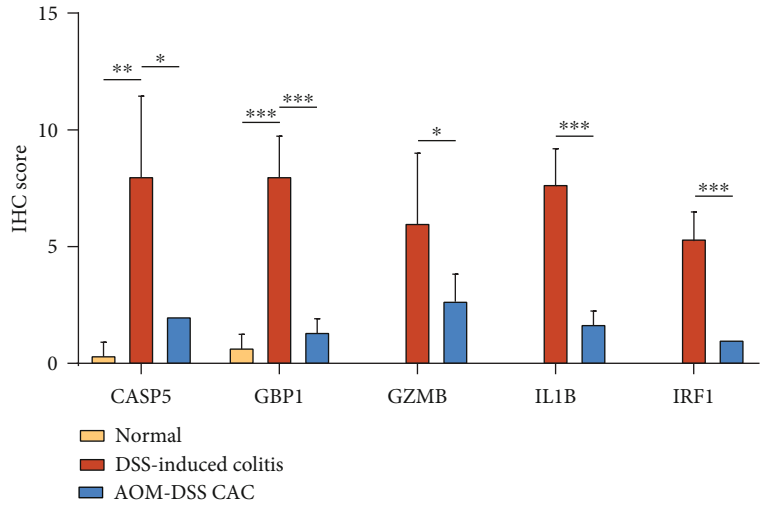

(c)

Figure 8: Validation of the levels of the PR-signature genes in vitro and in vivo. (a) The expressions of 5 PR-signature genes in normal NCM460 cells and TNF-α-stimulated inflammation cells. (b) Representative IHC images showing the expressions of 5 PR-signature genes in normal (left), DSS-induced colitis (middle), and AOM/DSS-induced CAC (right) tissues of mice. (c) Semiquantification of IHC staining of 5 PR-signature genes in normal, DSS-induced colitis, and AOM/DSS-induced CAC tissues of mice. CAC: colitis-associated colorectal cancer; IHC: immunohistochemistry. $^{*}P < .05$, $^{**}P < .01$, and $^{***}P < .001$.

UC is less reported. It is worth mentioning that CASP5 was highly expressed in the stromal compartment of inflammatory UC and CRC tissues [36]. Also, CASP5 is essential for heme-induced IL1B release and the heme-induced activation of CASP5 is a key mediator of inflammation in macrophages [37]. Our study points out that CASP5 was a key pyroptosis regulator associated with the occurrence of active UC, providing more insights for further studies. IRF1 is required for IFNs to induce MHC class I proteins and prime CD8+ T cell responses [38]. IRF1 regulates IL-15 expression and controls the development of NK1+ T cells, NK cells, and CD8+ intestinal intraepithelial lymphocytes [39]. Thus, IRF1 is close to immune activation and inflammatory response. Fang et al. reported that IRF1 was upregulated in pediatric IBD and experimental colitis [40]. During intestinal inflammation, the activation of TNF-α upregulates the expression of IRF1, resulting in aggravating apoptosis of the intestinal epithelial cells [41]. Our study also identified IRF1 as a key pyroptosis molecule involved in the inflammatory activity of UC. GZMB is a member of granzyme (GZM) family and also possesses the cytotoxic activities [42]. GZMB and CASP1 together activate GSDME to cause cell pyroptosis and participate in the inflammatory activity [43]. Significant upregulated expression of GBP1 was found in inflammatory disease such as rheumatoid arthritis [44]. Additionally, Zhang et al. observed that inflammatory macrophage was significantly enriched in severe COVID-19 samples and showed significantly elevated levels of proinflammatory genes, including GBP1 and IL1B [45]. Here, we demonstrated that the five PR-signature genes were highly upregulated in the inflammation cell model and DSS-induced colitis samples. Therefore, the five PR-signature genes were all proven to be positive pyroptosis regulators associated with the occurrence of active UC. Meanwhile, PR-Score was positively correlated with the interferon-α/γ, chronic inflammatory response, and IL6/JAK/STAT3 pathways, further proving that the PR-signature genes helped with inflammation.

This PR-signature contains molecules that are clearly associated with UC inflammation (IL1B, CASP5, and IRF1) as well as novel molecules rarely reported in UC (GZMB and GBP1), which together may better predict and differentiate the active UC from inactive UC. More importantly, we validated the diagnostic power of the PR-signature/PR-Score in multiple datasets, including not only tissue sample sets but also a blood sample set (GSE94648). The PR-signature/PR-Score showed outstanding diagnostic ability and may be utilized to be a novel signature detecting the occurrence of active UC even in blood samples. We also revealed that the PR-Score had a significant positive correlation with GSDMD, which is the most important pyroptosis executioner [8]. Collectively, the PR-signature genes could participate in the development of active UC by mediating pyroptosis, but the specific mechanism still needs further exploration. Many studies have revealed that the pathogenesis of IBD involves various immune cells, such as neutrophil [46], innate lymphoid cells [47], and subsets of CD4+ T cells [48]. Notably, PR-Score was positively correlated with the infiltration of neutrophil, active CD4+ T cells, and regulatory T cell (one subset of CD4+ T cells) in our study, suggesting the PR-signature genes were involved in inflammatory activity of UC by enriching these immune cells. This correlation was weak in the blood samples (GSE94648) on account of the low levels of immune cells in blood.

Another important finding of our study is that PR-Score was significantly associated with the response to anti-TNF treatment. Tang et al. demonstrated that TNF-α blockade can induce macrophage pyroptosis by inhibiting the IRF1

pathway and thus alleviate the inflammatory activity [41]. Anti-TNF-α or an NF-κB signaling pathway inhibitor would reduce the release of cytokines [49]. This can partially explain the decline of PR-Score after IFX and golimumab treatments. The responders of anti-TNF therapy had significantly lower PR-Score than the nonresponders, inferring low PR-Score could enhance and predict the response to anti-TNF antibodies. Consistently, Salvador-Martín et al. revealed [50] that GBP1 was downexpressed in responders compared with nonresponders in UC, and Lykowska-Szuber et al. reported [51] that IL1B was significantly downregulated in responders in Crohn's disease. Therefore, the PR-signature genes were potentially involved in the response process of anti-TNF therapy and can serve as promising predictors for anti-TNF therapy response in UC.

Pyroptosis is usually induced by inflammasome that is an important innate immune pathway [52, 53]. Recent studies demonstrated that inflammasome promote tumor progression in skin and breast cancer [54, 55]. However, on the intestinal mucosal surface, the intestinal barrier function and tumor surveillance depend on activation of inflammasome to product active IL1B and IL18 [52]. Previous studies showed that the inflammasome components provide protection against the development of colon cancer in the CAC model [56, 57]. In our study, PR-Score was negatively associated with the progress of inflamed dysplasia to adenocarcinoma, indicating that the PR-signature played a protective role in CAC. The in vivo experiments in CAC mouse model proved that the levels of PR-signature genes were indeed reduced in the CAC samples compared to UC. Besides, we found that PR-Score was positively correlated with the CAC/CRC inhibitory molecules, among which AIM2 was the most significant. Researches demonstrated that the expression of Aim2 is markedly reduced in tumor-associated tissues of mice, and mice lacking Aim2 are hypersusceptible to both colitis-associated and spontaneous colorectal tumorigenesis [58, 59]. This indirectly confirmed the effect of the PR-signature on suppressing CAC. Our study also found that the high-PR-Score group showed more MSI-H CRC and more active antitumor-related pathways/molecules. Collectively, high-PR-Score may be a protective factor against CRC and thus improve the survival outcomes.

5. Conclusions

In brief, we identified CASP5, GBP1, GZMB, IL1B, and IRF1 as key PRGs and established a novel PR-signature/PR-Score, which had great power to distinguish active UC from inactive UC. The in vitro and in vivo experiments validated that the PR-signature genes were overexpressed in UC pathologies. We also determined the therapeutic liability of the PR-signature genes in anti-TNF treatment for UC patients. The correlations between the PR-signature genes and CAC were clarified using public datasets and the CAC mouse model. Our study provided promising pyroptosis-related biomarkers for predicting the progressions of UC and CAC and guided individualized anti-TNF therapy for UC patients.

Data Availability

Publicly available datasets were analyzed in this study. These data can be found here: https://portal.gdc.cancer.gov/ and https://www.ncbi.nlm.nih.gov/geo/. All processed data and R codes used in this study can be obtained from the corresponding authors on reasonable request.

Conflicts of Interest

No potential conflicts of interest were disclosed.

Authors' Contributions

Y.N., H.W., and F.W. designed the study. K.L. and J.F. collected the data. Y.N. and H.W. analyzed the data. H.W., Q.Z., and J.F. supervised the data and provided statistical advice. Y.N. and K.L. wrote the primary manuscript. X.C., X.H., and L.L. were involved in manuscript modification and medical writing assistance. F.W. and H.W. reviewed the article. All authors read and approved the final manuscript. Yumei Ning, Kun Lin, and Jun Fang contributed equally to this work.

Acknowledgments

This study was funded by the Knowledge Innovation Special Project of Wuhan Science and Technology Bureau (No. 2022020801020490), the Program of Excellent Doctoral (Postdoctoral) of Zhongnan Hospital of Wuhan University (No. ZNYB2019003), the National Natural Science Foundation of China (No. 81870390), and the Engineering Construction Project of Improving Diagnosis and Treatment Ability of Difficult Diseases (oncology) (No. ZLYNXM202017).

Supplementary Materials

Figure S1: the principal component analysis of before and after batch correction of all samples in the training set. Figure S2: determination of soft-thresholding power in the coexpression network. Figure S3: the correlation of the PR-Score and PR-clusters. Figure S4: representative IHC images showing the expressions of 5 PR-signature genes in normal, DSS-induced colitis, and AOM/DSS-induced CAC tissues of mice. Table S1: detailed information of all datasets and included samples. Table S2: summary of 75 recognized pyroptosis-related genes. Table S3: the primer sequences of CASP5, GBP1, GZMB, IL1B, and IRF1. Table S4: differential expression analysis of pyroptosis-related genes in the training set (active UC vs. inactive UC). Table S5: differential expression analysis of pyroptosis-related genes in GSE75214 (active UC vs. inactive UC). Table S6: standard weight of each gene in WGCNA. Table S7: logistic regression analysis for the key PRGs. Table S8: correlation of clinicopathologic characteristics and PR-Score in GSE111889. Table S9: correlation of clinicopathologic characteristics and PR-Score in GSE94648. Table S10: correlation of clinicopathologic characteristics and PR-Score in TCGA. Table S11: correlation of clinicopathologic characteristics and PR-Score in GSE39582. *(Supplementary Materials)*

References

[1] S. C. Ng, H. Y. Shi, N. Hamidi et al., "Worldwide incidence and prevalence of inflammatory bowel disease in the 21st century: a systematic review of population-based studies," *The Lancet*, vol. 390, no. 10114, pp. 2769–2778, 2017.

[2] S. P. Short, J. M. Pilat, C. W. Barrett et al., "Colonic epithelial-derived selenoprotein P is the source for antioxidant-mediated protection in colitis-associated cancer," *Gastroenterology*, vol. 160, no. 5, pp. 1694–1708.e3, 2021.

[3] J.-W. Lu, A. Rouzigu, L.-H. Teng, and W.-L. Liu, "The construction and comprehensive analysis of inflammation-related ce RNA networks and tissue-infiltrating immune cells in ulcerative progression," *BioMed Research International*, vol. 2021, Article ID 6633442, 2021.

[4] B. S. Boland, Z. He, M. S. Tsai et al., "Heterogeneity and clonal relationships of adaptive immune cells in ulcerative colitis revealed by single-cell analyses," *Science immunology*, vol. 5, no. 50, 2020.

[5] B. L. Cohen and D. B. Sachar, "Update on anti-tumor necrosis factor agents and other new drugs for inflammatory bowel disease," *BMJ*, vol. 357, article j2505, 2017.

[6] Bank S, P. S. Andersen, J. Burisch et al., "Associations between functional polymorphisms in the NFκB signaling pathway and response to anti-TNF treatment in Danish patients with inflammatory bowel disease," *The pharmacogenomics journal*, vol. 14, no. 6, pp. 526–534, 2014.

[7] S. B. Kovacs and E. A. Miao, "Gasdermins: effectors of pyroptosis," *Trends in cell biology*, vol. 27, no. 9, pp. 673–684, 2017.

[8] J. Shi, W. Gao, and F. Shao, "Pyroptosis: gasdermin-mediated programmed necrotic cell death," *Trends in Biochemical Sciences*, vol. 42, no. 4, pp. 245–254, 2017.

[9] L. Gu, Y. Sun, T. Wu et al., "A novel mechanism for macrophage pyroptosis in rheumatoid arthritis induced by Pol β deficiency," *Cell Death & Disease*, vol. 13, no. 7, p. 583, 2022.

[10] X. Xia, X. Wang, Z. Cheng et al., "The role of pyroptosis in cancer: pro-cancer or pro-"host"?," *Cell Death & Disease*, vol. 10, no. 9, p. 650, 2019.

[11] E. García-Pras, A. Fernández-Iglesias, J. Gracia-Sancho, and S. Pérez-Del-Pulgar, "Cell death in hepatocellular carcinoma: pathogenesis and therapeutic opportunities," *Cancers*, vol. 14, no. 1, p. 48, 2022.

[12] C.-B. Zhou and J.-Y. Fang, "*The role of pyroptosis in gastrointestinal cancer and immune responses to intestinal microbial infection*," *Cancer*, vol. 1872, no. 1, pp. 1–10, 2019.

[13] G. Rogler, "Chronic ulcerative colitis and colorectal cancer," *Cancer letters*, vol. 345, no. 2, pp. 235–241, 2014.

[14] H. Yu, Y. Fu, Z. Tang et al., "A novel pyroptosis-related signature predicts prognosis and response to treatment in breast carcinoma," *Aging*, vol. 14, no. 2, pp. 989–1013, 2022.

[15] W. Lin, Y. Chen, B. Wu, Y. Chen, and Z. Li, "Identification of the pyroptosis-related prognostic gene signature and the associated regulation axis in lung adenocarcinoma," *Cell death discovery*, vol. 7, no. 1, p. 161, 2021.

[16] B. Chao, F. Jiang, H. Bai, P. Meng, L. Wang, and F. Wang, "Predicting the prognosis of glioma by pyroptosis-related signature," *Journal of Cellular and Molecular Medicine*, vol. 26, no. 1, pp. 133–143, 2022.

[17] P. Langfelder and S. Horvath, "WGCNA: an R package for weighted correlation network analysis," *BMC Bioinformatics*, vol. 9, no. 1, p. 559, 2008.

[18] J. C. Stoltzfus, "Logistic regression: a brief primer," *Academic Emergency Medicine*, vol. 18, no. 10, pp. 1099–1104, 2011.

[19] Z. Yang, G. Yan, L. Zheng et al., "YKT6, as a potential predictor of prognosis and immunotherapy response for oral squamous cell carcinoma, is related to cell invasion, metastasis, and CD8+ T cell infiltration," *Oncoimmunology*, vol. 10, no. 1, p. 1938890, 2021.

[20] W. Song, J. Ren, R. Xiang, C. Kong, and T. Fu, "Identification of pyroptosis-related subtypes, the development of a prognosis model, and characterization of tumor microenvironment infiltration in colorectal cancer," *Oncoimmunology*, vol. 10, no. 1, p. 1987636, 2021.

[21] R. Zeng, S. Huang, X. Qiu et al., "Predicting the prognosis of esophageal adenocarcinoma by a pyroptosis-related gene signature," *Frontiers in Pharmacology*, vol. 12, article 767187, 2021.

[22] E. Ravasz, A. L. Somera, D. A. Mongru, Z. N. Oltvai, and A. L. Barabási, "Hierarchical organization of modularity in metabolic networks," *Science*, vol. 297, no. 5586, pp. 1551–1555, 2002.

[23] M. D. Wilkerson and D. N. Hayes, "ConsensusClusterPlus: a class discovery tool with confidence assessments and item tracking," *Bioinformatics*, vol. 26, no. 12, pp. 1572-1573, 2010.

[24] S. Dong, Y. Lu, G. Peng et al., "Furin inhibits epithelial cell injury and alleviates experimental colitis by activating the Nrf2-Gpx4 signaling pathway," *Digestive and liver disease*, vol. 53, no. 10, pp. 1276–1285, 2021.

[25] M. Yassin, Z. Sadowska, D. Djurhuus et al., "Upregulation of PD-1 follows tumour development in the AOM/DSS model of inflammation-induced colorectal cancer in mice," *Immunology*, vol. 158, no. 1, pp. 35–46, 2019.

[26] M. De Robertis, E. Massi, M. L. Poeta et al., "The AOM/DSS murine model for the study of colon carcinogenesis: from pathways to diagnosis and therapy studies," *Journal of carcinogenesis*, vol. 10, no. 1, p. 9, 2011.

[27] L. Zhuang, Y. Yao, L. Peng et al., "Silencing GS homeobox 2 alleviates gemcitabine resistance in pancreatic cancer cells by activating SHH/GLI1 signaling pathway," *Digestive Diseases and Sciences*, vol. 67, no. 8, pp. 3773–3782, 2022.

[28] A. Takaya, W. X. Peng, K. Ishino et al., "Cystatin B as a potential diagnostic biomarker in ovarian clear cell carcinoma," *International Journal of Oncology*, vol. 46, no. 4, pp. 1573–1581, 2015.

[29] W. Xu, F. Liu, W. Tang et al., "The Mayo endoscopic score is a novel predictive indicator for malignant transformation in ulcerative colitis: a long-term follow-up multicenter study," *Frontiers in surgery*, vol. 9, article 832219, 2022.

[30] Y. Zuo, L. Chen, H. Gu et al., "GSDMD-mediated pyroptosis: a critical mechanism of diabetic nephropathy," *Expert Reviews in Molecular Medicine*, vol. 23, article e23, 2021.

[31] D. Pugliese, C. Felice, A. Papa et al., "Anti TNF-α therapy for ulcerative colitis: current status and prospects for the future," *Expert Review of Clinical Immunology*, vol. 13, no. 3, pp. 223–233, 2017.

[32] H. Joos, A. Wildner, C. Hogrefe, H. Reichel, and R. E. Brenner, "Interleukin-1 beta and tumor necrosis factor alpha inhibit migration activity of chondrogenic progenitor cells from non-fibrillated osteoarthritic cartilage," *Arthritis Research & Therapy*, vol. 15, no. 5, p. R119, 2013.

[33] L. Ma, X.-W. Li, S.-J. Zhang et al., "Interleukin-1 beta guides the migration of cortical neurons," *Journal of Neuroinflammation*, vol. 11, no. 1, p. 114, 2014.

[34] J. V. Patankar and C. Becker, "Cell death in the gut epithelium and implications for chronic inflammation," *Nature Reviews. Gastroenterology & Hepatology*, vol. 17, no. 9, pp. 543–556, 2020.

[35] D. F. Li, X. Chang, J. L. Zhao et al., "Colonic epithelial PHLPP2 deficiency promotes colonic epithelial pyroptosis by activating the NF-κB signaling pathway," *Oxidative Medicine and Cellular Longevity*, vol. 2021, Article ID 5570731, 14 pages, 2021.

[36] B. Flood, K. Oficjalska, D. Laukens et al., "Altered expression of caspases-4 and -5 during inflammatory bowel disease and colorectal cancer: diagnostic and therapeutic potential," *Clinical and Experimental Immunology*, vol. 181, no. 1, pp. 39–50, 2015.

[37] B. E. Bolívar, A. N. Brown-Suedel, B. A. Rohrman et al., "Non-canonical roles of caspase-4 and caspase-5 in heme-driven IL-1β release and cell death," *Journal of immunology*, vol. 206, no. 8, pp. 1878–1889, 2021.

[38] L. F. Reis, H. Harada, J. D. Wolchok, T. Taniguchi, and J. Vilcek, "Critical role of a common transcription factor, IRF-1, in the regulation of IFN-beta and IFN-inducible genes," *The EMBO Journal*, vol. 11, no. 1, pp. 185–193, 1992.

[39] T. Ohteki, H. Yoshida, T. Matsuyama, G. S. Duncan, T. W. Mak, and P. S. Ohashi, "The transcription factor interferon regulatory factor 1 (IRF-1) is important during the maturation of natural killer 1.1+ T cell receptor-alpha/beta+ (NK1+ T) cells, natural killer cells, and intestinal intraepithelial T cells," *The Journal of Experimental Medicine*, vol. 187, no. 6, pp. 967–972, 1998.

[40] K. Fang, M. B. Grisham, and C. G. Kevil, "Application of comparative transcriptional genomics to identify molecular targets for pediatric IBD," *Frontiers in immunology*, vol. 6, p. 165, 2015.

[41] R. Tang, G. Yang, S. Zhang, C. Wu, and M. Chen, "Opposite effects of interferon regulatory factor 1 and osteopontin on the apoptosis of epithelial cells induced by TNF-α in inflammatory bowel disease," *Inflammatory Bowel Diseases*, vol. 20, no. 11, pp. 1950–1961, 2014.

[42] M. L. Cupi, M. Sarra, I. Marafini et al., "Plasma cells in the mucosa of patients with inflammatory bowel disease produce granzyme B and possess cytotoxic activities," *Journal of immunology*, vol. 192, no. 12, pp. 6083–6091, 2014.

[43] K. Tsuchiya, "Switching from apoptosis to pyroptosis: gasdermin-elicited inflammation and antitumor immunity," *International journal of molecular sciences*, vol. 22, no. 1, p. 426, 2021.

[44] M. Haque, A. K. Singh, M. M. Ouseph, and S. Ahmed, "Regulation of synovial inflammation and tissue destruction by guanylate binding protein 5 in synovial fibroblasts from patients with rheumatoid arthritis and rats with adjuvant-induced arthritis," *Arthritis & Rhematology*, vol. 73, no. 6, pp. 943–954, 2021.

[45] F. Zhang, J. R. Mears, L. Shakib et al., "IFN-γ and TNF-α drive a CXCL10+ CCL2+ macrophage phenotype expanded in severe COVID-19 lungs and inflammatory diseases with tissue inflammation," *Genome Medicine*, vol. 13, no. 1, p. 64, 2021.

[46] B. Drury, G. Hardisty, R. D. Gray, and G.-T. Ho, "Neutrophil extracellular traps in inflammatory bowel disease: pathogenic mechanisms and clinical translation," *Cellular and Molecular Gastroenterology and Hepatology*, vol. 12, no. 1, pp. 321–333, 2021.

[47] S. M. Bal, K. Golebski, and H. Spits, "Plasticity of innate lymphoid cell subsets," *Nature reviews Immunology*, vol. 20, no. 9, pp. 552–565, 2020.

[48] J. Maul, C. Loddenkemper, P. Mundt et al., "Peripheral and intestinal regulatory CD4+CD25^{high} T cells in inflammatory bowel disease," *Gastroenterology*, vol. 128, no. 7, pp. 1868–1878, 2005.

[49] Z. Chen, M. Tang, D. Huang et al., "Real-time observation of leukocyte-endothelium interactions in tissue-engineered blood vessel," *Lab on a Chip*, vol. 18, no. 14, pp. 2047–2054, 2018.

[50] S. Salvador-Martín, B. Kaczmarczyk, R. Álvarez et al., "Whole transcription profile of responders to anti-TNF drugs in pediatric inflammatory bowel disease," *Pharmaceutics*, vol. 13, no. 1, p. 77, 2021.

[51] L. Lykowska-Szuber, M. Walczak, M. Skrzypczak-Zielinska et al., "Effect of anti-TNF therapy on mucosal apoptosis genes expression in Crohn's disease," *Frontiers in immunology*, vol. 12, article 615539, 2021.

[52] M. Kantono and B. Guo, "Inflammasomes and cancer: the dynamic role of the inflammasome in tumor development," *Frontiers in immunology*, vol. 8, p. 1132, 2017.

[53] X. Liu, Z. Zhang, J. Ruan et al., "Inflammasome-activated gasdermin D causes pyroptosis by forming membrane pores," *Nature*, vol. 535, no. 7610, pp. 153–158, 2016.

[54] F. L. Zhong, O. Mamaï, L. Sborgi et al., "Germline NLRP1 mutations cause skin inflammatory and cancer susceptibility syndromes via inflammasome activation," *Cell*, vol. 167, no. 1, pp. 187–202.e17, 2016.

[55] R. Kolb, L. Phan, N. Borcherding et al., "Obesity-associated NLRC4 inflammasome activation drives breast cancer progression," *Nature Communications*, vol. 7, no. 1, p. 13007, 2016.

[56] G. Y. Chen and G. Núñez, "Inflammasomes in intestinal inflammation and cancer," *Gastroenterology*, vol. 141, no. 6, pp. 1986–1999, 2011.

[57] I. C. Allen, E. M. TeKippe, R.-M. T. Woodford et al., "The NLRP3 inflammasome functions as a negative regulator of tumorigenesis during colitis-associated cancer," *The Journal of Experimental Medicine*, vol. 207, no. 5, pp. 1045–1056, 2010.

[58] S. M. Man, Q. Zhu, L. Zhu et al., "Critical role for the DNA sensor AIM2 in stem cell proliferation and cancer," *Cell*, vol. 162, no. 1, pp. 45–58, 2015.

[59] J. E. Wilson, A. S. Petrucelli, L. Chen et al., "Inflammasome-independent role of AIM2 in suppressing colon tumorigenesis via DNA-PK and Akt," *Nature medicine*, vol. 21, no. 8, pp. 906–913, 2015.

Hindawi
Journal of Immunology Research
Volume 2023, Article ID 4452414, 8 pages
https://doi.org/10.1155/2023/4452414

Review Article

Berberine in Sepsis: Effects, Mechanisms, and Therapeutic Strategies

Tingxia Lv, Chunpan Zhang, Lan Hu, Chao Wang, Shirong Li, He Wang, and Wenjie Qi

Department of Infectious Diseases, Beijing Friendship Hospital, Capital Medical University, Beijing 100050, China

Correspondence should be addressed to Wenjie Qi; qi_wenjie@ccmu.edu.cn

Received 15 July 2022; Revised 10 September 2022; Accepted 10 October 2022; Published 25 January 2023

Academic Editor: Meng-Hao Huang

Sepsis is defined as a dysregulated immune response to infection that leads to multiple organ dysfunction. To date, though a growing body of knowledge has gained insight into the clinical risk factors, pathobiology, treatment response, and recovery methods, sepsis remains a significant concern and clinical burden. Therefore, further study is urgently needed to alleviate the acute and chronic outcomes. Berberine (BBR), a traditional Chinese medicine with multiple actions and mechanisms, has been investigated in cellular and rodent animal models of sepsis mainly based on its anti-inflammatory effect. However, the practical application of BBR in sepsis is still lacking, and it is imperative to systematically summarize the study of BBR in sepsis. This review summarized its pharmacological activities and mechanisms in septic-related organ injuries and the potential BBR-based therapeutic strategies for sepsis, which will provide comprehensive references for scientific research and clinical application.

1. Introduction

Sepsis is a life-threatening clinical syndrome characterized by multiple organ dysfunction caused by the body's dysregulated response to infection. Despite better supportive therapy and care, sepsis and sepsis shock have led to a high morbidity and mortality rate in recent years [1]. Just as intricated immune or inflammatory factors drive multiple metabolic diseases [2, 3], the exact mechanisms responsible for sepsis are also complex, involving coagulation abnormalities, uncontrolled release of inflammatory mediators, excessive innate immune response, endothelial capillary leakage syndrome, and organ dysfunction [4]. Though progress has been made regarding recognizing and managing clinical sepsis, incidence and mortality rates remain high. For example, in 2017, an estimated 48.9 million incident cases of sepsis and 11.0 million sepsis-related deaths were reported, representing 19.7% of all global deaths [5, 6]. Furthermore, clinical trials of therapeutics have failed to obtain promising results, and it likely got even worse during the coronavirus disease 2019 (COVID-19) pandemic due to the limited intensive care unit resources [7]. Given the lack of effective treatment for sepsis, Chinese herbal medicines, i.e., Chinese patent medicines, Chinese herbal prescriptions, and single Chinese herbs, have therapeutic actions promising in treating sepsis through multicomponent, multipathway, and multitargeting abilities [8].

Berberine (BBR), an isoquinoline alkaloid, is widely distributed in many medicinal plants, such as *Coptis chinensis* and *Berberis vulgaris*, and is usually regarded as an ingredient of Chinese herbal medicines [9]. It has a molecular weight of 336.37 Da and can be obtained through de novo synthesis. Though BBR was approved to be an antibacterial agent, it also plays a crucial therapeutic role in infectious diseases, cardiovascular diseases, neurodegenerative diseases, and rheumatoid arthritis due to its antimicrobial, antioxidant, anti-inflammatory, and metabolic regulation effects [10, 11]. BBR can act on a diverse range of molecular targets by binding to the active cavities with specific structural and physiochemical properties. Among the related conditions, sepsis is characterized by the host's excessive and complex inflammatory response and is linked with bacterial and viral infections during its occurrence and progression. In recent years, though no studies about BBR for treating sepsis in

clinical practice, its protective effect and mechanism on sepsis have been explored extensively in cellular and animal models [12–15]. Whether BBR could be a potential therapeutic drug for sepsis and septic complications remains unclear in the real world. Given that dysregulated host systemic inflammatory and immune response during sepsis usually lead to life-threatening organ dysfunction, this paper summarizes the protective role of BBR for organ injury and related mechanism and, finally, prospects the potential BBR-based therapeutic strategies in sepsis.

2. Effects and Mechanisms of BBR in Sepsis-Related Organ Dysfunction

2.1. BBR in Sepsis-Related Intestinal Barrier Injury. The intestinal barrier and the subsequent translocation of intestinal bacteria play a critical role in multiple organ dysfunction syndromes during sepsis [16]. Lipopolysaccharide (LPS) produced by intestinal bacteria might damage gut-vascular integrity, increase permeability, and reduce tight junction and adherens junction protein production [17]. Several studies have shown that pretreatment with BBR protects against intestinal injury in sepsis-challenged animals with various mechanisms. For example, in male Sprague-Dawley (SD) rats undergoing cecal ligation and puncture (CLP), TNF-α and IL-6 were significantly lower, while the tight junction protein level, the percentage of cell death in intestinal epithelial cells, and the mucosal permeability were significantly elevated after treatment by BBR [12]. The overall effects were consistent with other studies [18, 19]. Further investigation showed that the mRNA level of intestinal Toll-like receptors 2 (TLR2) and TLR4 was also increased [18, 20], indicating that BBR might protect the intestinal mucosal barrier in the early phase of sepsis through the TLR-NF-κB signaling pathway [20]. Moreover, BBR protected the damaged gut-vascular barrier (GVB) via modulation of the hepatic apolipoprotein M/S1P pathway in the polymicrobial sepsis model [21] and attenuated the impairment of glutamine transport and glutaminase activity in rats [19]. BBR also inhibited inducible cyclooxygenase-2 (COX-2) overexpression in rat small intestinal mucosa via activation of the peroxisome proliferator-activated receptor-gamma (PPARγ) pathway and inhibited the effects of LPS in a rat model of endotoxemia [13]. However, although NOD-like receptors (NLR) play a crucial role in host defense against intestinal infection, there is no evidence that the NLR pathway was related to the preventive effect of BBR for sepsis [12]. In contrast, Wnt/beta-catenin signaling pathway was related to the protective effect of BBR on the gut-vascular barrier during sepsis [17].

Zinc deficiency is prevalent in the gut and might drive bacterial translocation and toxin dissemination, while zinc redistribution could protect the intestinal barrier in sepsis [22–24]. It was reported that BBR could regulate the trace elements of zinc's metabolism and exert intestinal protection role. He et al. demonstrated that BBR (50 mg/kg/day, gavage) improved survival rates of septic rats in the rat CLP sepsis model (BBR vs. CLP group: 80% vs. 46.7% at 48 hours) and reduced plasma endotoxin levels and intestinal mucosal permeability of septic rats, which were accompanied by the increased zinc levels [25]. In cellular studies, BBR treatment increased intracellular zinc transporter Zrt-Irt-like protein 14 (ZIP14) mRNA and protein expression in LPS-treated human colorectal adenocarcinoma cell line Caco-2 cells and upregulated LPS-decreased claudin-1 and occludin generation [25]. From the above evidence, we could conclude that BBR has a definite protective effect on intestinal barrier dysfunction, and this aspect might be the first breakthrough of BBR in treating organ injury in sepsis.

2.2. BBR in Sepsis-Related Lung Injury. Lung injury and acute respiratory distress syndrome (ARDS) are common challenges in sepsis. Microbial infections are usually responsible for pneumonia or sepsis, which cause altered respiratory function, pulmonary edema, and accumulation of inflammatory cells, including polymorphonuclear neutrophils (PMNs), circulating monocytes, and tissue-resident macrophages. The protective role of BBR for lung injury in sepsis was mainly derived from its anti-inflammatory effect. BBR was endowed with pronounced anti-inflammatory property, which was probably associated with suppressing the activation of the NF-κB signaling pathway and the subsequent gene expressions and productions of proinflammatory mediators [26, 27], as well as suppressing the phosphorylation of MAPKs, such as p38, ERK, and JNK, and the level of reactive oxygen species in macrophages [28]. Berberine pretreatment maintained the integrity of endothelial glycocalyx, inhibited NF-κB signaling pathway activation, and decreased the production of proinflammatory cytokines TNF-α, IL-1β, and IL-6 in mice with LPS-induced ARDS [29]. Pretreatment with neutral sulfate berberine attenuates lung and small intestine tissue injury and improves survival in endotoxemic mice, which may be mediated, at least in part, by the inhibition of proinflammatory mediators TNF-α and IFN-γ and NO production and upregulation of IL-10 release [1]. Wang et al. also reported that BBR inhibited LPS or CpG-ODN-induced proinflammatory cytokine expression at 12 and 24 h post BBR treatment in bone marrow-derived macrophages (BMDM) and LPS/D-galactosamine-challenged septic mouse model in vivo. They demonstrated that BBR significantly attenuated lung tissue injury and potently increased the survival rate in the septic mice with negligible side effects by suppressing NF-κB- and IL-6-mediated STAT3 activation [30]. Additionally, BBR could protect the permeability of pulmonary microvascular endothelial cells (HPMECs) and decrease the expression of IL-1β and IL-18 by suppressing the expression of phosphorylated NF-κB and further restraining the downstream gene nucleotide-binding domain and leucine-rich repeat protein-3 (Nlrp3) [31]. This limited evidence hints that the anti-inflammatory roles might be the core mechanisms for BBR in treating sepsis-related lung injury.

2.3. BBR in Sepsis-Related Acute Kidney Injury. Septic acute kidney injury (S-AKI), which is characterized by a rapid deterioration of renal function, accounts for about half of all patients with AKI syndrome treated in the intensive care unit (ICU) [32]. The mechanisms of sepsis-associated acute kidney injury involve ischemia-reperfusion, inflammation,

oxidative stress, tubular cell damage, dysregulated microcirculation, morphofunctional alterations in the mitochondria, and apoptosis. The pathogen-associated molecular patterns (PAMP) and damage-associated molecular patterns (DAMP) participate in the pathological process [33, 34]. Sepsis-causing pathogens include bacteria, fungi, and viruses, and the widely used models of S-AKI in basic research were usually induced by bacteria or isolated bacterial pathogenic substances [33]. As an alkaloid with well antibacterial activity and even an alternative to antibiotics, few studies reported the application of BBR in S-AKI. Al-Kuraishy et al. revealed that BBR has no significant effect on AKI biomarkers except on serum kidney injury molecules (KIM-1) in diclofenac-induced AKI, whereas combined use of BBR and pentoxifylline significantly reduced renal biomarkers such as blood urea, serum creatinine, and glomerular filtration rate (eGFR) [35]. Berberine is the main bioactive component in *Rhizoma Coptidis* [36]. Integrating metabolomics and network pharmacology showed that *Rhizoma Coptidis extracts* increased the nuclear translocation of nuclear factor-erythroid 2-related factor-2 (Nrf2), the protein expression of heme oxygenase-1 (HO-1), and the mRNA expression of PPARα and reduced nitric oxide synthase 2 (NOS2) activity [37]. Of note, BBR also exerts renoprotective effects caused by other inducers such as cisplatin and gentamicin in rodent models through upregulating mitophagy or its antioxidant, anti-inflammatory, and antiapoptotic properties [38–40].

2.4. BBR in Sepsis-Related Liver Injury. Disturbed liver function and drastic changes in hepatic gene and protein expression during sepsis induce inflammatory pathway activation and downregulate house-keeping functions such as metabolic, biotransformation, or bile transport activities [41]. During systemic infections, the liver regulates immune defenses via bacterial clearance, production of acute-phase proteins (APPs) and cytokines, and metabolic adaptation to inflammation. The release of APPs with various biological functions in the systemic circulation contributes to the systemic activation of immune responses, while mitochondrial and endoplasmic reticulum (ER) dysfunctions during the acute phase response elicited by systemic inflammation lead to liver failure in sepsis [3, 41, 42]. To date, the molecular mechanism studies for hepatoprotection of BBR in sepsis were insufficient. Limited investigations revealed that BBR inhibits LPS-induced oxidative stress markers NO protein and iNOS expression in RAW 264.7 and THP-1 macrophage cells [14] and further alleviates ALT, AST, malondialdehyde (MDA), and myeloperoxidase (MPO) activity in sepsis rat model [15]. Moreover, BBR reduced proapoptotic protein cleaved caspase-3 and increased antiapoptotic protein Bcl-2 in CLP-induced liver injury, which were associated with a reduction in intestinal permeability and CLP-induced distant organ cell apoptosis as compared with mice on vehicle treatment [43]. Among the numerous mediators in sepsis, the high mobility group box 1 (HMGB1) is an endogenous DAMP that mediates downstream effects within the inflammatory cascade. It was reported that AMPK activation could significantly inhibit LPS-induced HMGB1 release in RAW264.7 cells [44]. A berberine derivative, 13-ethylberberine (13-EBR), could reduce HMGB1 release by activating AMPK under septic conditions and protect endotoxemic mice from liver damage [45]. Similarly, other researchers also have verified the inhibition of BBR-loaded nanostructured lipid carriers for HMGB1/TLR4/NF-κB signaling and protective roles for warm hepatic ischemia/reperfusion-induced lesion [46]. Therefore, based on this limited evidence, inhibiting the key inflammatory mediators and pathways is still a dominant mechanism of BBR in treating sepsis-related liver injury.

2.5. BBR in Sepsis-Induced Disseminated Intravascular Coagulation. Disseminated intravascular coagulation (DIC) was recognized as a deadly complication in sepsis. In addition to the activation of coagulation induced by pathogens, damage-associated molecular patterns, neutrophil extracellular traps, extracellular vesicles, and glycocalyx damage are also involved in the pathogenesis of sepsis-induced DIC. Tissue factor (TF) plays a crucial role in the coagulation of sepsis [47]. It was reported that BBR could inhibit LPS-induced TF activity and expression and downregulate NF-κB, Akt, and MAPK/JNK/p38/ERK pathways in THP-1 cells, which provides some new insights into its mechanism for sepsis treatment [48]. Yang et al.'s study showed that caspase-11, as a cytosolic LPS receptor, could enhance the activation of tissue factor and subsequent phosphatidylserine exposure independent of cell death, while deletion of caspase-11 or neutralization of phosphatidylserine or TF prevented LPS-induced DIC [49]. Berberine inhibits caspase-11-dependent coagulation in bacterial sepsis by blocking Msr1, thus preventing coagulation syndrome [50]. Mechanistically, Wang et al. first reported the possible targets and mechanisms of BBR and its primary metabolite berberrubine in inhibiting platelet activation. That is, BBR significantly inhibited ADP-induced integrin αIIbβ3 activation, reduced the level of P-selectin on the platelet membrane, and suppressed the binding of fibrinogen to the platelets, which was derived from the inhibition roles of BBR for the PI3K/Akt pathway, Rasa3 membrane translocation, and Rap1 activation [51]. These existing studies open a promising direction for BBR in treating sepsis-induced disseminated intravascular coagulation.

3. Berberine-Based Therapeutic Strategies in Sepsis

Although many studies have reported the protective effects and multiple mechanisms of BBR in sepsis-related animal or cell models (Table 1), unfortunately, there is no clinical practice at present. We speculated that to treat this kind of systemic severe inflammatory disease, it still needs to improve the drug concentration of BBR in blood, discover compounds with better efficacy based on the structure of BBR, and explore drug combination strategies in the future. Definitely, the poor oral bioavailability of BBR limited its therapeutic potential, and fortunately, BBR solid lipid nanoparticles (BBR-SLNs) were previously developed and showed significant improvement in bioavailability and reduction in systemic adverse reactions [52]. In recent years,

Table 1: The protective effects and mechanisms of berberine in sepsis-related animal or cell model.

In vivo/vitro	Animal or cell model	Therapeutic dose	Effects and mechanisms	Reference
In vivo	Cecal slurry-induced neonatal sepsis in C57BL/6J mice (5-7 days)	50/100 μg/mouse, i.p.	↑Survival rate; ↓intestinal injury; ↓IL-6, IL-1β, and TNF-α; ↑miR-132-3p; ↓FOXA1, p-IκBα, and p65; and ↑IκBα	[60]
In vivo	Mouse model of E. coli sepsis	5 mg/kg, i.p.	↑Survival rate; ↓IL-6, TNF-α, and CD4+ and CD8+ lymphocyte population in septic mice	[61]
In vivo	LPS/D-gal-induced C57BL/6 septic mouse model (6-8 weeks)	200 μg/mouse, i.v.	↓Lung tissue injury; ↑survival rate; ↓IL-6, TNF-α, and IL-1β; (-) B cells%, T cells%, and subtypes of T cells in the spleen; and (-) CD11b + Gr-1+ cells in bone marrow cells	[30]
In vivo	LPS-induced male BALB/c mice (6-8 weeks)	50 mg/kg, i.g.	↓Ileum injury (injury score, intestinal villus height, gut mucosal weight, and intestinal permeability); ↓enterocyte apoptosis; and ↓TLR4 mRNA, p-IκBα, MIP-2 production, and MPO activity	[18]
In vivo	CLP-induced male Wistar rats (260-300 g)	25/50/100 mg/kg/d, i.g.	↓Sepsis-related mortality; ↑hepatic and plasma ApoM level; ↓hyperglycemia, TNF-α, and IL-1β; and ↓sepsis-induced gluconeogenesis expression	[62]
In vivo	CLP-induced male Long-Evans rats (270-300 g)	25/50 mg/kg/d, i.p.	↓Microvascular permeability, serum endotoxemia levels	[17]
In vivo	CLP-induced male Wistar rats (270-310 g)	50 mg/kg/d, i.g.	↑Survival rates; ↓endotoxin levels and intestinal mucosal permeability; and ↑Zn^{2+} in intestinal mucosa, ZIP14 expression	[25]
In vivo	CLP-induced male SD rats (200-230 g)	50 mg/kg, i.g.	↓TNF-α, IL-6; ↓claudin-4, mucosal permeability; and ↓intestinal epithelial cell mortality	[12]
In vivo	CLP-induced SD rat (200-230 g)	50 mg/kg, i.g.	↓Intestinal epithelial cell death; ↓TLR2/4, TNF-α, and IL-6; and ↑zonula occludens-1	[20]
In vivo	Outer membrane vesicles (used for delivering LPS) challenged mice (25-30 g)	5 mg/kg	↓Vessel occlusion and fibrin deposition in liver microvasculature; ↓DIC markers (TAT and PAI-1); ↓multiorgan dysfunction and death rate; and ↓caspase-11-mediated coagulation activation	[50]
In vivo	LPS-induced male C57BL/6 mice (8 weeks)	10 mg/kg, injected into peritoneal cavity	↓Lung damage and injury scores; ↓injury of pulmonary permeability; ↓ROS level, IL-6/-18/-1β, and TNF-α; ↑IL-10; and ↓p-NF-κB, Nlrp3	[31]
In vitro	HepG2 cells	5/10/20 μM	↓TLR4 mRNA	[62]
In vitro	LPS or CpG-ODN-induced BMDM	5 μM	↓IL-6, TNF-α, and IL-1β; ↓p-IκBα/β, p-IκBα, and NF-κB nuclear translocation	[30]
In vitro	LPS-induced RIMECs	10/20 μM	↓RIMEC permeability; ↑transendothelial electrical resistance; and ↑β-catenin, claudin-12, and VE-cadherin	[17]
In vitro	LPS-induced Caco-2 cells	20 μM	↑Intracellular zinc content; ↑ZIP14, claudin-1, and occludin expression	[25]
In vitro	LPS-stimulated HPMECs	2.5 μM	↓ROS level, IL-6/-18/-1β, and TNF-α; ↑IL-10; and ↓Nlrp3	[31]
In vitro	*E. coli*-stimulated primary macrophages and THP-1 cells	5 μM	↓Cytotoxicity; ↓pyroptosis; and ↓caspase-11 pathway	[50]
In vitro	LPS-induced HUVECs	1.25/2.5/5 μM	↓Endothelial glycocalyx degradation; ↓endothelial glycocalyx damage factors (ROS, heparanase, and MMP9)	[29]

ApoM: apolipoprotein M; BMDM: bone marrow-derived macrophages; CLP: ligation and puncture; D-gal: D-galactosamine; HUVECs: human umbilical endothelial cells; HPMECs: human pulmonary microvascular endothelial cells; i.g.: intragastric gavage; i.p.: intraperitoneal injection; i.v.: intravenous injection; RIMECs: rat intestinal microvascular endothelial cells; ROS: reactive oxygen species.

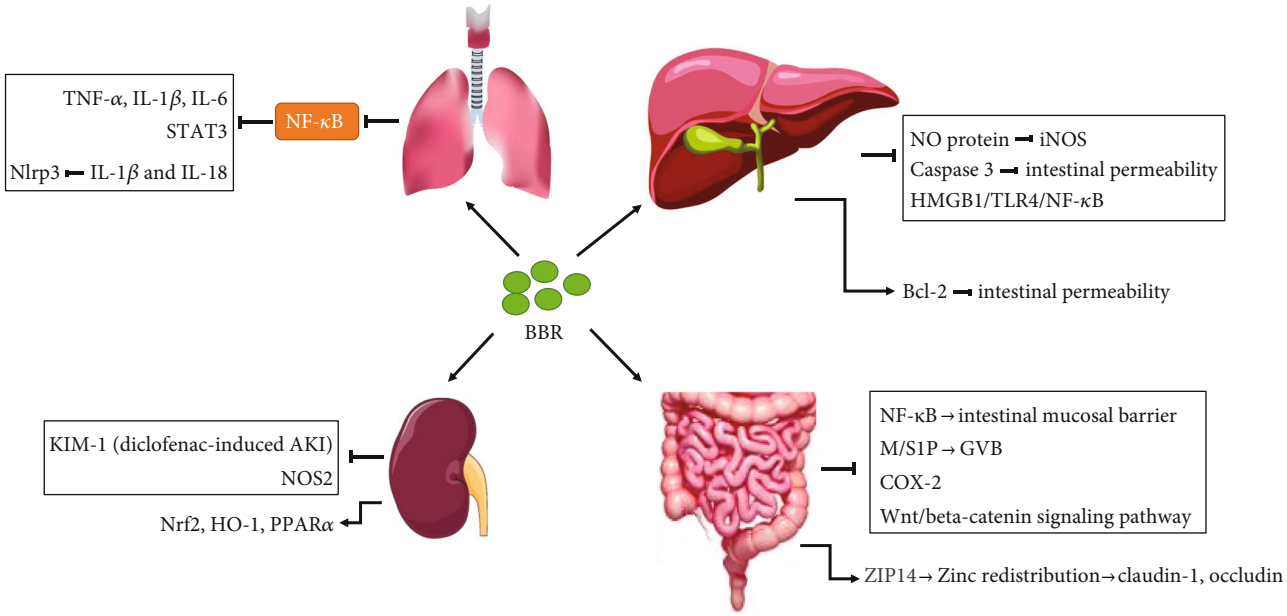

Figure 1: The protective effect and mechanism of berberine for sepsis-related organ injury.

BBR-SLNs have been applied for the management of ulcerative colitis [53, 54], bacterial infection [55], and infections of traumatic wounds [56], which are essential sepsis triggers. The effect of immunomodulatory activity and inhibition for the expression of multiple inflammatory factors were demonstrated, suggesting that BBR-SLNs might be developed to enhance the therapeutic effects of BBR as an antisepsis drug. Besides, several derivatives of BBR were reported to have better pharmaceutical effects. For example, the natural oxoderivative oxyberberine (OBB) was endowed with more pronounced anti-inflammatory properties than BBR, which was likely to be associated with suppressing the activation of the NF-κB, the subsequent gene expressions and productions of proinflammatory mediators [26]. Tetrahydroberberrubine (THBru), a berberine derivative, significantly decreased TNF-α and nitrate/nitrite content in the plasma, reduced the MPO activity in LPS-induced acute lung injury, and suppressed the activation of the MAPKs, AKT, and the NF-κB subunit p65 in LPS-induced THP-1 cells [57]. Similarly, another berberine derivative, 13-ethylberberine (13-EBR), reduces HMGB1 release through AMPK activation in LPS-activated RAW264.7 cells and protects endotoxemic mice from lung and liver damage [45]. Wang et al. considered that BBR might also serve as a promising adjuvant that could be used in conjunction with other medications for the treatment of septic patients [30]. For example, combinatorial liposomes of BBR and curcumin could inhibit biofilm formation and intracellular methicillin-resistant *Staphylococcus aureus* infections and associated inflammation, with five times more efficient than clindamycin [58]. The combined use of sodium new houttuyfonate and berberine chloride presented synergistic antibacterial effects against growing and persistent methicillin-resistant and vancomycin-intermediate *Staphylococcus aureus*, which is likely related to the interruption of the cell membrane [59]. These combined antibacterial effects of BBR with other agents predicted their potential application in sepsis. Taken together, the strategies for improving the bioavailability, discovering more powerful and effective berberine derivatives, and drug combinations might contribute to the application of BBR in treating sepsis in the future.

4. Conclusion and Perspective

BBR, as a natural modulator of inflammatory signaling in multiple immune and infectious diseases, could also effectively protect the various organs in sepsis from severe damage and increase the survival rate in rodent models. Currently, BBR could be considered to act as a multitarget drug to antagonize sepsis. The primary mechanism mainly derives from the regulation for inflammatory signaling pathways (i.e., NF-κB, JAK/STAT, Akt, and MAPK), the key inflammatory mediators (i.e., HMGB1 and tissue factor), the subsequent anti-/proinflammatory cytokines (i.e., TNF-α, IL-6, and IL-10), and the dysregulated endoplasmic reticulum/oxidative stress and apoptosis (Figure 1). BBR exhibited potential therapeutic effects for sepsis-related intestinal barrier injury, lung injury, acute kidney injury, liver injury, and disseminated intravascular coagulation. Given the exact antibacterial effect of BBR and a large number of experimental reports in intestinal regulation, it is expected to be first used to protect against sepsis-induced intestinal injury in the clinic. Also, owing to its poor oral bioavailability and current unsatisfied therapeutic effects, as well as lack of practical application of BBR in sepsis, the nanostructured lipid carrier of BBR, more effective BBR derivatives, and drug combination strategies need to be investigated in various well-designed clinical trials in the future.

Data Availability

The data used to support the review are included in the article.

Conflicts of Interest

The authors declare that there is no conflict of interest regarding the publication of this paper.

Acknowledgments

This study was supported by the Capital's Funds for Health Improvement and Research (2020-2-2027), Funding Support for Key Clinical Projects in Beijing (WJQ), and Youyi Zhongzi Plan (YYZZ202043).

References

[1] Y. Y. Zhang and B. T. Ning, "Signaling pathways and intervention therapies in sepsis," *Signal Transduction and Targeted Therapy*, vol. 6, no. 1, p. 407, 2021.

[2] X. C. Dong, K. Chowdhury, M. Huang, and H. G. Kim, "Signal transduction and molecular regulation in fatty liver disease," *Antioxidants & Redox Signaling*, vol. 35, no. 9, pp. 689–717, 2021.

[3] H. Li, M. H. Huang, J. D. Jiang, and Z. G. Peng, "Hepatitis C: from inflammatory pathogenesis to anti-inflammatory/hepatoprotective therapy," *World Journal of Gastroenterology*, vol. 24, no. 47, pp. 5297–5311, 2018.

[4] T. van der Poll, F. L. van de Veerdonk, B. P. Scicluna, and M. G. Netea, "The immunopathology of sepsis and potential therapeutic targets," *Nature Reviews. Immunology*, vol. 17, no. 7, pp. 407–420, 2017.

[5] K. E. Rudd, S. C. Johnson, K. M. Agesa et al., "Global, regional, and national sepsis incidence and mortality, 1990-2017: analysis for the Global Burden of Disease Study," *The Lancet*, vol. 395, no. 10219, pp. 200–211, 2020.

[6] M. Cecconi, L. Evans, M. Levy, and A. Rhodes, "Sepsis and septic shock," *The Lancet*, vol. 392, no. 10141, pp. 75–87, 2018.

[7] A. C. Kalil, "Sepsis and septic shock," *Seminars in Respiratory and Critical Care Medicine*, vol. 42, no. 5, pp. 639-640, 2021.

[8] C. Cheng and X. Yu, "Research progress in Chinese herbal medicines for treatment of sepsis: pharmacological action, phytochemistry, and pharmacokinetics," *International Journal of Molecular Sciences*, vol. 22, no. 20, p. 11078, 2021.

[9] H. Li, N. N. Liu, J. R. Li et al., "Combined use of bicyclol and berberine alleviates mouse nonalcoholic fatty liver disease," *Frontiers in Pharmacology*, vol. 13, article 843872, 2022.

[10] W. J. Kong, C. Vernieri, M. Foiani, and J. D. Jiang, "Berberine in the treatment of metabolism-related chronic diseases: a drug cloud (dCloud) effect to target multifactorial disorders," *Pharmacology & Therapeutics*, vol. 209, article 107496, 2020.

[11] Y. Wang, X. Zhou, D. Zhao et al., "Berberine inhibits free fatty acid and LPS-induced inflammation via modulating ER stress response in macrophages and hepatocytes," *PLoS One*, vol. 15, no. 5, article e0232630, 2020.

[12] G. X. Li, X. M. Wang, T. Jiang, J. F. Gong, L. Y. Niu, and N. Li, "Berberine prevents damage to the intestinal mucosal barrier during early phase of sepsis in rat through mechanisms independent of the NOD-like receptors signaling pathway," *European Journal of Pharmacology*, vol. 730, pp. 1–7, 2014.

[13] A. W. Feng, W. Gao, G. R. Zhou et al., "Berberine ameliorates COX-2 expression in rat small intestinal mucosa partially through PPARγ pathway during acute endotoxemia," *International Immunopharmacology*, vol. 12, no. 1, pp. 182–188, 2012.

[14] J. S. Shin, H. E. Choi, S. Seo, J. H. Choi, N. I. Baek, and K. T. Lee, "Berberine decreased inducible nitric oxide synthase mRNA stability through negative regulation of human antigen R in lipopolysaccharide-induced macrophages," *The Journal of Pharmacology and Experimental Therapeutics*, vol. 358, no. 1, pp. 3–13, 2016.

[15] Y. Lv, J. Wang, D. Xu et al., "Comparative study of single/combination use of Huang-Lian-Jie-Du decoction and berberine on their protection on sepsis induced acute liver injury by NMR metabolic profiling," *Journal of Pharmaceutical and Biomedical Analysis*, vol. 145, pp. 794–804, 2017.

[16] C. Wang, Q. Li, and J. Ren, "Microbiota-immune interaction in the pathogenesis of gut-derived infection," *Frontiers in Immunology*, vol. 10, p. 1873, 2019.

[17] Y. He, X. Yuan, H. Zuo, Y. Sun, and A. Feng, "Berberine exerts a protective effect on gut-vascular barrier via the modulation of the Wnt/beta-catenin signaling pathway during sepsis," *Cellular Physiology and Biochemistry*, vol. 49, no. 4, pp. 1342–1351, 2018.

[18] H. M. Li, Y. Y. Wang, H. D. Wang et al., "Berberine protects against lipopolysaccharide-induced intestinal injury in mice via alpha 2 adrenoceptor-independent mechanisms," *Acta Pharmacologica Sinica*, vol. 32, no. 11, pp. 1364–1372, 2011.

[19] L. Niu, W. Qiao, Z. Hu et al., "Berberine attenuates lipopolysaccharide-induced impairments of intestinal glutamine transport and glutaminase activity in rat," *Fitoterapia*, vol. 82, no. 3, pp. 323–330, 2011.

[20] G. X. Li, X. M. Wang, T. Jiang, J. F. Gong, L. Y. Niu, and N. Li, "Berberine prevents intestinal mucosal barrier damage during early phase of sepsis in rat through the Toll-like receptors signaling pathway," *The Korean Journal of Physiology & Pharmacology*, vol. 19, no. 1, pp. 1–7, 2015.

[21] Y. Li, J. Zhou, J. Qiu et al., "Berberine reduces gut-vascular barrier permeability via modulation of ApoM/S1P pathway in a model of polymicrobial sepsis," *Life Sciences*, vol. 261, article 118460, 2020.

[22] J. Souffriau and C. Libert, "Mechanistic insights into the protective impact of zinc on sepsis," *Cytokine & Growth Factor Reviews*, vol. 39, pp. 92–101, 2018.

[23] S. S. Siddiqui, C. Dhar, V. Sundaramurthy et al., "Sialoglycan recognition is a common connection linking acidosis, zinc, and HMGB1 in sepsis," *Proceedings of the National Academy of Sciences of the United States of America*, vol. 118, no. 10, 2021.

[24] I. Wessels and R. J. Cousins, "Zinc dyshomeostasis during polymicrobial sepsis in mice involves zinc transporter Zip14 and can be overcome by zinc supplementation," *American Journal of Physiology. Gastrointestinal and Liver Physiology*, vol. 309, no. 9, pp. G768–G778, 2015.

[25] Y. He, X. Yuan, H. Zuo, X. Li, Y. Sun, and A. Feng, "Berberine induces ZIP14 expression and modulates zinc redistribution to protect intestinal mucosal barrier during polymicrobial sepsis," *Life Sciences*, vol. 233, article 116697, 2019.

[26] C. L. Li, L. H. Tan, Y. F. Wang et al., "Comparison of anti-inflammatory effects of berberine, and its natural oxidative

and reduced derivatives from Rhizoma Coptidis *in vitro* and *in vivo*," *Phytomedicine*, vol. 52, pp. 272–283, 2019.

[27] K. K. Reddi, H. Li, W. Li, and S. D. Tetali, "Berberine, a phytoalkaloid, inhibits inflammatory response induced by LPS through NF-kappaβ pathway: possible involvement of the IKKα," *Molecules*, vol. 26, no. 16, p. 4733, 2021.

[28] H. W. Jeong, K. C. Hsu, J. W. Lee et al., "Berberine suppresses proinflammatory responses through AMPK activation in macrophages," *American Journal of Physiology. Endocrinology and Metabolism*, vol. 296, no. 4, pp. E955–E964, 2009.

[29] L. Huang, X. Zhang, X. Ma et al., "Berberine alleviates endothelial glycocalyx degradation and promotes glycocalyx restoration in LPS-induced ARDS," *International Immunopharmacology*, vol. 65, pp. 96–107, 2018.

[30] Y. Wang, P. Du, and D. Jiang, "Berberine functions as a negative regulator in lipopolysaccharide -induced sepsis by suppressing NF-κB and IL-6 mediated STAT3 activation," *Pathogens and Disease*, vol. 78, no. 7, 2020.

[31] J. Chen, Y. Huang, X. Bian, and Y. He, "Berberine ameliorates inflammation in acute lung injury via NF-κB/Nlrp3 signaling pathway," *Frontiers in Nutrition*, vol. 9, article 851255, 2022.

[32] R. Bellomo, J. A. Kellum, C. Ronco et al., "Acute kidney injury in sepsis," *Intensive Care Medicine*, vol. 43, no. 6, pp. 816–828, 2017.

[33] T. Li, J. Y. Liu, J. F. Liu, M. Duan, and A. Li, "The correlation between the types of initial bacterial infection and clinical prognosis in patients with septic AKI," *Frontiers in Medicine (Lausanne)*, vol. 8, article 800532, 2021.

[34] L. S. Chawla, R. L. Amdur, S. Amodeo, P. L. Kimmel, and C. E. Palant, "The severity of acute kidney injury predicts progression to chronic kidney disease," *Kidney International*, vol. 79, no. 12, pp. 1361–1369, 2011.

[35] H. M. Al-Kuraishy, A. I. Al-Gareeb, and N. R. Hussien, "Synergistic effect of berberine and pentoxifylline in attenuation of acute kidney injury," *International Journal of Critical Illness and Injury Science*, vol. 9, no. 2, pp. 69–74, 2019.

[36] B. L. Ma, C. Yin, B. K. Zhang et al., "Naturally occurring proteinaceous nanoparticles in _Coptidis Rhizoma_ extract act as concentration-dependent carriers that facilitate berberine absorption," *Scientific Reports*, vol. 6, no. 1, p. 20110, 2016.

[37] Y. Zheng, X. Shi, J. Hou et al., "Integrating metabolomics and network pharmacology to explore _Rhizoma Coptidis_ extracts against sepsis-associated acute kidney injury," *Journal of Chromatography. B, Analytical Technologies in the Biomedical and Life Sciences*, vol. 1164, article 122525, 2021.

[38] J. Shen, W. Wang, X. Shao et al., "Integrated analysis of m6A methylome in cisplatin-induced acute kidney injury and berberine alleviation in mouse," *Frontiers in Genetics*, vol. 11, article 584460, 2020.

[39] J. Qi, Q. Xue, L. Kuang, L. Xie, R. Luo, and X. Nie, "Berberine alleviates cisplatin-induced acute kidney injury by regulating mitophagy via PINK 1/Parkin pathway," *Translational Andrology and Urology*, vol. 9, no. 4, pp. 1712–1724, 2020.

[40] M. Adil, A. D. Kandhare, G. Dalvi et al., "Ameliorative effect of berberine against gentamicin-induced nephrotoxicity in rats via attenuation of oxidative stress, inflammation, apoptosis and mitochondrial dysfunction," *Renal Failure*, vol. 38, no. 6, pp. 996–1006, 2016.

[41] P. Strnad, F. Tacke, A. Koch, and C. Trautwein, "Liver – guardian, modifier and target of sepsis," *Nature Reviews. Gastroenterology & Hepatology*, vol. 14, no. 1, pp. 55–66, 2017.

[42] H. Li, J. R. Li, M. H. Huang et al., "Bicyclol attenuates liver inflammation induced by infection of hepatitis C virus via repressing ROS-mediated activation of MAPK/NF-κB signaling pathway," *Frontiers in Pharmacology*, vol. 9, p. 1438, 2018.

[43] D. Qiu, W. Zhang, Z. Song et al., "Berberine suppresses cecal ligation and puncture induced intestinal injury by enhancing Treg cell function," *International Immunopharmacology*, vol. 106, article 108564, 2022.

[44] K. Tsoyi, H. J. Jang, I. T. Nizamutdinova et al., "Metformin inhibits HMGB1 release in LPS-treated RAW 264.7 cells and increases survival rate of endotoxaemic mice," *British Journal of Pharmacology*, vol. 162, no. 7, pp. 1498–1508, 2011.

[45] D. U. Lee, Y. S. Ko, H. J. Kim, and K. C. Chang, "13-Ethylberberine reduces HMGB1 release through AMPK activation in LPS- activated RAW264.7 cells and protects endotoxemic mice from organ damage," *Biomedicine & Pharmacotherapy*, vol. 86, pp. 48–56, 2017.

[46] A. M. Gendy, M. R. Elnagar, M. M. Allam et al., "Berberine-loaded nanostructured lipid carriers mitigate warm hepatic ischemia/reperfusion-induced lesion through modulation of HMGB1/TLR4/NF-κB signaling and autophagy," *Biomedicine & Pharmacotherapy*, vol. 145, article 112122, 2022.

[47] T. van der Poll, "Tissue factor as an initiator of coagulation and inflammation in the lung," *Critical Care*, vol. 12, Supplement 6, p. S3, 2008.

[48] M. Y. Gao, L. Chen, L. Yang, X. Yu, J. P. Kou, and B. Y. Yu, "Berberine inhibits LPS-induced TF procoagulant activity and expression through NF-κB/p65, Akt and MAPK pathway in THP-1 cells," *Pharmacological Reports*, vol. 66, no. 3, pp. 480–484, 2014.

[49] X. Yang, X. Cheng, Y. Tang et al., "Bacterial endotoxin activates the coagulation cascade through gasdermin D-dependent phosphatidylserine exposure," *Immunity*, vol. 51, no. 6, article e986, pp. 983–996.e6, 2019.

[50] C. Yuan, M. Wu, Q. Xiao et al., "Blocking Msr1 by berberine alkaloids inhibits caspase-11-dependent coagulation in bacterial sepsis," *Signal Transduction and Targeted Therapy*, vol. 6, no. 1, p. 92, 2021.

[51] C. Wang, Y. Cheng, Y. Zhang et al., "Berberine and its main metabolite berberrubine inhibit platelet activation through suppressing the class I PI3Kβ/Rasa3/Rap1 pathway," *Frontiers in Pharmacology*, vol. 12, article 734603, 2021.

[52] M. Xue, M. X. Yang, W. Zhang et al., "Characterization, pharmacokinetics, and hypoglycemic effect of berberine loaded solid lipid nanoparticles," *International Journal of Nanomedicine*, vol. 8, pp. 4677–4687, 2013.

[53] J. Deng, Z. Wu, Z. Zhao et al., "Berberine-loaded nanostructured lipid carriers enhance the treatment of ulcerative colitis," *International Journal of Nanomedicine*, vol. 15, pp. 3937–3951, 2020.

[54] L. Zhao, X. Du, J. Tian et al., "Berberine-loaded carboxylmethyl chitosan nanoparticles ameliorate DSS-induced colitis and remodel gut microbiota in mice," *Frontiers in Pharmacology*, vol. 12, article 644387, 2021.

[55] T. Li, P. Wang, W. Guo et al., "Natural berberine-based Chinese herb medicine assembled nanostructures with modified antibacterial application," *ACS Nano*, vol. 13, no. 6, pp. 6770–6781, 2019.

[56] Z. Liu, Y. Liu, T. Fang, J. Xia, N. Ma, and Y. Wang, "Application of berberine-loaded albumin nanoparticles in infections

of traumatic wounds," *International Journal of Burns and Trauma*, vol. 12, no. 1, pp. 28–34, 2022.

[57] X. Yu, S. Yu, L. Chen et al., "Tetrahydroberberrubine attenuates lipopolysaccharide-induced acute lung injury by down-regulating MAPK, AKT, and NF-κB signaling pathways," *Biomedicine & Pharmacotherapy*, vol. 82, pp. 489–497, 2016.

[58] E. Bhatia, S. Sharma, K. Jadhav, and R. Banerjee, "Combinatorial liposomes of berberine and curcumin inhibit biofilm formation and intracellular methicillin resistant Staphylococcus aureus infections and associated inflammation," *Journal of Materials Chemistry B*, vol. 9, no. 3, pp. 864–875, 2021.

[59] X. Li, P. Wang, X. Hu et al., "The combined antibacterial effects of sodium new houttuyfonate and berberine chloride against growing and persistent methicillin-resistant and vancomycin-intermediate Staphylococcus aureus," *BMC Microbiology*, vol. 20, no. 1, p. 317, 2020.

[60] B. Li, S. Niu, H. Geng, C. Yang, and C. Zhao, "Berberine attenuates neonatal sepsis in mice by inhibiting FOXA1 and NF-κB signal transduction via the induction of MiR-132-3p," *Inflammation*, vol. 44, no. 6, pp. 2395–2406, 2021.

[61] E. Pierpaoli, O. Cirioni, O. Simonetti et al., "Potential application of berberine in the treatment of Escherichia coli sepsis," *Natural Product Research*, vol. 35, no. 22, pp. 4779–4784, 2021.

[62] A. A. Alalwan, A. Taher, and A. H. Alaradi, "A hemodialysis patient with severe COVID-19 pneumonia," *Cureus*, vol. 12, no. 5, article e7995, 2020.

Hindawi
Journal of Immunology Research
Volume 2022, Article ID 2931214, 8 pages
https://doi.org/10.1155/2022/2931214

Review Article

Sushi-Repeat-Containing Protein X-Linked 2: A Potential Therapeutic Target for Inflammation and Cancer Therapy

Jinhua Chen,[1] Zhenhua Yin,[2] Wenping Song,[1] Baoxia He,[1] and Wenzhou Zhang[1]

[1]*The Affiliated Cancer Hospital of Zhengzhou University & Henan Cancer Hospital, Henan Engineering Research Center for Tumor Precision Medicine and Comprehensive Evaluation, Henan Provincial Key Laboratory of Anticancer Drug Research, Zhengzhou 450008, China*
[2]*Comprehensive Utilization of Edible and Medicinal Plant Resources Engineering Technology Research Center, Zhengzhou Key Laboratory of Synthetic Biology of Natural Products, Henan Joint International Research Laboratory of Drug Discovery of Small Molecules, Huanghe Science and Technology College, Zhengzhou 450063, China*

Correspondence should be addressed to Wenzhou Zhang; hnzzzwzx@sina.com

Received 24 May 2022; Revised 13 June 2022; Accepted 7 July 2022; Published 28 July 2022

Academic Editor: Yisong Qian

Accumulating evidence has showed that sushi-repeat-containing protein X-linked 2 (SRPX2) is an abnormal expression in a variety of cancers and involved in cancer carcinogenesis, chemosensitivity, and prognosis, which mainly promote cancer cell metastasis, invasion, and migration by regulating the uPAR/integrins/FAK signaling pathway, epithelial-mesenchymal transition (EMT), angiogenesis, and glycosylation. Inflammation has been regarded as a key role in regulating cancer initiation, progression, EMT, and therapeutics. Furthermore, SRPX2 exhibited excellent antifibrosis effect *via* the TGFβR1/SMAD3/SRPX2/AP1/SMAD7 signaling pathway. Therefore, this review provides compelling evidence that SRPX2 might be a therapeutic target for inflammation and cancer-related inflammation for future cancer therapeutics.

1. Introduction

Sushi-repeat-containing protein X-linked 2 (SRPX2) is first found in 1999 by Kurosawa et al. that it is a downstream molecule of the *E2A-HLF* fusion gene in t (17;19)-positive leukemia cells. It is also called as sushi-repeat protein upregulated in leukemia (SRPUL) [1]. There are five genes in this family, including *SRPX2*, *SRPX* (*sushi-repeat-containing protein*, *X-linked*), *SVEP1* (*selectin-like protein*), *SELE* (*selectin E precursor*), and *SELP* (*selectin P precursor*) [2]. An increasing number of studies showed that SRPX2 is identified as a ligand for the urokinase plasminogen activator surface receptor (uPAR, CD87) [3]. As a crucial component of the extracellular plasminogen proteolysis system, uPAR is closely correlated with cancer invasion and metastasis, which is a transmembrane glycoprotein containing three distinct domains (D1, D2, and D3) [4, 5]. SRPX2 interacts with the D1 and D2-D3 extracellular domains of uPAR to enhance cancer invasion and metastasis by regulating multiple downstream signaling pathways, including the integrins/FAK pathway, the MAPK pathway, and the PI3K/Akt pathway [6, 7]. Roll et al. also found that transcription factor FOXP2, mutations of which caused severe speech and language disorders, could repress the interaction of SRPX2 and uPAR by directly binding to the promoter regions of SRPX2 (SRP1 and SRP2) and uPAR (UP2 and UP6) [8–10]. In addition, SRPX2 is regulated by its upstream molecules including TGF-β1, NFATC3, MAN1 (LEM) domain containing 1 (LEMD1), miR-192, miR-215, and miR-149 [11–14].

SRPX2 is an abnormal expression in a variety of cancers, such as pancreatic cancer, colorectal cancer, and gastric cancer [15–17]. Its overexpression in cancer has showed to relate with chemosensitivity, including cisplatin, nedaplatin, and temozolomide [14, 18]. Moreover, it might be a prognostic biomarker in cancer [17, 19]. Accumulating evidence has showed that inflammatory signaling pathways are closely involved in tumorigenesis, therapy resistance, and

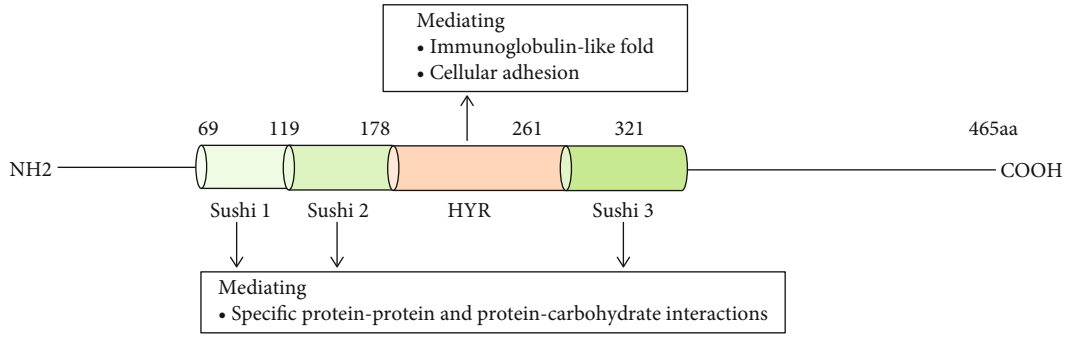

Figure 1: Schematic structure of SRPX2 protein. Sushi: sushi domain; sushi 1: 69-119AA; sushi 2: 120-178AA; sushi 3: 262-321AA; HYR: hyaline domain, 177-261AA; AA: amino acid.

metastasis [20–22]. SRPX2 also exhibited excellent antifibrosis effect *via* TGFβR1/SMAD3/SRPX2/AP1/SMAD7-positive feedback loop, indicating that SRPX2 might be a therapeutic target for inflammation and cancer-related inflammation for future cancer therapeutics [11]. Therefore, the purpose of this review is to consider and analyze the role of SRPX2 in inflammation and carcinogenesis to provide insight into potential shared mechanisms.

2. Structure and Expression

On chromosome Xq22.1, the *SRPX2* gene encodes a secreted extracellular matrix protein SRPX2 (GenBank NP_055282), which was identified as a chondroitin sulfate proteoglycan later [23]. SRPX2 protein consists of 465 amino acids containing three consensus sushi domains and one hyaline (HYR) domain (Figure 1) [3]. A sushi domain, also known as a complement control protein (CCP) module or a short consensus repeat, mostly exists in proteins of the complement system and other diverse proteins including the selectin family. It consists of ~60 amino acids including four invariant cysteine residues forming two disulfide-bridges (I-III and II-IV), a highly conserved tryptophan, and conserved glycine, proline, and hydrophobic residues [24, 25]. Studies demonstrated that it was involved in the interactions of specific protein and protein or carbohydrate, such as interacting with hepatocyte growth factor (HGF) and uPAR [23]. Moreover, some eukaryotic proteins also have HYR domains in their structures, often relating with sushi domain. It is probably related to the immunoglobulin-like fold and involved in cellular adhesion [26].

Tanaka et al. found that the levels of *SRPX2 mRNA* in the placenta, lung, trachea, uterus, and adrenal gland were high expression, whereas the levels were relatively low in the peripheral blood, brain, and bone marrow by detecting 24 normal human tissues with real-time RT-PCR [27]. In terms of studies on the understanding of the *SRPX2* gene and its functions in cancer, the mRNA expression from the TCGA and GTEx database (including 29 types of cancer) was analyzed, and *SRPX2* was found to abnormally express in multiple tumors (Figure 2). There is a significant higher expression in several tumor tissues than that of the appropriate normal tissues, including colon adenocarcinoma, lymphoid neoplasm diffuse large B cell lymphoma, glioblastoma multiforme, pancreatic adenocarcinoma, and rectum adenocarcinoma, while there is a significant lower expression in several tumor tissues than that of the appropriate normal tissues, including adrenocortical carcinoma, esophageal carcinoma, kidney chromophobe, kidney renal papillary cell carcinoma, ovarian serous cystadenocarcinoma, prostate adenocarcinoma, thyroid carcinoma, and uterine corpus endometrial carcinoma. Survival analysis indicated that the high expression of *SRPX2* had a shorter overall survival time than that of low expression of *SRPX2*. These findings indicated that abnormal expression of *SRPX2* was closely related to tumor.

3. SRPX2 and Inflammation

Idiopathic pulmonary fibrosis (IPF) is a severe lung disease. Its progression is closely related with oxidative stress, mitochondrial dysfunction, and endoplasmic reticulum stress [28]. Fibroblast-to-myofibroblast transition (FMT) has an important role for IPF. Wang et al. used deep-RNA sequencing to analyze the transcriptome between *in vitro* fibroblasts and myofibroblasts. Results showed that SRPX2 was overexpressed, while SRPX2 family other genes, SELE and SELP, were downregulated between *in vitro* fibroblasts and myofibroblasts. In line with *in vitro* results, the expression of SRPX2 in IPF patients' lung was higher than that of control subjects. And it found that TGF-β1 mediated the upregulation of SRPX2 *via* the TGFβR1/SMAD3/SRPX2/AP1/SMAD7 signaling pathway. Moreover, this study further demonstrated that SRPX2 siRNA-loaded liposomes, administrated by the intratracheal way, displayed good antifibrosis effects on BLM-induced pulmonary fibrosis in mice and significantly reduced FMT [11]. These findings showed that SRPX2 was very important in the progression of pulmonary fibrosis and suggested that targeting SRPX2 might be a good strategy to treat pulmonary fibrosis in clinical setting.

4. SRPX2 and Cancer

4.1. SRPX2 Involved in Cancer Metastasis, Invasion, and Migration. This process of cancer spread is known as metastasis. A major process of metastasis is the proteolytic degradation of the extracellular matrix (ECM) to promote tumor cell migration and invasion [29]. Currently, metastatic and

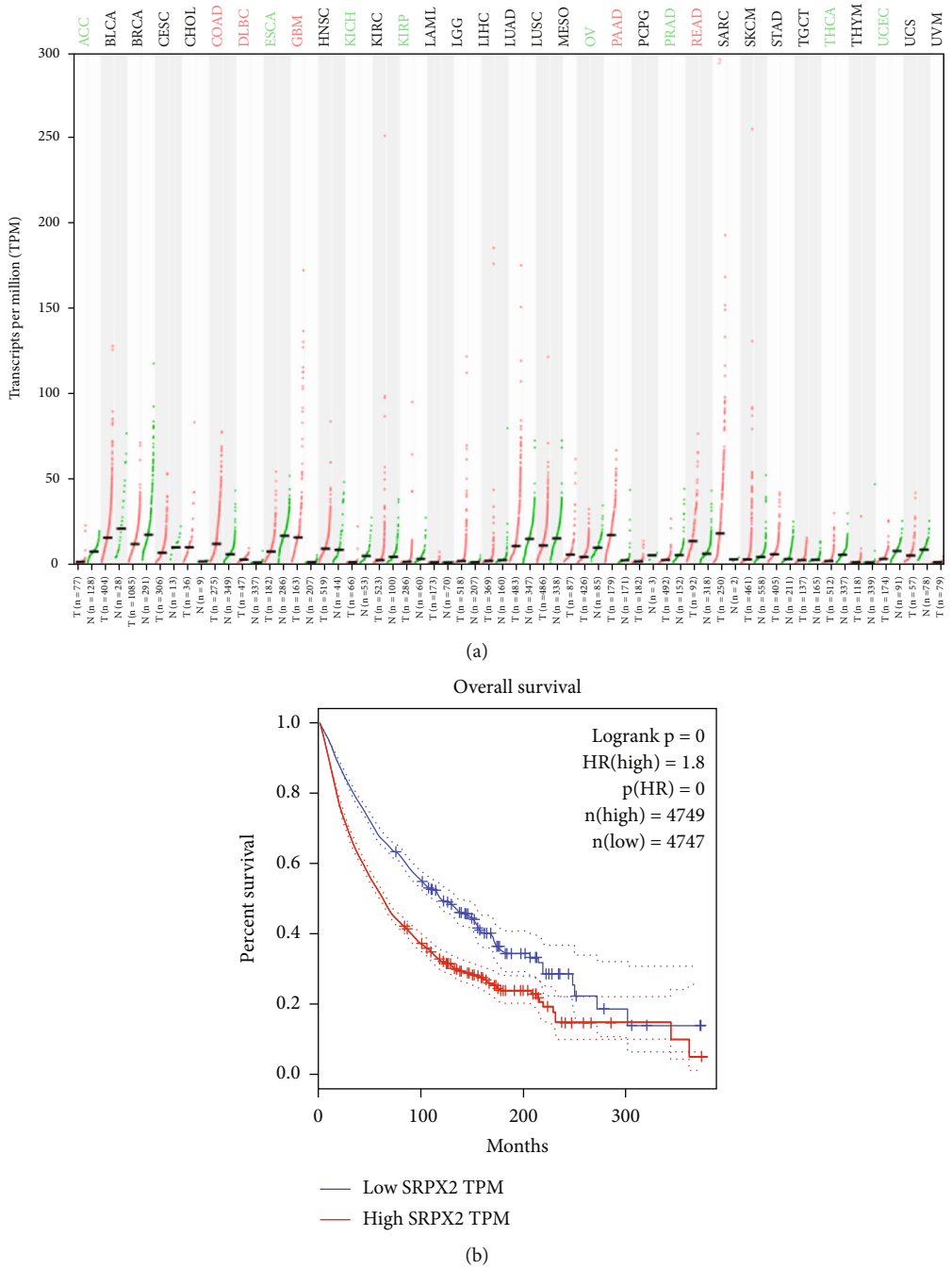

Figure 2: mRNA expression of *SRPX2* and survival analysis from the TCGA and GTEx database. (a) mRNA expression of *SRPX2* in 29 types of tumors. Green font represents that there is a lower expression of *SRPX2* in tumor tissue than that of the appropriate normal tissue. Red font represents that there is a higher expression in tumor tissue than that of the appropriate normal tissue. Black font represents that there is no significant difference in tumor tissue and the appropriate normal tissue. (b) The overall survival time of the SRPX2 high expression group ($n = 4749$) and the SRPX2 low expression group ($n = 4747$). ACC: adrenocortical carcinoma; BLCA: bladder urothelial carcinoma; BRCA: breast invasive carcinoma; CESC: cervical squamous cell carcinoma and endocervical adenocarcinoma; CHOL: cholangiocarcinoma; COAD: colon adenocarcinoma; DLBC: lymphoid neoplasm diffuse large B cell lymphoma; ESCA: esophageal carcinoma; GBM: glioblastoma multiforme; HNSC: head and neck squamous cell carcinoma; KICH: kidney chromophobe; KIRC: kidney renal clear cell carcinoma; KIRP: kidney renal papillary cell carcinoma; LAML: acute myeloid leukemia; LGG: brain lower-grade glioma; LIHC: liver hepatocellular carcinoma; LUAD: lung adenocarcinoma; LUSC: lung squamous cell carcinoma; MESO: mesothelioma; OV: ovarian serous cystadenocarcinoma; PAAD: pancreatic adenocarcinoma; PCPG: pheochromocytoma and paraganglioma; PRAD: prostate adenocarcinoma; READ: rectum adenocarcinoma; SARC: sarcoma; SKCM: skin cutaneous melanoma; STAD: stomach adenocarcinoma; TGCT: testicular germ cell tumors; THCA: thyroid carcinoma; THYM: thymoma; UCEC: uterine corpus endometrial carcinoma; UCS: uterine carcinosarcoma; UVM: uveal melanoma.

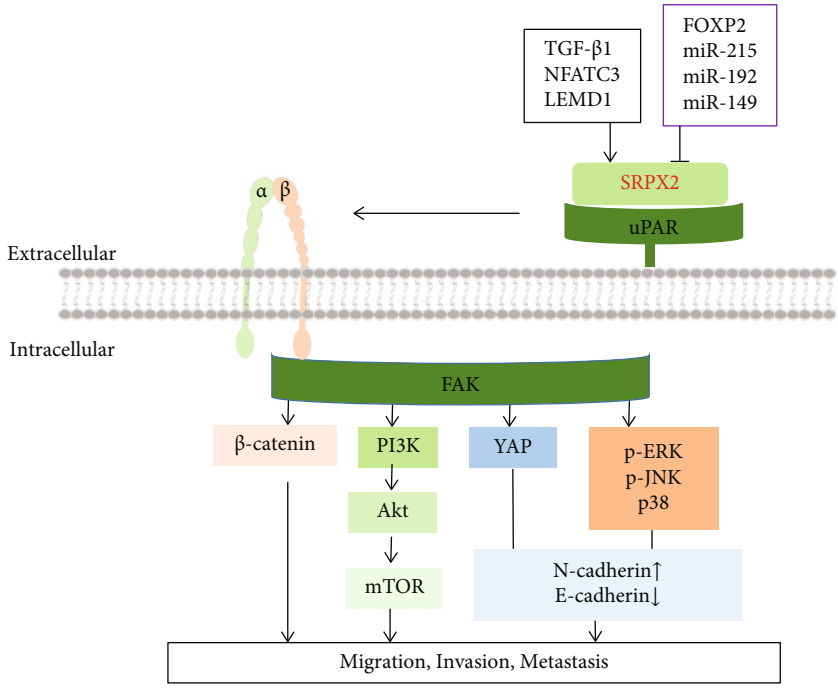

Figure 3: SRPX2 regulates cancer cell metastasis, migration, and invasion by regulating various signaling pathways.

invasive cancers remain largely incurable. The abnormal expression of SRPX2 is a common molecular characteristic of human cancers and enhanced cell metastasis and invasion by regulating the focal adhesion kinase (FAK) signaling pathway, epithelial-mesenchymal transition (EMT), angiogenesis, and glycosylation (Figure 3).

4.1.1. Regulation of the Focal Adhesion Kinase (FAK) Signaling Pathway. FAK is a nonreceptor tyrosine kinase and aggregates to the cytoplasmic tails of integrins to regulate cellular adhesion, migration, invasion, and metastasis by activating a series of cellular signaling pathways such as the matrix metalloproteinases (MMPs), PI3K/Akt, and Wnt/β-catenin pathway [30–33]. Researchers showed that elevated SRPX2 in gastric cancer and pancreatic ductal adenocarcinoma enhanced migration and adhesion through increasing phosphorylation levels of FAK [27, 34]. In hepatocellular carcinoma, SRPX2 knockdown suppressed pulmonary metastasis of hepatocellular carcinoma HCCLM3 cells in nude mice, which the mechanisms were through inhibiting FAK/AKT pathway-mediated MMP2/9 expression [23]. Moreover, the inhibition of SRPX2 by siRNA also inhibited the invasion of colorectal cancer HCT116 cells through downregulating Wnt/β-catenin pathway-mediated MMP2/9 expression [16]. SRPX2 has been demonstrated to be a ligand for uPAR, and uPAR-integrin interaction is frequently associated with the activation of FAK [35]. Therefore, the uPAR/integrins/FAK/MMPs signaling pathway may play an central role in SRPX2-induced tumor metastasis and invasion.

4.1.2. Regulation of Epithelial-Mesenchymal Transition (EMT). EMT is a highly dynamic process characterized by transformation of polarized epithelial cells into highly invasive mesenchymal cells, resulting in the increased capacity of migration and invasion [36]. The events occurring during EMT include the loss of adherent junctions, the downregulation of E-cadherin, and upregulation of N-cadherin, Twist, Snail, Slug, fibronectin, MMP-2, and MMP-9 [37]. Wu et al. found that SRPX2 knockdown inhibited osteosarcoma invasion by decreasing N-cadherin levels and increasing E-cadherin level *in vivo*. Further study showed SRPX2 knockdown increased the phosphorylation of Yes-associated protein (YAP), thus decreasing nuclear translocation to activate the Hippo signaling pathway, suggesting that SRPX2 might activate the Hippo signaling pathway to increase cell invasion in osteosarcoma [38]. It was also observed that SRPX2 knockdown inhibited migration and invasion by reducing N-cadherin level and increasing E-cadherin level in prostate cancer cells (LNCaP cells and DU-145cells). Furthermore, SRPX2 knockdown obviously inhibited the phosphorylation of PI3K, Akt, and mTOR, and the treatment with PI3K inhibitor LY294002 efficiently enhanced the inhibitory effects of sh-SRPX2 on LNCap cell migration, suggesting SRPX2 regulates the migration and invasion *via* the EMT process by mediating the PI3K/Akt/mTOR signaling pathway [7]. In glioblastoma, SRPX2 knockdown significantly decreased the expression of EMT markers (N-cadherin, fibronectin, Twist, Snail, and Slug) and increased E-cadherin expression, while SRPX2 overexpression increased N-cadherin and fibronectin expression and decreased E-cadherin expression. In the meantime, it was observed that knockdown of SRPX2 decreased the MAPK signaling pathway (p-ERK, p-JNK, and p-p38) proteins, but blocking the MAPK signaling pathway by PD098059 inhibited glioblastoma metastasis, not cell invasion and

Table 1: Roles for SRPX2 in cancer metastasis, invasion, migration, drug resistance, and prognosis.

Cancer type	Downstream signaling pathway	Upstream signaling pathway	Effects	Prognostic value	References
Gastric cancer	FAK	/	Migration and adhesion induction	Lower OS and worse prognosis; independent predictor of outcomes	[15, 27]
Colorectal cancer	Wnt/β-catenin pathway-mediated MMP2/9	miR-192, miR-215, miR-149	Invasion induction	/	[16]
Pancreatic ductal adenocarcinoma	FAK; PI3K/AKT/mTOR	/	Migration and adhesion induction; 5-Fu and gemcitabine resistance	Shorter DFS and OS	[17, 34, 52]
Prostate cancer	PI3K/Akt/mTOR	/	Migration and adhesion induction	Shorter OS	[7, 53]
Oral squamous cell carcinomas	/	LEMD1	Adhesion induction; nedaplatin and cisplatin resistance	/	[10]
Glioblastoma	p-ERK, p-JNKp38	/	Metastasis induction; temozolomide resistance	/	[18]
Hepatocellular carcinoma	FAK/AKT pathway-mediated MMP2/9	/	Metastasis induction	/	[19]
Osteosarcoma	Yes-associated protein (YAP)	/	Invasion induction	/	[38]
Esophageal squamous cell carcinoma	Wnt/β-catenin	/	Metastasis induction; cisplatin resistance	/	[39]
Papillary thyroid cancer	/	/	/	Independent prognostic factor	[54]

migration in the cells with downregulation of SRPX2, suggesting that SRPX2 promoted the EMT process to enhance glioblastoma metastasis through the MAPK signaling pathway [18]. In addition, knockdown of SRPX2 inhibited metastasis in esophageal squamous cell carcinoma cells by preventing the EMT process via the inactivation of the Wnt/β-catenin signaling pathway [39]. Therefore, EMT process plays an important role for SRPX2 to induce cancer invasion and metastasis by various pathways including the Hippo signaling pathway, PI3K/Akt/mTOR signaling pathway, MAPK signaling pathway, and Wnt/β-catenin signaling pathway.

4.1.3. Regulation of Angiogenesis. Angiogenesis is the process through which novel blood vessels are formed from the existing blood vessels, and provides sufficient supply of nutrients and oxygen to cells. Tumor angiogenesis is closely related with tumor growth, progression, and metastasis [40]. Miljkovic-Licina et al. used in situ mRNA hybridization and immunostaining to detect SRPX2 expression in de novo formation of the blood vessels in angiogenic tissues and found SRPX2-specific expression in tumor endothelial sprouts. This study further demonstrated that silencing of SRPX2 delayed angiogenic sprout formation and SRPX2 bound to vascular uPAR by pull-down experiments [41]. Because SRPX2 is a secretory proteoglycan in extracellular matrix, other study used SRPX2 recombinant protein to further demonstrate that SRPX2 could significantly increase the angiogenic ability of human umbilical vein endothelial cells (HUVECs) through the uPAR/integrin/FAK pathway, which activated the PI3K/Akt and Ras/MAPK pathways [42].

4.1.4. Regulation of Glycosylation. Glycosylation is the most ubiquitous molecular modification, which regulates many biological functions [43]. Compared with *O*-glycans in healthy tissues, cancer-associated *O*-glycans are often truncated [44, 45]. Abnormal glycosylation in cancer is associated with cancer progression and metastasis [46]. MKN45 SC cells and AGS SC cells are derived from two gastric cancer cell lines, MKN45 and AGS, by knocking out the *COSMC* gene, which is essential for *O*-glycan elongation [47, 48]. Freitas and coworkers found that truncation of *O*-glycans in MKN45 SC cells and AGS SC cells promoted invasive features. The results of the transcriptomic analysis exhibited that *COSMC* knockout in MKN45 SC cells and AGS SC cells resulted in a significant alteration in the transcription profile in comparison with the respective parental cells, especially the most upregulated *SRPX2* gene, suggesting that SRPX2 may promote cancer invasion through regulating cell glycosylation [49].

4.2. SRPX2 Involved in Cancer Chemosensitivity. Cancer resistance is still the greatest challenge in improving the outcomes for cancer patients [50]. Accumulating evidence demonstrated that SRPX2 was involved in chemosensitivity. Platinum-based chemotherapeutic drugs have been used

extensively to treat various human cancers such as esophageal cancer, head and neck cancer, and lung cancer [51]. It has shown that downregulation of SRPX2 restored the sensitivity of oral squamous cell carcinoma cells to nedaplatin and cisplatin and increased the sensitivity of esophageal squamous cell carcinoma cells towards cisplatin [14, 39]. The study by Tang et al. showed that overexpression of SRPX2 induced temozolomide resistance in glioblastoma [18]. Additionally, it was observed that SRPX2 level of pancreatic cancer patients with stable disease and progressive disease after chemotherapy was above that before chemotherapy, while SRPX2 level of pancreatic cancer patients with partial remission after chemotherapy was lower than that before chemotherapy, suggesting that SRPX2 was closely associated with chemotherapeutic efficacy of pancreatic cancer patients. Further study indicated that silencing of SRPX2 sensitized pancreatic cancer cells against 5-Fu and gemcitabine by deactivating the PI3K/AKT/mTOR signaling pathway [52].

4.3. SRPX2 as a Prognosic Marker in Cancer. Researchers have found SRPX2 may yield several clinically relevant insights in patients with cancers. Li and coworkers demonstrated that patients with elevated SRPX2 expression are related to shorter disease-free survival (DFS) and overall survival (OS) than patients with low SRPX2 expression by detecting 200 tissue microarray specimens from patients (79 training and 121 validation) with curative pancreatectomy for pancreatic ductal adenocarcinoma [17]. Furthermore, elevated SRPX2 expression was significantly associated with shorter OS in prostate cancer [53]. In patients with papillary thyroid cancer, high SRPX2 expression was demonstrated to as an independent prognostic factor [54]. Moreover, it was also reported that gastric cancer patients with overexpression of SRPX2 presented a lower OS and worse prognosis in comparison to patients with low SPRX2, and SRPX2 was considered a useful independent predictor of outcomes [15]. However, other study detected 112 gastric cancer patients' peripheral blood karyocytes and did not find SRPX2 was related with prognosis [55]. Therefore, SRPX2 may be a prognostic biomarker in tumor tissue, but it needed to further explore the role in peripheral blood karyocytes.

5. Conclusion and Perspective

Since its discovery in 1999, SRPX2 is demonstrated to associate with the progression of various types of cancers. Research interest in cancer mainly focused on cancer metastasis, invasion, migration, and drug resistance through regulating the FAK signaling pathway, EMT, angiogenesis, and glycosylation (Table 1). Moreover, SRPX2 was a prognostic factor with OS and DFS through analyzing the tumor tissue, but not in peripheral blood karyocytes (Table 1). Furthermore, SRPX2 exhibited excellent antifibrosis effect *via* the TGFβR1/SMAD3/SRPX2/AP1/SMAD7 pathway *in vitro* and *in vivo*. Thus, these findings indicated that SRPX2 might be a potential therapeutic target for treatment of highly metastatic cancers, cancer resistance, and inflammation. Inflammatory signaling pathways are closely involved in tumorigenesis, therapy resistance, and metastasis. A better understanding of the roles of SRPX2 in inflammation will be helpful to treat cancer-related inflammation to slow the progression of cancer. Additionally, it is a pity that there is little connection between SRPX2 and drug development at current. Therefore, in-depth understanding of structure and functions of SRPX2 will provide the theoretical foundations to drug design.

Data Availability

The data supporting this review are from previously reported studies and datasets, which have been cited. The processed data generated or analyzed during this study are included in this article.

Conflicts of Interest

The authors declare that they have no conflicts of interest.

Acknowledgments

This work was supported by the Tackling-plan Project of Henan Department of Science and Technology under Grant (212102310325) and the Tackling-plan Project of Henan Medical Science and Technology under Grant (LHGJ20200164).

References

[1] H. Kurosawa, K. Goi, T. Inukai et al., "Two candidate downstream target genes for E2A-HLF," *Blood*, vol. 93, no. 1, pp. 321–332, 1999.

[2] B. Royer, D. C. Soares, P. N. Barlow et al., "Molecular evolution of the human SRPX2 gene that causes brain disorders of the Rolandic and Sylvian speech areas," *BMC Genetics*, vol. 8, no. 1, p. 72, 2007.

[3] B. Royer-Zemmour, M. Ponsole-Lenfant, H. Gara et al., "Epileptic and developmental disorders of the speech cortex: ligand/receptor interaction of wild-type and mutant SRPX2 with the plasminogen activator receptor uPAR," *Human Molecular Genetics*, vol. 17, no. 23, pp. 3617–3630, 2008.

[4] M. J. Duffy, "The urokinase plasminogen activator system: role in malignancy," *Current Pharmaceutical Design*, vol. 10, no. 1, pp. 39–49, 2004.

[5] N. Mahmood, C. Mihalcioiu, and S. A. Rabbani, "Multifaceted role of the urokinase type plasminogen activator (uPA) and its receptor (uPAR): diagnostic, prognostic, and therapeutic applications," *Frontiers in Oncology*, vol. 8, pp. 1–21, 2018.

[6] X. Li, J. Liu, H. Sun et al., "SRPX2 promotes cell proliferation and invasion via activating FAK/SRC/ERK pathway in non-small cell lung cancer," *Acta Biochimica Polonica*, vol. 67, no. 2, pp. 165–172, 2020.

[7] X. Hong, X. Hong, H. Zhao, and C. He, "Knockdown of SRPX2 inhibits the proliferation, migration, and invasion of prostate cancer cells through the PI3K/Akt/mTOR signaling pathway," *Journal of Biochemical and Molecular Toxicology*, vol. 9, article e22237, 2018.

[8] K. D. MacDermot, E. Bonora, N. Sykes et al., "Identification of FOXP2 truncation as a novel cause of developmental speech

and language deficits," *American Journal of Human Genetics*, vol. 76, no. 6, pp. 1074–1080, 2005.

[9] P. Roll, S. C. Vernes, N. Bruneau et al., "Molecular networks implicated in speech-related disorders: FOXP2 regulates the SRPX2/uPAR complex," *Human Molecular Genetics*, vol. 19, no. 24, pp. 4848–4860, 2010.

[10] T. Sasahira, M. Kurihara-Shimomura, Y. Nishiguchi, H. Shimomura, and T. Kirita, "Sushi repeat containing protein X-linked 2 is a downstream signal of LEM domain containing 1 and acts as a tumor-promoting factor in oral squamous cell carcinoma," *International Journal of Molecular Sciences*, vol. 21, no. 10, p. 3655, 2020.

[11] Q. Wang, J. Liu, Y. Hu et al., "Local administration of liposomal-based Srpx 2 gene therapy reverses pulmonary fibrosis by blockading fibroblast-to-myofibroblast transition," *Theranostics*, vol. 11, no. 14, pp. 7110–7125, 2021.

[12] H. Chen, Y. Zeng, M. Shao et al., "Calcineurin A gamma and NFATc3/SRPX2 axis contribute to human embryonic stem cell differentiation," *Journal of Cellular Physiology*, vol. 236, no. 8, pp. 5698–5713, 2021.

[13] J. Zhao, J. Xu, and R. Zhang, "SRPX2 regulates colon cancer cell metabolism by miR-192/215 via PI3K-Akt," *American Journal of Translational Research*, vol. 10, no. 2, pp. 483–490, 2018.

[14] B. Øster, L. Linnet, L. L. Christensen et al., "Non-CpG island promoter hypomethylation and miR-149 regulate the expression of SRPX2 in colorectal cancer," *International Journal of Cancer*, vol. 132, no. 10, pp. 2303–2315, 2013.

[15] T. Yamada, T. Oshima, K. Yoshihara et al., "Impact of overexpression of sushi repeat-containing protein X-linked 2 gene on outcomes of gastric cancer," *Journal of Surgical Oncology*, vol. 109, no. 8, pp. 836–840, 2014.

[16] K. L. Liu, J. Wu, Y. Zhou, and J. H. Fan, "Increased sushi repeat-containing protein X-linked 2 is associated with progression of colorectal cancer," *Medical Oncology*, vol. 32, no. 4, p. 99, 2015.

[17] H. Li, S. R. Zhang, H. X. Xu et al., "SRPX2 and RAB31 are effective prognostic biomarkers in pancreatic cancer," *Journal of Cancer*, vol. 10, no. 12, pp. 2670–2678, 2019.

[18] H. Tang, J. Zhao, L. Zhang, J. Zhao, Y. Zhuang, and P. Liang, "SRPX2 enhances the epithelial-mesenchymal transition and temozolomide resistance in glioblastoma cells," *Cellular and Molecular Neurobiology*, vol. 36, no. 7, pp. 1067–1076, 2016.

[19] X. Lin, W. Chang, Y. Wang, M. Tian, and Z. Yu, "SRPX2, an independent prognostic marker, promotes cell migration and invasion in hepatocellular carcinoma," *Biomedicine & Pharmacotherapy*, vol. 93, pp. 398–405, 2017.

[20] M. H. Park and J. T. Hong, "Roles of NF-κB in cancer and inflammatory diseases and their therapeutic approaches," *Cell*, vol. 5, no. 2, p. 15, 2016.

[21] H. Li, M. H. Huang, J. D. Jiang, and Z. G. Peng, "Hepatitis C: from inflammatory pathogenesis to anti-inflammatory/hepatoprotective therapy," *World Journal of Gastroenterology*, vol. 24, no. 47, pp. 5297–5311, 2018.

[22] S. Hibino, T. Kawazoe, H. Kasahara et al., "Inflammation-induced tumorigenesis and metastasis," *International Journal of Molecular Sciences*, vol. 22, no. 11, p. 5421, 2021.

[23] K. Tanaka, T. Arao, D. Tamura et al., "SRPX2 is a novel chondroitin sulfate proteoglycan that is overexpressed in gastrointestinal cancer," *PLoS One*, vol. 7, no. 1, article e27922, 2012.

[24] J. M. O'Leary, K. Bromek, G. M. Black et al., "Backbone dynamics of complement control protein (CCP) modules reveals mobility in binding surfaces," *Protein Science*, vol. 13, no. 5, pp. 1238–1250, 2004.

[25] K. B. Reid and A. J. Day, "Structure-function relationships of the complement components," *Immunology Today*, vol. 10, no. 6, pp. 177–180, 1989.

[26] I. Callebaut, D. Gilgès, I. Vigon, and J. P. Mornon, "HYR, an extracellular module involved in cellular adhesion and related to the immunoglobulin-like fold," *Protein Science*, vol. 9, no. 7, pp. 1382–1390, 2000.

[27] K. Tanaka, T. Arao, M. Maegawa et al., "SRPX2 is overexpressed in gastric cancer and promotes cellular migration and adhesion," *International Journal of Cancer*, vol. 124, no. 5, pp. 1072–1080, 2009.

[28] T. H. G. Phan, P. Paliogiannis, G. K. Nasrallah et al., "Emerging cellular and molecular determinants of idiopathic pulmonary fibrosis," *Cellular and Molecular Life Sciences*, vol. 78, no. 5, pp. 2031–2057, 2021.

[29] S. A. Rabbani and A. P. Mazar, "Evaluating distant metastases in breast cancer: from biology to outcomes," *Cancer and Metastasis Reviews*, vol. 26, no. 3-4, pp. 663–674, 2007.

[30] P. Tapial Martínez, P. López Navajas, and D. Lietha, "FAK structure and regulation by membrane interactions and force in focal adhesions," *Biomolecules*, vol. 10, no. 2, p. 179, 2020.

[31] N. N. Mon, S. Ito, T. Senga, and M. Hamaguchi, "FAK signaling in neoplastic disorders: a linkage between inflammation and cancer," *Annals of the New York Academy of Sciences*, vol. 1086, no. 1, pp. 199–212, 2006.

[32] K. Katoh, "FAK-dependent cell motility and cell elongation," *Cell*, vol. 9, no. 1, p. 192, 2020.

[33] J. Wörthmüller and C. Rüegg, "The crosstalk between FAK and Wnt signaling pathways in cancer and its therapeutic implication," *International Journal of Molecular Sciences*, vol. 21, no. 23, p. 9107, 2020.

[34] Z. Gao, J. Zhang, M. Bi et al., "SRPX2 promotes cell migration and invasion via FAK dependent pathway in pancreatic cancer," *International Journal of Clinical and Experimental Pathology*, vol. 8, no. 5, pp. 4791–4798, 2015.

[35] J. A. Aguirre Ghiso, "Inhibition of FAK signaling activated by urokinase receptor induces dormancy in human carcinoma cells in vivo," *Oncogene*, vol. 21, no. 16, pp. 2513–2524, 2002.

[36] J. P. Thiery, H. Acloque, R. Y. Huang, and M. A. Nieto, "Epithelial-mesenchymal transitions in development and disease," *Cell*, vol. 139, no. 5, pp. 871–890, 2009.

[37] D. Ribatti, R. Tamma, and T. Annese, "Epithelial-mesenchymal transition in cancer: a historical overview," *Translational Oncology*, vol. 13, no. 6, article 100773, 2020.

[38] Z. Wu, C. Wang, Y. Chen, Z. Sun, and W. Yan, "SRPX2 promotes cell proliferation and invasion in osteosarcoma through regulating Hippo signaling pathway," *Onco Targets and Therapy*, vol. 13, pp. 1737–1749, 2020.

[39] F. He, H. Wang, Y. Li et al., "SRPX2 knockdown inhibits cell proliferation and metastasis and promotes chemosensitivity in esophageal squamous cell carcinoma," *Biomedicine & Pharmacotherapy*, vol. 109, pp. 671–678, 2019.

[40] R. I. Teleanu, C. Chircov, A. M. Grumezescu, and D. M. Teleanu, "Tumor angiogenesis and anti-angiogenic strategies for cancer treatment," *Journal of Clinical Medicine*, vol. 9, no. 1, p. 84, 2020.

[41] M. Miljkovic-Licina, P. Hammel, S. Garrido-Urbani, P. F. Bradfield, P. Szepetowski, and B. A. Imhof, "Sushi repeat

protein X-linked 2, a novel mediator of angiogenesis," *FASEB Journal*, vol. 23, no. 12, pp. 4105–4116, 2009.

[42] K. Liu, J. Fan, and J. Wu, "Sushi repeat-containing protein X-linked 2 promotes angiogenesis through the urokinase-type plasminogen activator receptor dependent integrin $\alpha v\beta 3$/focal adhesion kinase pathways," *Drug Discoveries and Therapeutics*, vol. 11, no. 4, pp. 212–217, 2017.

[43] A. Varki, "Biological roles of glycans," *Glycobiology*, vol. 27, no. 1, pp. 3–49, 2017.

[44] I. Brockhausen, "Mucin-type O-glycans in human colon and breast cancer: glycodynamics and functions," *EMBO Reports*, vol. 7, no. 6, pp. 599–604, 2006.

[45] M. R. Kudelka, T. Ju, J. Heimburg-Molinaro, and R. D. Cummings, "Simple sugars to complex disease—mucin-type O-glycans in cancer," *Advances in Cancer Research*, vol. 126, pp. 53–135, 2015.

[46] S. Cascio and O. J. Finn, "Intra- and extra-cellular events related to altered glycosylation of MUC1 promote chronic inflammation, tumor progression, invasion, and metastasis," *Biomolecules*, vol. 6, no. 4, p. 39, 2016.

[47] D. Campos, D. Freitas, J. Gomes et al., "Probing the O-glycoproteome of gastric cancer cell lines for biomarker discovery∗ [S]," *Molecular & Cellular Proteomics*, vol. 14, no. 6, pp. 1616–1629, 2015.

[48] T. Ju, R. P. Aryal, M. R. Kudelka, Y. Wang, and R. D. Cummings, "The Cosmc connection to the Tn antigen in cancer," *Cancer Biomarkers*, vol. 14, no. 1, pp. 63–81, 2014.

[49] D. Freitas, D. Campos, J. Gomes et al., "*O* -glycans truncation modulates gastric cancer cell signaling and transcription leading to a more aggressive phenotype," *eBioMedicine*, vol. 40, pp. 349–362, 2019.

[50] M. M. Gottesman, O. Lavi, M. D. Hall, and J. P. Gillet, "Toward a better understanding of the complexity of cancer drug resistance," *Annual Review of Pharmacology and Toxicology*, vol. 56, no. 1, pp. 85–102, 2016.

[51] S. Dilruba and G. V. Kalayda, "Platinum-based drugs: past, present and future," *Cancer Chemotherapy and Pharmacology*, vol. 77, no. 6, pp. 1103–1124, 2016.

[52] Z. Gao, J. Wu, X. Wu, J. Zheng, and Y. Ou, "SRPX2 boosts pancreatic cancer chemoresistance by activating PI3K/AKT axis," *Open Medicine (Warsaw)*, vol. 15, no. 1, pp. 1072–1082, 2020.

[53] M. Zhang, X. Li, Z. Fan et al., "High SRPX2 protein expression predicts unfavorable clinical outcome in patients with prostate cancer," *Onco Targets and Therapy*, vol. 11, pp. 3149–3157, 2018.

[54] M. Shibata, T. Inaishi, T. Ichikawa et al., "Identifying the tumor-progressive gene expression profile in high-risk papillary thyroid cancer," *Surgery Today*, vol. 51, no. 10, pp. 1703–1712, 2021.

[55] Y. Y. Wang, L. Li, Z. S. Zhao, and H. J. Wang, "Clinical utility of measuring expression levels of KAP1, TIMP1 and STC2 in peripheral blood of patients with gastric cancer," *World Journal of Surgical Oncology*, vol. 11, no. 1, p. 81, 2013.